International Journal of Plasticity, Volume 38, November 2012, Pages 47–85

Manuscript number INTPLA-D-11-00170R1

Modelling of Dynamic Behaviour of Orthotropic Metals Including Damage and Failure

R. Vignjevic[a], *N. Djordjevic*[a], *V. Panov*

[a] Department of Applied Mechanics and Astronautics, School of Engineering,
Cranfield University, Cranfield, Bedfordshire,
MK43 0AL, United Kingdom

e-mail: v.rade@cranfield.ac.uk
tel: +44 (0) 1234 754736 fax: +44 (0) 1234 758207

Abstract

A physically based material model for metals, with elastic plastic and damage/failure orthotropy is proposed in this paper. The model is defined within the frameworks of irreversible thermodynamics and configurational continuum mechanics and integrated in the isoclinic configuration. The use of the multiplicative decomposition of deformation gradient makes the model applicable to arbitrary plastic and damage deformations. To account for the physical mechanisms of failure, the concept of thermally activated damage initially proposed by Klepaczko (Klepaczko, 1990) was adopted as the basis for the new damage evolution model. This makes the proposed damage/failure model compatible with the Mechanical Threshold Strength (MTS) model (Follansbee and Kocks, 1988; Chen and Gray, 1996; Goto et al., 2000; Gray et al., 1999; Chen et al., 1998) which was used to control evolution of flow stress during plastic deformation. In addition the constitutive model is coupled with a shock equation of state which allows for modelling of shock wave propagation in the material. The new model was implemented in DYNA3D and our in-house non-linear transient SPH code, MCM (Meshless Continuum Mechanics).

Parameters for the new constitutive model for AA7010 (a polycrystalline aluminium alloy, whose orthotropy is a consequence of grain morphology), were derived on the basis of the tensile tests and Taylor anvil tests. The tensile tests were performed for the range of temperatures between 343.15K and 413.15K, and strain rates between $6.4\times10^{-4}s^{-1}$ and $6.4\times10^{1}s^{-1}$.

The new model was validated in two stages. The first stage comprised a series of single element tests design to separately validate elasticity, plasticity and damage related parts of the model. The second stage comprised a series of numerical simulations of Taylor anvil and plate impact tests for AA7010 and comparison of the numerical results with the experimental data. The numerical results illustrate the ability of the new model to predict experimentally observed behaviour.

Keywords: orthotropic damage-elastoplasticity, thermally activated damage, structural tensors, isotropic free energy function (invariant representation)

1 Introduction

It has long been recognized that the mechanical properties of many common engineering materials display a pronounced anisotropy. This can occur at the unit-cell level, for example, in single crystals; in the grain structure due to preferred orientations caused by processing; or in multiphase materials due to directional orientation of secondary phases (e.g. directional fibre-reinforced composites). These effects have been studied extensively at quasi-static strain rates, e.g. (Smallman, 1985; Vignjevic et al., 2002, Sinha and Ghosh, 2006). A significant amount of work has been done on behaviour of materials under shock loading, see for instance (Meredith and Khan, 2011; Khan and Meredith, 2010; Furnish and Chhabildas, 1998; Minich et al., 2004; Kanel et al., 2009; Zaretsky and Kanel, 2011; Khan et al., 2009; Colvin et al., 2009). However, the influence of anisotropy on material behaviour at high strain rates, including shock wave propagation, has only recently attracted attention e.g. (Smallman, 1985; Vignjevic et al., 2002; Gray et al., 2003; Sitko et al., 2010; Meredith and Khan, 2011; Khan et al., 2009; Khan et al., 2007a; Khan et al., 2007b; Nakamachi et al., 2007). The proposed model is intended for modelling of dynamic behaviour in the presence of shockwaves for orthotropic metals, such as Tantalum and rolled aluminium alloy (AA) 7010. Initial validation of the model was done on AA 7010, for which extensive experimental data was available.

One of the first detailed investigations of the shock response of AAs was made by Rosenberg (Rosenberg et al., 1983), who showed that for AA2024 the Hugoniot Elastic Limit (HEL) and spall strengths, in differently heat treated states, followed the same trends as the quasi-statically measured properties. Furthermore, Rosenberg showed that solution treated specimens possess the lowest strengths under both testing regimes. Work by Butcher (Butcher, 1968) and Rubin (Rubin, 1990) on AA6061-T6 predicted that the spall strength should vary in accordance with the one-dimensional stress yield strength according to orientation, but they concluded that directionality has no significant effect on crack formation. Other works have also investigated the spall response of AAs, with Stevens and Tuler (Stevens and Tuler, 1971) observing that the degree of pre compression, in other words the shock amplitude, had no effect on the spall strength of AA6061-T6. While Schmidt (Schmidt et al., 1978) showed that the spall strength of AA2024-T86 decreased with increasing temperature. Analysis of BCC tantalum, conducted by Gray and Maudlin, (Maudlin et al., 1999a; Maudlin et al., 1999b; Bronkhorst et al., 2006), through a number of Taylor impact tests, shows that evolution of texture does not affect the plastic deformation observed at continuum level, and that yield surface shape was the same for a range of strain rates. This finding was used to support the assumption of isotropic hardening in the proposed model.

Prior to failure, ductile materials undergo significant plastic deformation, which has a major influence on damage evolution. These materials usually fail as the result of nucleation, growth and coalescence of micro-voids, resulting in the loss of the load carrying capacity of the material. Experimental observations show that plastic deformation and accumulation of micro-damage have a

tendency to localise, see for instance (Krajcinovic, 1989; Skoczeń et al., 2010). The physical process of progressive degradation of the material mechanical properties up to complete failure is commonly referred to as the damage process.

These two distinct dissipative mechanical processes, i.e. plasticity and damage, are the main causes of non-linear material behaviour. A large number of multi-dissipative models, for this type of behaviour, for ductile metals have been proposed. Some include damage micromechanics (micromechanical damage models, e.g. (Smallman, 1985; Vignjevic et al., 2002; Gray et al., 2003; Sinha and Ghosh, 2006; Neil and Agnew, 2009; Neil et al., 2010; Chen and Ghosh 2011; Nicot et al., 2012)), whilst others are based on Continuum Damage Theory (phenomenological damage models, e.g. (Rosenberg et al., 1983; Butcher, 1968; Brünig, 2001; Brünig, 2003; Gerke and Brünig, 2010; Brünig et al., 2011a; Brünig and Gerke, 2011; Brünig et al., 2011b; Egner and Skoczeń, 2010; Garion and Skoczen, 2003; Bielski et al., 2006; Skoczeń et al., 2010; Li and Wierzbicki, 2010; Li and Karr, 2009)). The proposed model belongs to the latter category and, to some extent, is similar to the model proposed in (Brünig, 2001; Brünig, 2003; Brünig et al., 2011a; Brünig et al., 2011b) for initially isotropic configuration.

The new constitutive model has rate form, i.e. defines relationship between the rate of stress and the rate of strain and a set of internal variables locally for every point in a body. It satisfies the principle of material frame invariance with respect to arbitrary rigid-body translations and rotations.

The model has two parts, an equation of state (EOS) which defines the response of the material to uniform compression (change of volume) and a deviatoric (strength) part of the model, which defines the response of the material to shear deformation (change of shape). For orthotropic materials this separation of material response is complicated by the fact that an isotropic state of strain induces anisotropic state of stress in the material (Vignjevic et al., 2008).

The coupling between plasticity and damage is based on the assumption that there exists two separate damage and plasticity loading surfaces (potentials), with two independent associative flow rules. This type of starting assumption has been used by number of authors, for instance (Rubin, 1990; Stevens and Tuler, 1971; Schmidt et al., 1978; Liu, 2004; Bielski et al., 2006; Hiermaier, 2008; Brünig et al., 2011a).

The proposed model was developed using a structured approach, which combines the framework of irreversible thermodynamics with internal variables, and configurational finite deformation kinematics of elastoplasticity with damage. The constitutive equations are integrated in the isoclinic intermediate configuration, following (Mandel, 1972; Mandel, 1974; Itskov and Aksel, 2004; Vujosevic and Lubarda, 2002; Hansen and Schreyer, 1994; Menzel and Steinmann, 2007).

The hyperelastic part to the material model was based on the assumption that initial elastic anisotropy remains unaltered, does not evolve, during plastic deformation. In other words, initial principal material orthotropy directions remain unchanged, while elastic material parameters evolve due to damage.

Plastic behaviour is modelled using associative plasticity and Hill's orthotropic quadratic yield function (Hill, 1950) with the aid of the structural tensors. Hill's yield criterion was chosen due to its simplicity and accuracy in describing behaviour of the ductile metals of interest. The yield function was defined in terms of the Mandel stress tensor. Plastic orthotropy is assumed unaltered during plastic deformation. Material isotropic hardening is controlled by the reference stress strain curve defined by the Mechanical Threshold Stress (MTS) model (Follansbee and Kocks, 1988; Chen et al., 1998). It is important to note that the MTS model, in addition to flow stress, provides accurate approximation of temperature, strain and strain rate dependant plastic hardening rate. *In the proposed model this hardening rate is used as the parameter that controls the initiation of damage.*

Damage part of the constitutive model is described by an orthotropic damage potential, which evolves following a referential damage hardening law. This isotropic hardening law was developed on the basis of Klepaczko's thermally activated damage concept (Klepaczko, 1990). This makes the damage model consistent with the MTS model, which is used for the evolution of the plastic potential.

The model was implemented into the public domain version of the Lagrangian hydrocode DYNA3D (Liu, 2004) originating from Lawrence Livermore National Laboratory (LLNL). Validation of the model was done through comparison with experimental data from Taylor anvil and plate impact tests, showing the effects of orientation of a hot rolled 7010-T6 alloy (Vignjevic et al., 2002).

The adopted framework for model development incorporates: 1) the multiplicative decomposition of the deformation gradient used to define necessary kinematic parameters and the isoclinic configuration; 2) the irreversible thermodynamics of deformation processes; 3) associative plasticity combined with the MTS flow stress evolution equations; 4) associative damage with a new energy based damage evolution law; and 5) the assumption that principle directions of elastic, plastic and damage material anisotropy are not influenced by plastic deformation and damage i.e. the mutual relations between the structural tensors do not change during the deformation process. The model is applicable for arbitrary plastic and damage deformation and small elastic deformation.

This paper is structured as follows: sections 2 and 3 give brief background on relevant kinematics and thermodynamics of the deformation processes; section 4 describes the elastic-damage and elastic-plastic behaviour, i.e. thermodynamic potentials for damage and plasticity. The summary of constitutive equations, numerical implementation and coupling are given in section 5, followed by an outline description of the material characterisation in the section 6. A two stage validation process of the new model is presented in section 7. The paper concludes with a summary in Section 8 and Appendices A and B, which respectively provide a description of the hyperelastic orthotropic constitutive model and the derivation of consistency condition for damage process.

2 Relevant Kinematics of Large Deformations

Constitutive theories in Continuum mechanics usually employ intermediate configurations, which are obtained through the multiplicative decomposition of the deformation gradient. Following (Stojanovic et al., 1964; Jaric, 1988 Brünig, 2003) among others, the deformation gradient **F** may be multiplicatively decomposed as:

$$\mathbf{F} = \mathbf{F}_e \mathbf{F}_d \mathbf{F}_p \tag{2.1}$$

where: $\mathbf{F}_e$ represents thermo-elastic part of the deformation, $\mathbf{F}_d$ represents deformation due to damage (initiation and evolution of voids and/or micro-cracks) and $\mathbf{F}_p$ represents the part of the deformation due to plastic deformation (dislocation mechanics). The intermediate (generally non-Euclidean) configuration, which corresponds to elastically unloaded material, i.e. $\mathbf{F}_e = \mathbf{I}$, is called the elastic reference configuration. This configuration is, by definition, stress free and at an elastic reference temperature. It can be physically obtained by elastic unloading of material which has not been damaged, regardless the state of plastic deformation, since plasticity does not influence elastic material response. After damage is initiated, the elastic unloading path of damaged material differs from the elastic unloading path of undamaged material. The elastically unloaded state of the undamaged material cannot be physically obtained. Consequently, the elastic unloading path of damaged material is used in this work for the definition of an isoclinic (intermediate) configuration in which the constitutive model was formulated. All the other intermediate configurations introduced by the multiplicative decomposition (2.1) are used to describe irreversible processes of plastic deformation and damage.

The work described in this paper is based on the assumption that the principal directions of material elastic and plastic orthotropy coincide and are not influenced by inelastic deformation. This assumption is supported by experimental evidence that there is a strong correlation between elastic and plastic material symmetries, see for instance (Man, 1995). The description of the material orthotropy utilises structural tensors (Boehler, 1987) where a structural tensor $\mathbf{M} = \mathbf{e} \otimes \mathbf{e}$ is a tensor product of unit vectors $\mathbf{e}$ which are parallel with the intersections of the material symmetry planes. In the case of orthotropic materials three unit vectors $\mathbf{e}_i$ form an orthogonal triad, i.e. $\mathbf{e}_i \cdot \mathbf{e}_j = \boldsymbol{\delta}_{ij}$, $i, j = 1,2,3$. The three related structural tensors used in the definition of the thermodynamic potentials, e.g. free energy function, are given as $\mathbf{M}^i = \mathbf{e}_i \otimes \mathbf{e}_i$, $i = 1,2,3$ (see for instance (Mandel, 1972; Mandel, 1974; Itskov and Aksel, 2004; Boehler, 1987)).

Push forward transformations of the structural tensors from an initial to elastically unloaded configuration are $\mathbf{M}_e^i = \mathbf{F}_{dp} \mathbf{M}^i \mathbf{F}_{dp}^{-1}$. It is simple to demonstrate that this transformation preserves the invariants of the structural tensors and, in general, does not preserve the invariance of the unit vectors

(Sansour and Bocko, 2003). This property allows for definition of an isotropic internal energy function in an intermediate configuration in terms of invariants and pseudo invariants of the right Green Lagrange strain tensor and structural tensors. Similarly, the thermodynamic potentials used in the subsequent sections are expressed in terms of invariants and pseudo invariants.

The structural tensors $\mathbf{M}_e^i$ are pulled back from the elastically unloaded to the isoclinic configuration by un-rotating for a rigid rotation due to plastic and damage related deformations as given by the following orthonormal transformation.

$$\bar{\mathbf{M}}^i = \mathbf{Q}_{dp}^T \mathbf{M}_e^i \mathbf{Q}_{dp} \tag{2.2}$$

where $\mathbf{Q}_{dp}$ is an orthonormal tensor which defines the rotation induced by irreversible deformation.

The choice of the isoclinic configuration for formulation of the constitutive model was driven by 1) the physical nature of the elastic unloading of damaged plastically deformed material and 2) definition of damage deformation gradient and convenience of the invariant representation of the constitutive functions. Since the material compliance changes due to damage, the intermediate configuration C_{dp} shown in Figure 1 cannot be physically obtained. Consequently, the isoclinic configuration is defined from the (effective) intermediate configuration C^1 by rotating back for the (remaining) plastically induced rigid body rotation. The effective configuration is obtained from the elastically unloaded intermediate configuration by the inverse mapping with damage deformation gradient as shown in Figure 1. In this configuration the effective stress and strain are mutually related by the stiffness and compliance tensors of undamaged material. Therefore, the elastic strain energy is defined in terms of invariants and pseudo invariants of the effective elastic strain.

Near Figure 1

The multiplicative decomposition of the deformation gradient in equation (2.1) can be expressed in the isoclinic configuration as:

$$\mathbf{F} = \mathbf{F}_e \mathbf{F}_d \mathbf{F}_p = \mathbf{F}_e \mathbf{F}_d \mathbf{R}_p \mathbf{R}_p^T \mathbf{F}_p = \mathbf{F}_e \bar{\mathbf{F}}_d \bar{\mathbf{F}}_p = \bar{\mathbf{F}}_{ed} \bar{\mathbf{F}}_p \tag{2.3}$$

where $\bar{\mathbf{F}}_d = \mathbf{F}_d \mathbf{R}_p$, $\bar{\mathbf{F}}_p = \mathbf{R}_p^T \mathbf{F}_p = \mathbf{R}_p^T \mathbf{R}_p \mathbf{U}_p = \mathbf{U}_p$, $\bar{\mathbf{F}}_{ed} = \mathbf{F}_e \bar{\mathbf{F}}_d$ and $\mathbf{R}_p$ is an orthogonal tensor obtained by the polar decomposition of plastic deformation gradient (rotation induced by plastic deformation). The rotation induced by plastic deformation is assigned to $\mathbf{F}_d$ and $\mathbf{F}_p$ so that there is no rotation of the material principal axes of orthotropy in the isoclinic intermediate configuration.

Based on the above decomposition, the other related measures of deformation, strain and strain rate can be defined. For instance, total Green-Lagrange strain $\mathbf{E}$ can be additively decomposed as:

$$\mathbf{E}=\frac{1}{2}\left(\mathbf{F}^{T}\mathbf{F}-\mathbf{I}\right)=\frac{1}{2}\left(\bar{\mathbf{C}}_{p}-\mathbf{I}\right)+\bar{\mathbf{F}}_{p}^{T}\left(\frac{1}{2}\left(\bar{\mathbf{C}}_{d}-\mathbf{I}\right)\right)\bar{\mathbf{F}}_{p}+\bar{\mathbf{F}}_{p}^{T}\bar{\mathbf{F}}_{d}^{T}\left(\frac{1}{2}\left(\mathbf{C}_{e}-\mathbf{I}\right)\right)\bar{\mathbf{F}}_{d}\bar{\mathbf{F}}_{p}= \\ =\mathbf{E}_{p}+\bar{\mathbf{F}}_{p}^{T}\bar{\mathbf{E}}_{d}\bar{\mathbf{F}}_{p}+\bar{\mathbf{F}}_{p}^{T}\bar{\mathbf{F}}_{d}^{T}\tilde{\mathbf{E}}_{e}\bar{\mathbf{F}}_{d}\bar{\mathbf{F}}_{p}=\mathbf{E}_{p}+\mathbf{E}_{d}+\mathbf{E}_{e} \tag{2.4}$$

The above decomposition of Green-Lagrange strain, when expressed in the isoclinic configuration, takes the following form:

$$\bar{\mathbf{E}}\ =\bar{\mathbf{F}}_{p}^{-T}\left(\frac{1}{2}\left(\bar{\mathbf{C}}_{p}-\mathbf{I}\right)\right)\bar{\mathbf{F}}_{p}^{-1}+\left(\frac{1}{2}\left(\bar{\mathbf{C}}_{d}-\mathbf{I}\right)\right)+\bar{\mathbf{F}}_{d}^{T}\left(\frac{1}{2}\left(\mathbf{C}_{e}-\mathbf{I}\right)\right)\bar{\mathbf{F}}_{d}= \\ =\bar{\mathbf{F}}_{p}^{-T}\mathbf{E}_{p}\bar{\mathbf{F}}_{p}^{-1}+\bar{\mathbf{E}}_{d}+\bar{\mathbf{F}}_{d}^{T}\tilde{\mathbf{E}}_{e}\bar{\mathbf{F}}_{d}=\bar{\mathbf{E}}_{p}+\bar{\mathbf{E}}_{d}+\bar{\mathbf{E}}_{e} \tag{2.5}$$

where right Cauchy-Green tensors: $\bar{\mathbf{C}}_{p}$ is a measure of deformation between the isoclinic and initial configuration, $\bar{\mathbf{C}}_{d}$ is a measure of deformation between the elastically unloaded and the isoclinic configuration, $\mathbf{C}_{e}$ is a measure of deformation between current and the elastically unloaded configuration and $\mathbf{C}$ is a measure of deformation between current and initial configuration.

Similarly, the multiplicative decomposition given in equation (2.3) allows for the velocity gradient ($\mathbf{l}=\dot{\mathbf{F}}\mathbf{F}^{-1}$) to be decomposed additively as follows:

$$\mathbf{l}=\dot{\mathbf{F}}\mathbf{F}^{-1}=\frac{\partial}{\partial t}\left(\mathbf{F}_{e}\bar{\mathbf{F}}_{d}\bar{\mathbf{F}}_{p}\right)\left(\mathbf{F}_{e}\bar{\mathbf{F}}_{d}\bar{\mathbf{F}}_{p}\right)^{-1}=\dot{\mathbf{F}}_{e}\mathbf{F}_{e}^{-1}+\mathbf{F}_{e}\dot{\bar{\mathbf{F}}}_{d}\bar{\mathbf{F}}_{d}^{-1}\mathbf{F}_{e}^{-1}+\mathbf{F}_{e}\bar{\mathbf{F}}_{d}\dot{\bar{\mathbf{F}}}_{p}\bar{\mathbf{F}}_{p}^{-1}\bar{\mathbf{F}}_{d}^{-1}\mathbf{F}_{e}^{-1} \tag{2.6}$$

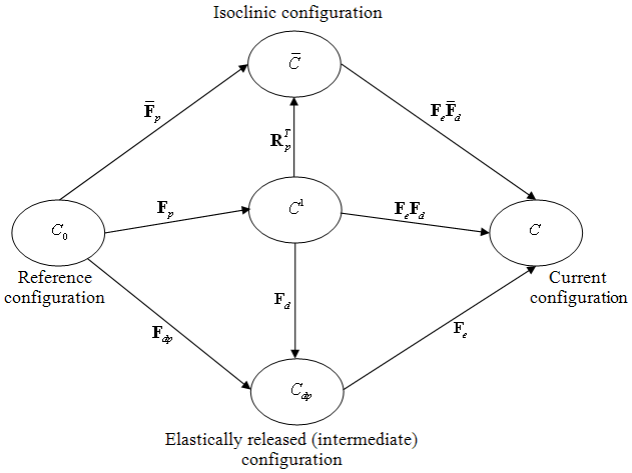

Figure 1 Definition of isoclinic configuration

This decomposition when expressed in the isoclinic configuration takes the following form:

$$\bar{\mathbf{l}} = \bar{\mathbf{F}}_d^{-1}\mathbf{F}_e^{-1}\mathbf{l}\mathbf{F}_e\,\bar{\mathbf{F}}_d = \bar{\mathbf{F}}_d^{-1}\mathbf{F}_e^{-1}\dot{\mathbf{F}}_e\bar{\mathbf{F}}_d + \bar{\mathbf{F}}_d^{-1}\dot{\bar{\mathbf{F}}}_d + \dot{\bar{\mathbf{F}}}_p\bar{\mathbf{F}}_p^{-1} = \bar{\mathbf{l}}_e + \bar{\mathbf{l}}_d + \bar{\mathbf{l}}_p \tag{2.7}$$

Note that pull back transformation of the velocity gradient is defined by the first equation in (2.7)**.** The plastic part of the deformation is assumed incompressible; i.e. $\det\bar{\mathbf{F}}_p = 1$, which implies that $tr\bar{\mathbf{l}}_p = 0$ and consequently the density in the isoclinic configuration is equal to the density in the initial configuration ρ_0.

The velocity gradient $\bar{\mathbf{l}}$ and its components $\bar{\mathbf{l}}_e$, $\bar{\mathbf{l}}_d$ and $\bar{\mathbf{l}}_p$ resulting from the additive decomposition in equation (2.7) can be divided into the symmetric rate of deformation tensor $\bar{\mathbf{d}}$ and the anti-symmetric spin tensor $\bar{\mathbf{w}}$.

$$\bar{\mathbf{l}} = \frac{1}{2}\left(\bar{\mathbf{l}} + \bar{\mathbf{l}}^T\right) + \frac{1}{2}\left(\bar{\mathbf{l}} - \bar{\mathbf{l}}^T\right) = \bar{\mathbf{d}} + \bar{\mathbf{w}} \tag{2.8}$$

The components of velocity gradient given in (2.6) and (2.7) define the elastic strain rate in the isoclinic configuration as:

$$\dot{\bar{\mathbf{E}}}_e = \frac{1}{2}\bar{\mathbf{C}}_e\left(\bar{\mathbf{l}} - \bar{\mathbf{l}}_p\right) + \frac{1}{2}\left(\bar{\mathbf{l}}^T - \bar{\mathbf{l}}_p^T\right)\bar{\mathbf{C}}_e - \frac{1}{2}\bar{\mathbf{C}}_d\bar{\mathbf{l}}_d - \frac{1}{2}\bar{\mathbf{l}}_d^T\bar{\mathbf{C}}_d = \left[\bar{\mathbf{C}}_e\left(\bar{\mathbf{l}} - \bar{\mathbf{l}}_p\right)\right]_{sym} - \left[\bar{\mathbf{C}}_d\bar{\mathbf{l}}_d\right]_{sym} \tag{2.9}$$

The thermodynamics analysis, presented in Section 3, is based on the second law in the form of Clausius – Duhem (CD) inequality expressed in the isoclinic configuration. In order to define the CD inequality it is necessary to introduce relevant conjugate variable pairs, starting with the stress power:

$$\mathcal{P}_s = \boldsymbol{\tau} : \mathbf{l} = \det\mathbf{F}\boldsymbol{\sigma} : \mathbf{l} = \mathbf{S} : \dot{\mathbf{E}} = \bar{\mathbf{F}}_{ed}^T\boldsymbol{\tau}\bar{\mathbf{F}}_{ed}^{-T} : \bar{\mathbf{l}} = \bar{\boldsymbol{\Sigma}} : \bar{\mathbf{l}} \tag{2.10}$$

where $\boldsymbol{\tau}$ is Kirchhoff stress, $\boldsymbol{\sigma} = \left(\det\mathbf{F}\right)^{-1}\boldsymbol{\tau}$ is Cauchy stress, $\mathbf{S} = \mathbf{F}^{-1}\boldsymbol{\tau}\mathbf{F}^{-T}$ is second Piola Kirchhoff stress and $\bar{\boldsymbol{\Sigma}} = \bar{\mathbf{F}}_{ed}^T\boldsymbol{\tau}\bar{\mathbf{F}}_{ed}^{-T}$ is Mandel stress in the isoclinic configuration (Mandel, 1972; Mandel, 1974).

Using symmetry of Mandel stress (Vladimirov et al., 2008; Reese and Vladimirov, 2008), the stress power $\mathcal{P}_s$ may now be decomposed into elastic, damage and plastic parts as:

$$\mathcal{P}_s = \bar{\boldsymbol{\Sigma}} : \bar{\mathbf{d}} = \bar{\boldsymbol{\Sigma}} : (\bar{\mathbf{d}}_e + \bar{\mathbf{d}}_p + \bar{\mathbf{d}}_d) = \mathcal{P}_e + \mathcal{P}_p + \mathcal{P}_d \tag{2.11}$$

where: $\mathcal{P}_e = \bar{\boldsymbol{\Sigma}} : \bar{\mathbf{d}}_e$ is elastic stress power, $\mathcal{P}_p = \bar{\boldsymbol{\Sigma}} : \bar{\mathbf{d}}_p$ is plastic stress power and $\mathcal{P}_d = \bar{\boldsymbol{\Sigma}} : \bar{\mathbf{d}}_d$ is damage stress power. The power terms consist of the conjugate pairs which are further discussed in the next section.

3 Thermodynamics of deformation process

The constitutive model is developed in the framework of irreversible thermodynamics with internal variables, where the internal energy (consequently Helmholtz free energy) is assumed to be a

constitutive function of elastic strain, and temperature (the observable variables) and an array v of internal variables (scalars and tensors) that characterize the microscopic dissipative effects associated with the material defect structure. The model is intended for adiabatic deformation processes and consequently the internal/free energy is composed of reversible elastically stored energy and irreversible energy associated with the change in microstructure caused by plastic deformation and damage. The stress and other state variables are assumed to be derivable from constitutive laws expressed in the isoclinic configuration.

Rate of change of internal energy per unit volume, $\bar{\rho}\dot{u}$, is according to the first law of thermodynamics:

$$\bar{\rho}\dot{u} = \bar{\mathbf{\Sigma}} : \bar{\mathbf{l}} + \bar{\rho} r - \nabla_{\bar{X}} \cdot \bar{\mathbf{q}} \tag{3.1}$$

where $\bar{\rho}$, r and $\bar{\mathbf{q}}$ respectively denote density, heat source/supply and heat flux vector in the isoclinic configuration. The second law of thermodynamics in the form of CD inequality, when expressed in the isoclinic configuration has the following form:

$$\bar{\rho}\dot{s} - \bar{\rho}\frac{r}{\theta} + \nabla_{\bar{X}} \cdot \left(\frac{\bar{\mathbf{q}}}{\theta}\right) \geq 0 : \tag{3.2}$$

where $\bar{\rho}\dot{s}$ denotes rate of change of entropy per unit volume. By making use of the first law of thermodynamics (3.1), the second law for adiabatic processes can be expressed in terms of a rate of change of internal dissipation (dissipation power) Δ_{ad} as:

$$\Delta_{ad} = \bar{\rho}\theta\dot{s} - \bar{\rho}\dot{u} + \bar{\mathbf{\Sigma}} : \bar{\mathbf{l}} \geq 0 \tag{3.3}$$

where the subscript *ad* stands for adiabatic process and hence, the term related to the heat flux is excluded. The rate of internal dissipation (3.3) can be defined in terms of Helmholtz free energy, using Legendre transformation $\psi = u - \theta s$, as:

$$\Delta_{ad} = \bar{\mathbf{\Sigma}} : \bar{\mathbf{l}} - \bar{\rho}\dot{\psi} - \bar{\rho} s \dot{\theta} \geq 0 \tag{3.4}$$

where free energy ψ, entropy s and the Mandel stress $\bar{\mathbf{\Sigma}}$, are assumed to be the constitutive functions of the same set of variables: $\bar{\mathbf{E}}_e$, θ and v. The proposed model uses one internal variable to describe evolution of each irreversible process. The evolution of plastic deformation is governed by an isotropic hardening law defined in terms of effective plastic strain ε_{pl}. Similarly, damage evolution is governed by an isotropic damage hardening law defined in terms of a damage hardening parameter ω^H. In addition to these variables, the arguments in the constitutive functions are the structural tensors defined by the Equation (2.2).

To develop a thermodynamically consistent material model, the specific heat c, which in general is a function of the set of variables, has to be determined:

$$c\left(\bar{\mathbf{E}}_e, \bar{\mathbf{M}}^1, \bar{\mathbf{M}}^2, \theta, \varepsilon_{pl}, \omega^H\right) = -\bar{\rho}\theta\frac{\partial^2 \psi}{\partial \theta^2} \tag{3.5}$$

The assumption was made that the free energy is additively decomposed into a thermo-elastic free energy $\bar{\psi}$, energy related to the plastic hardening and energy related to the damage hardening, respectively denoted as u_{pl} and u_d (see for instance (Germain and Lee, 1973; Lubliner, 1972)):

$$\psi\left(\bar{\mathbf{E}}_e,\bar{\mathbf{M}}^1,\bar{\mathbf{M}}^2,\theta,\varepsilon_{pl},\omega^H\right)=\bar{\psi}\left(\bar{\mathbf{E}}_e,\bar{\mathbf{M}}^1,\bar{\mathbf{M}}^2,\theta\right)+u_{pl}\left(\varepsilon_{pl},\theta\right)+u_d\left(\omega^H,\theta\right) \tag{3.6}$$

The additive decomposition (3.6) holds if the specific heat and stress are not functions of the hardening variables and if the hardenings in the two irreversible processes (plasticity and damage) are decoupled (Rosakis et al., 2000). Note that the hardening terms u_{pl} and u_d are functions of absolute temperature and that the free energy is a function of effective stain $\bar{\mathbf{E}}_e=\bar{\mathbf{F}}_d^T\tilde{\mathbf{E}}_e\bar{\mathbf{F}}_d$ and undamaged stiffness matrix because the material in the isoclinic configuration is in an undamaged state. For instance, the elastically stored energy in the current configuration, where the material is in damaged state is a function of damaged elastic stiffness tensor.

$$\bar{\psi}=\frac{1}{2}\bar{\mathbf{E}}_e:\bar{\mathbb{C}}:\bar{\mathbf{E}}_e \qquad\qquad \bar{\psi}^{(damaged)}=\frac{1}{2}\tilde{\mathbf{E}}_e:\tilde{\mathbb{C}}:\tilde{\mathbf{E}}_e \tag{3.7}$$

where $\bar{\mathbb{C}}$ is a stiffness matrix of undamaged material defined in the isoclinic configuration and $\tilde{\mathbb{C}}$ is a stiffness matrix of damaged material defined in the current configuration. The rate of change of free energy function is defined as:

$$\dot{\psi}\left(\bar{\mathbf{E}}_e,\bar{\mathbf{M}}^1,\bar{\mathbf{M}}^2,\theta,\varepsilon_{pl},\omega^H\right)=\frac{\partial\bar{\psi}}{\partial\bar{\mathbf{E}}_e}:\dot{\bar{\mathbf{E}}}_e+\frac{\partial\bar{\psi}}{\partial\bar{\mathbf{M}}^1}:\dot{\bar{\mathbf{M}}}^1+\frac{\partial\bar{\psi}}{\partial\bar{\mathbf{M}}^2}:\dot{\bar{\mathbf{M}}}^2+\frac{\partial\psi}{\partial\theta}\dot{\theta}+\frac{\partial u_{pl}}{\partial\varepsilon_{pl}}\dot{\varepsilon}_{pl}+\frac{\partial u_d}{\partial\omega^H}\dot{\omega}^H \tag{3.8}$$

This equation is simplified by excluding the evolution of structural tensors ($\dot{\bar{\mathbf{M}}}^i=\mathbf{0}$, $i=1,2,3$) from the current model development. By making use of the simplified form of the last equation and with the aid of the kinematic definitions from (2.6) to (2.9) one can express the rate of internal dissipation (3.4) as:

$$\begin{aligned}\Delta_{ad}&=\bar{\boldsymbol{\Sigma}}:\bar{\mathbf{l}}-\bar{\rho}\dot{\psi}-\bar{\rho}\dot{\theta}s=\bar{\boldsymbol{\Sigma}}:\bar{\mathbf{l}}-\bar{\rho}\frac{\partial\bar{\psi}}{\partial\bar{\mathbf{E}}_e}:\dot{\bar{\mathbf{E}}}_e-\bar{\rho}\frac{\partial\psi}{\partial\theta}\dot{\theta}-\bar{\rho}\frac{\partial u_{pl}}{\partial\varepsilon_{pl}}\dot{\varepsilon}_{pl}-\bar{\rho}\frac{\partial u_d}{\partial\omega^H}\dot{\omega}^H-\bar{\rho}\dot{\theta}s=\\&=\left(\bar{\boldsymbol{\Sigma}}-\bar{\rho}\bar{\mathbf{C}}_e\frac{\partial\bar{\psi}}{\partial\bar{\mathbf{E}}_e}\right):\bar{\mathbf{l}}+\bar{\rho}\bar{\mathbf{C}}_e\frac{\partial\bar{\psi}}{\partial\bar{\mathbf{E}}_e}:\bar{\mathbf{l}}_p+\bar{\rho}\frac{\partial\bar{\psi}}{\partial\bar{\mathbf{E}}_e}:\bar{\mathbf{C}}_d\bar{\mathbf{l}}_d-\bar{\rho}\frac{\partial u_{pl}}{\partial\varepsilon_{pl}}\dot{\varepsilon}_{pl}-\bar{\rho}\frac{\partial u_d}{\partial\omega^H}\dot{\omega}^H-\bar{\rho}\left(\frac{\partial\psi}{\partial\theta}+s\right)\dot{\theta}\end{aligned} \tag{3.9}$$

where:

$$s\left(\bar{\mathbf{E}}_e,\bar{\mathbf{M}}^1,\bar{\mathbf{M}}^2,\theta,\varepsilon_{pl},\omega^H\right)=-\frac{\partial\psi}{\partial\theta} \qquad\qquad \bar{\boldsymbol{\Sigma}}\left(\bar{\mathbf{E}}_e,\bar{\mathbf{M}}^1,\bar{\mathbf{M}}^2,\theta\right)=\bar{\rho}\bar{\mathbf{C}}_e\frac{\partial\bar{\psi}}{\partial\bar{\mathbf{E}}_e} \tag{3.10}$$

are entropy and Mandel stress in the isoclinic configuration and $\bar{\mathbf{C}}_e=\bar{\mathbf{F}}_d^T\mathbf{F}_e^T\mathbf{F}_e\bar{\mathbf{F}}_d=\bar{\mathbf{F}}_d^T\mathbf{C}_e\bar{\mathbf{F}}_d$. Consequently, the expression for the rate of internal dissipation (3.9) simplifies to:

$$\begin{aligned}\Delta_{ad}&=\bar{\rho}\frac{\partial\bar{\psi}}{\partial\bar{\mathbf{E}}_e}:\bar{\mathbf{C}}_e\bar{\mathbf{l}}_p+\bar{\rho}\frac{\partial\bar{\psi}}{\partial\bar{\mathbf{E}}_e}:\bar{\mathbf{C}}_d\bar{\mathbf{l}}_d-\bar{\rho}\frac{\partial u_{pl}}{\partial\varepsilon_{pl}}\dot{\varepsilon}_{pl}-\bar{\rho}\frac{\partial u_d}{\partial\omega^H}\dot{\omega}^H=\\&=\left(\bar{\boldsymbol{\Sigma}}:\bar{\mathbf{l}}_p-\Upsilon\dot{\varepsilon}_{pl}\right)+\left(\bar{\mathbf{S}}:\bar{\mathbf{C}}_d\bar{\mathbf{l}}_d-\Omega\dot{\omega}^H\right)=\Delta_p+\Delta_d\end{aligned} \tag{3.11}$$

Where: $\bar{\rho}\dfrac{\partial u_{pl}}{\partial \varepsilon_{pl}} = \Upsilon$ is a thermodynamic force conjugate to the internal variable for isotropic plastic hardening ε_{pl} and $\bar{\rho}\dfrac{\partial u_d}{\partial \omega^H} = \Omega$ is a thermodynamic force conjugate to the variable which describes damage hardening ω^H. For clarity, the derivatives of the free energy are used in the subsequent relations, rather than the newly introduced thermodynamic forces, which are discussed in detail in the following section.

Damage induced dissipation rate in (3.11) is determined by the damage part of velocity gradient, which is related to the second order damage tensor $\bar{\boldsymbol{\omega}}$, as detailed in the subsection 4.1. As a result, the damage part of dissipation rate can be expressed as a product of the rate of change of damage tensor and its thermodynamically conjugate force $\bar{\mathbf{Y}}$. The thermodynamic potential for damage is defined in terms of this conjugate force. For the unidirectional loading, the conjugate force is called damage energy release rate, and can be obtained from the complementary energy or Gibbs free energy as one half of the variation of elastic strain energy due to damage variation at constant stress (Lemaitre and Chaboche, 1990). Although it refers to the second order stress tensor, this name is used in the remainder of this paper.

Note, rate of dissipation given in the equation above is independent of gradient of temperature. The inequality must be satisfied for each irreversible process (plasticity and damage) taking place individually as well as in the case when the processes are simultaneous.

The constitutive equations for free energy, entropy, stress and internal energy may now be assumed in the following general forms, similarly to (Rosakis et al., 2000):

$$\begin{aligned}
&\psi\left(\bar{\mathbf{E}}_e, \bar{\mathbf{M}}^1, \bar{\mathbf{M}}^2, \theta, \varepsilon_{pl}, \omega^H\right) = \bar{\psi}\left(\bar{\mathbf{E}}_e, \bar{\mathbf{M}}^1, \bar{\mathbf{M}}^2, \theta\right) - \theta\left[s_{pl}\left(\varepsilon_{pl}\right) + s_d\left(\omega^H\right)\right] + \bar{u}_{pl}\left(\varepsilon_{pl}, \theta\right) + \bar{u}_d\left(\omega^H, \theta\right) \\
&s\left(\bar{\mathbf{E}}_e, \bar{\mathbf{M}}^1, \bar{\mathbf{M}}^2, \theta, \varepsilon_{pl}, \omega^H\right) = -\frac{\partial \bar{\psi}}{\partial \theta}\left(\bar{\mathbf{E}}_e, \bar{\mathbf{M}}^1, \bar{\mathbf{M}}^2, \theta\right) + s_{pl}\left(\varepsilon_{pl}\right) + s_d\left(\omega^H\right) \\
&\bar{\mathbf{S}}\left(\bar{\mathbf{E}}_e, \bar{\mathbf{M}}^1, \bar{\mathbf{M}}^2, \theta\right) = \bar{\rho}\frac{\partial \bar{\psi}}{\partial \bar{\mathbf{E}}_e}\left(\bar{\mathbf{E}}_e, \bar{\mathbf{M}}^1, \bar{\mathbf{M}}^2, \theta\right) \\
&u\left(\bar{\mathbf{E}}_e, \bar{\mathbf{M}}^1, \bar{\mathbf{M}}^2, \theta, \varepsilon_{pl}, \omega^H\right) = \bar{u}\left(\bar{\mathbf{E}}_e, \bar{\mathbf{M}}^1, \bar{\mathbf{M}}^2, \theta\right) + \bar{u}_{pl}\left(\varepsilon_{pl}, \theta\right) + \bar{u}_d\left(\omega^H, \theta\right)
\end{aligned} \tag{3.12}$$

where: $\bar{u}\left(\bar{\mathbf{E}}_e, \bar{\mathbf{M}}^1, \bar{\mathbf{M}}^2, \theta\right) = \bar{\psi}\left(\bar{\mathbf{E}}_e, \bar{\mathbf{M}}^1, \bar{\mathbf{M}}^2, \theta\right) - \theta\dfrac{\partial \bar{\psi}}{\partial \theta}\left(\bar{\mathbf{E}}_e, \bar{\mathbf{M}}^1, \bar{\mathbf{M}}^2, \theta\right)$, $s_{pl}\left(\varepsilon_{pl}\right)$ and $s_d\left(\omega^H\right)$ are irreversible parts of entropy related to plastic and damage deformation. The absolute temperature in the hardening terms $\bar{u}_{pl}$ and $\bar{u}_d$ appears only as a parameter and not as a state variable.

For the range of temperatures of interest, current development of the constitutive model assumes: that specific heat is constant and that free energy is a quadratic function of the effective elastic strain (linear constitutive relationship between the stress and elastic strain). Consequently the system of constitutive equations (3.12), when expressed in terms of irreducible strain invariants, simplifies to the following form:

$$\psi\left(\bar{\mathbf{E}}_e,\bar{\mathbf{M}}^1,\bar{\mathbf{M}}^2,\theta,\varepsilon_{pl},\omega^H\right)=\frac{1}{2}\bar{\alpha}_1\bar{J}_1^2+\bar{\alpha}_2\bar{J}_2+\frac{1}{2}\bar{\alpha}_3\bar{J}_4^2+\bar{\alpha}_4\bar{J}_5+\frac{1}{2}\bar{\alpha}_5\bar{J}_6^2+\bar{\alpha}_6\bar{J}_7+\bar{\alpha}_7\bar{J}_1\bar{J}_4+\bar{\alpha}_8\bar{J}_1\bar{J}_6+\bar{\alpha}_9\bar{J}_4\bar{J}_6-$$
$$\bar{\boldsymbol{\beta}}\left(\bar{\mathbf{M}}^1,\bar{\mathbf{M}}^2,\bar{\mathbf{E}}_e\right):\bar{\mathbf{E}}_e\left(\theta-\theta_0\right)-c\theta\ln\left(\frac{\theta}{\theta_0}\right)+\bar{u}_{pl}\left(\varepsilon_{pl},\theta\right)+\bar{u}_d\left(\omega^H,\theta\right)-\theta\left[s_{pl}\left(\varepsilon_{pl}\right)+s_d\left(\omega^H\right)\right]$$

$$s\left(\bar{\mathbf{E}}_e,\bar{\mathbf{M}}^1,\bar{\mathbf{M}}^2,\theta,\varepsilon_{pl},\omega^H\right)=\bar{\boldsymbol{\beta}}\left(\bar{\mathbf{M}}^1,\bar{\mathbf{M}}^2,\bar{\mathbf{E}}_e\right):\bar{\mathbf{E}}_e+c\left(\ln\left(\frac{\theta}{\theta_0}\right)+1\right)+s_{pl}\left(\varepsilon_{pl}\right)+s_d\left(\omega^H\right) \tag{3.13}$$

$$\bar{\mathbf{S}}=\alpha_1\bar{J}_1\frac{\partial\bar{J}_1}{\partial\bar{\mathbf{E}}_e}+\alpha_2\frac{\partial\bar{J}_2}{\partial\bar{\mathbf{E}}_e}+\alpha_3\bar{J}_4\frac{\partial\bar{J}_4}{\partial\bar{\mathbf{E}}_e}+\alpha_4\frac{\partial\bar{J}_5}{\partial\bar{\mathbf{E}}_e}+\alpha_5\bar{J}_6\frac{\partial\bar{J}_6}{\partial\bar{\mathbf{E}}_e}+\alpha_6\frac{\partial\bar{J}_7}{\partial\bar{\mathbf{E}}_e}+\alpha_7\bar{J}_4\frac{\partial\bar{J}_1}{\partial\bar{\mathbf{E}}_e}+\alpha_7\bar{J}_1\frac{\partial\bar{J}_4}{\partial\bar{\mathbf{E}}_e}+$$
$$\alpha_8\bar{J}_6\frac{\partial\bar{J}_1}{\partial\bar{\mathbf{E}}_e}+\alpha_8\bar{J}_1\frac{\partial\bar{J}_6}{\partial\bar{\mathbf{E}}_e}+\alpha_9\bar{J}_6\frac{\partial\bar{J}_4}{\partial\bar{\mathbf{E}}_e}+\alpha_9\bar{J}_4\frac{\partial\bar{J}_6}{\partial\bar{\mathbf{E}}_e}-\bar{\boldsymbol{\beta}}\left(\bar{\mathbf{M}}^1,\bar{\mathbf{M}}^2,\bar{\mathbf{E}}_e\right)\left(\theta-\theta_0\right)$$

$$u\left(\bar{\mathbf{E}}_e,\bar{\mathbf{M}}^1,\bar{\mathbf{M}}^2,\theta,\varepsilon_{pl},\omega^H\right)=\frac{1}{2}\alpha_1J_1^2+\alpha_2J_2+\frac{1}{2}\alpha_3J_4^2+\alpha_4J_5+\frac{1}{2}\alpha_5J_6^2+\alpha_6J_7+\alpha_7J_1J_4+\alpha_8J_1J_6+\alpha_9J_4J_6-$$
$$\bar{\boldsymbol{\beta}}\left(\bar{\mathbf{M}}^1,\bar{\mathbf{M}}^2,\bar{\mathbf{E}}_e\right):\bar{\mathbf{E}}_e\theta_0+c\theta+\bar{u}_{pl}\left(\varepsilon_{pl},\theta\right)+\bar{u}_d\left(\omega^H,\theta\right)$$

where $\bar{J}_i$, α_i $(i=1,....,7)$ and $\bar{\boldsymbol{\beta}}\left(\bar{\mathbf{M}}^1,\bar{\mathbf{M}}^2,\bar{\mathbf{E}}_e\right)=\frac{\partial\bar{\mathbf{S}}}{\partial\theta}$ are respectively: the irreducible set of strain tensor invariants and pseudo invariants defined in (1.1), corresponding material constants and a tensor conjugate to the tensor of thermal expansion. This is a convenient point to introduce the Gruneisen tensor $\bar{\boldsymbol{\gamma}}=\bar{\boldsymbol{\beta}}/\rho_0c_0$, which is later used in the expression for the shock equation of state (EOS). Note that specific heat c and $\bar{\boldsymbol{\beta}}$ are parameters which define material properties per unit volume.

To integrate the system of equations (3.13) and calculate energy dissipation (3.11) and/or (3.21) for a general inelastic material response, the functional forms of free energy in terms of internal variables (the thermodynamic forces Υ and Ω) and evolution equations for the internal variables have to be defined within constraints of associative plasticity and damage. These additional equations are obtained from the principle of maximum dissipation (Hill, 1950), which states that among all admissible processes, the actual thermodynamic state in space of thermodynamic forces $\bar{\boldsymbol{\Sigma}}$ and $\bar{\mathbf{Y}}$ corresponds to the extremum of the dissipation function.

The two pseudo potentials, used to describe evolution of plastic deformation and damage, define the constraints that the dissipation (3.11) has to be maximised within. This is mathematically expressed as:

$$L=\bar{\boldsymbol{\Sigma}}:\bar{\mathbf{I}}_p-\Upsilon\dot{\varepsilon}_{pl}+\bar{\mathbf{Y}}:\dot{\bar{\boldsymbol{\omega}}}-\Omega\dot{\omega}^H-\dot{\lambda}_{pl}f_{pl}-\dot{\lambda}_df_d \tag{3.14}$$

where L is an objective function, $\dot{\lambda}_{pl}$ and f_{pl} are a Lagrange multiplier and a plastic potential function, $\dot{\lambda}_d$ and f_d are a Lagrange multiplier and a damage potential function. To determine extremum of L , the conditions (3.15) have to be satisfied.

$$\frac{\partial L}{\partial\bar{\boldsymbol{\Sigma}}}=0 \qquad\qquad \frac{\partial L}{\partial\bar{\mathbf{Y}}}=0 \tag{3.15}$$

This leads to the following evolution equations (normality conditions):

$$\bar{\mathbf{I}}_p = \dot{\lambda}_{pl} \frac{\partial f_{pl}}{\partial \bar{\boldsymbol{\Sigma}}} \qquad \dot{\bar{\boldsymbol{\omega}}} = \dot{\lambda}_d \frac{\partial f_d}{\partial \bar{\mathbf{Y}}} \tag{3.16}$$

Note, that principle of maximum dissipation also implies that the rates of plastic deformation and damage tensor (3.16) are collinear with their conjugate forces (Hill, 1950) and the evolution of the plastic deformation and damage are described by the monotonically increasing Lagrange multipliers.

Similarly, equations for evolution of hardening parameters are:

$$\dot{\varepsilon}_{pl} = -\dot{\lambda}_{pl} \frac{\partial f_{pl}}{\partial \Upsilon} \qquad \dot{\omega}^H = -\dot{\lambda}_d \frac{\partial f_d}{\partial \Omega} \tag{3.17}$$

The Hertz–Signorini–Moreau (Kuhn-Tucker) or loading/unloading conditions for the plastic deformation and damage are:

$$f_{pl} \le 0 \qquad \dot{\lambda}_{pl} \ge 0 \qquad \dot{\lambda}_{pl} f_{pl} = 0 \tag{3.18}$$

$$f_d \le 0 \qquad \dot{\lambda}_d \ge 0 \qquad \dot{\lambda}_d f_d = 0 \tag{3.19}$$

The Lagrange multipliers are determined from the consistency conditions. Note that the conjugate variables, which describe the plastic and damage hardening, define the relationships between the free energy (state potential) and dissipation potentials. The evolution of temperature is derived directly from the definition of internal dissipation as shown in the remainder of this section. The specific functional forms of the potentials are introduced in Section 4. The hyperelastic orthotropic constitutive model is, for completeness, given in Appendix A.

Material heating due to deformation

Using entropy-form of the energy balance equation, which can be obtained from equations (3.1), (3.10) and (3.11), and assuming that the process is adiabatic, one can calculate the rate of change of material temperature as follows:

$$\begin{aligned} &\bar{\rho}\theta\dot{s} = \Delta_{ad} \\ &-\bar{\rho}\theta\left(\frac{\partial^2 \bar{\psi}}{\partial\theta\partial\bar{\mathbf{E}}_e} : \dot{\bar{\mathbf{E}}}_e + \frac{\partial^2 \bar{\psi}}{\partial\theta^2}\dot{\theta} + \frac{\partial^2 u_{pl}}{\partial\theta\partial\varepsilon_{pl}}\dot{\varepsilon}_{pl} + \frac{\partial^2 u_d}{\partial\theta\partial\omega^H}\dot{\omega}^H \right) = \bar{\boldsymbol{\Sigma}} : \bar{\mathbf{I}}_p + \bar{\mathbf{Y}} : \dot{\bar{\boldsymbol{\omega}}} - \bar{\rho}\frac{\partial u_{pl}}{\partial\varepsilon_{pl}}\dot{\varepsilon}_{pl} - \bar{\rho}\frac{\partial u_d}{\partial\omega^H}\dot{\omega}^H \end{aligned} \tag{3.20}$$

which yields:

$$c\dot{\theta} = \theta\frac{\partial \bar{\mathbf{S}}}{\partial\theta} : \dot{\bar{\mathbf{E}}}_e + \bar{\boldsymbol{\Sigma}} : \bar{\mathbf{I}}_p - \bar{\rho}\left(\frac{\partial u_{pl}}{\partial\varepsilon_{pl}} - \theta\frac{\partial^2 u_{pl}}{\partial\theta\partial\varepsilon_{pl}} \right)\dot{\varepsilon}_{pl} + \bar{\mathbf{Y}} : \dot{\bar{\boldsymbol{\omega}}} - \bar{\rho}\left(\frac{\partial u_d}{\partial\omega^H} - \theta\frac{\partial^2 u_d}{\partial\theta\partial\omega^H} \right)\dot{\omega}^H \tag{3.21}$$

Where: $c = -\bar{\rho}\theta\frac{\partial^2\psi}{\partial\theta^2}$. The right hand side of the equation above consists of thermal contributions: Q_e due to thermo-elastic expansion, Q_p heat generated by plastic deformation and Q_d heat generated by damage.

$$Q_e = \bar{\rho}\theta \frac{\partial^2 \bar{\psi}}{\partial\theta\partial\bar{\mathbf{E}}_e} : \dot{\bar{\mathbf{E}}}_e = \theta \frac{\partial \bar{\mathbf{S}}}{\partial\theta} : \dot{\bar{\mathbf{E}}}_e = \theta\bar{\boldsymbol{\beta}}\left(\bar{\mathbf{M}}^1, \bar{\mathbf{M}}^2, \bar{\mathbf{E}}_e\right) : \dot{\bar{\mathbf{E}}}_e$$

$$Q_p = \bar{\boldsymbol{\Sigma}} : \bar{\mathbf{I}}_p - \bar{\rho}\left(\frac{\partial u_{pl}}{\partial \varepsilon_{pl}} - \theta \frac{\partial^2 u_{pl}}{\partial\theta\partial\varepsilon_{pl}}\right)\dot{\varepsilon}_{pl} \tag{3.22}$$

$$Q_d = \bar{\mathbf{Y}} : \dot{\bar{\boldsymbol{\omega}}} - \bar{\rho}\left(\frac{\partial u_d}{\partial \omega^H} - \theta \frac{\partial^2 u_d}{\partial\theta\partial\omega^H}\right)\dot{\omega}^H$$

$$c\dot{\theta} = Q_e + Q_p + Q_d \tag{3.23}$$

Equation (3.23) allows for accurate calculation of the temperature increase due to an inelastic deformation if all necessary functional dependencies of the free energy on internal variables are known. Due to the limited amount of data available a simplified approach, based on experimental data for a number of metals (Dillon, 1967; Farren and Taylor, 1925), was adopted in this work. The assumption was made that ninety percent of plastic power, i.e. $0.9\bar{\boldsymbol{\Sigma}} : \bar{\mathbf{I}}_p$ and all damage power $\bar{\mathbf{Y}} : \dot{\bar{\boldsymbol{\omega}}}$ is dissipated as heat.

4 Thermodynamic potentials and evolution equations for orthotropic material

Thermodynamic potentials which define the evolution of the two irreversible processes are considered in this section in the order they occur during the unloading of plastically deformed damaged material, as illustrated in Figure 2. The specific configurational continuum mechanics framework adopted in this work, illustrated in the Figure 1, together with the concept of effective stress and strain allow for damage to be represented through deterioration of the material elastic stiffness in the current configuration. In this case the material elastic unloading includes strain related to damage as shown in Figure 2.a, (elastic unloading brings the material in the state that corresponds to point A).

Furthermore, if the same unloading process is represented in the isoclinic configuration, where the material is in a fictitious undamaged state, than damage related strain can be represented as irreversible strain similar to plastic strain. This is consistent with the schematic representation in Figure 2.b., which illustrates the elastic unloading and reloading of the undamaged material. The thermodynamic state denoted by point B corresponds to elastically unloaded undamaged material, which represents a fictitious physically non obtainable state.

Considering the intermediate configuration C_{dp}, unloading following a load/strain increment occurs along the path determined by the damaged material stiffness tensor, here denoted as $\tilde{\mathbb{C}}$. The elastic increment is obtained by unloading along the path defined by the undamaged (virgin) material stiffness tensor $\bar{\mathbb{C}}$; the remaining part of the strain is the plastic component. Note that the only

physically obtainable and uniquely defined stress free state in this configuration is denoted by point A in Figure 2.a). As illustrated in Figure 1, isoclinic configuration $\bar{C}$ is conveniently defined from the intermediate configuration C_{dp} by mapping with the damage part of deformation gradient and rotation induced by inelastic deformation. Consequently, the stress and elastic strain in this configuration are mutually related by the undamaged (virgin) material stiffness tensor, providing the expressions similar to the results obtained from the notion of energy equivalence (as shown in the end of subsection 4.1.1). Therefore, this configuration was chosen for the definition/integration of the constitutive equations.

The part of the constitutive model related to elastic behaviour of damaged material is described in the subsection 4.1, followed by the description of plasticity related part of the model given in the subsection 4.2; the hyperelastic response in the absence of damage is, for the completeness, presented in the Appendix A.

Near Figure 2

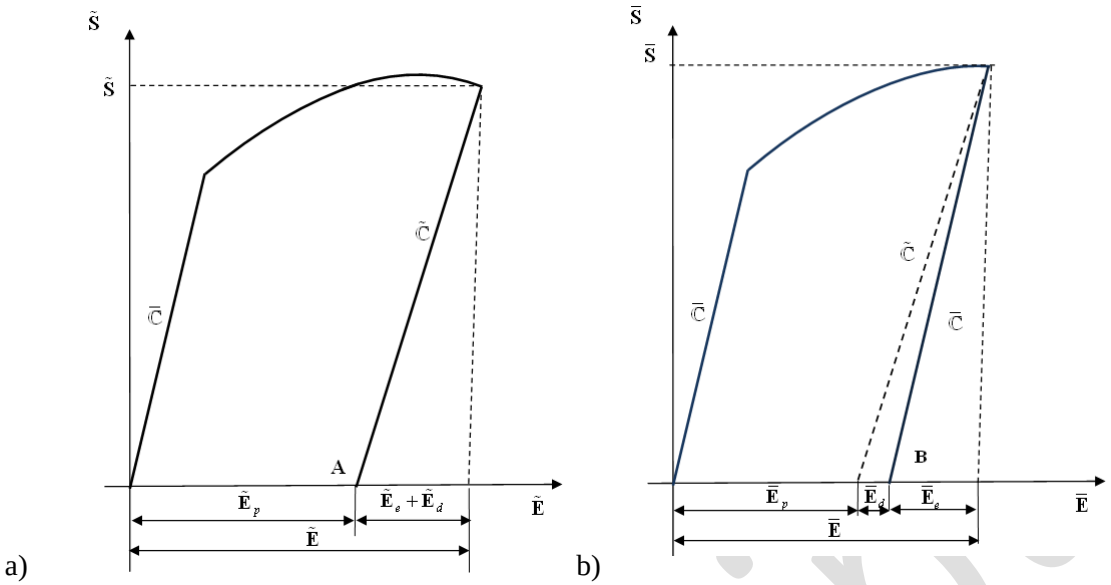

Figure 2 Kinematics and kinetics of deformation of a generalised loading-unloading curve in a) current configuration and b) isoclinic intermediate configuration

4.1 Elastic behaviour of damaged material

4.1.1 The damage model

The material model is based on the assumption that damage is irreversible and that it permanently reduces material elastic stiffness and strength. As described above, it can be considered either as a kinematic measure of the deformation which corresponds to damage (see for instance (Bammann and Solanki, 2010; Ekh et al., 2004) among others) or as a damage effect tensor operating on the material elastic stiffness tensor (see for instance (Hansen and Schreyer, 1994; Krajcinovic, 1996)).

According to the kinematics of deformation derived in the Section 2, damage in this work is represented by damage deformation gradient and damage part of velocity gradient. Damage deformation gradient maps elastically unloaded effective (undamaged) configuration to the elastically unloaded intermediate configuration which is stress free but includes damage, see Figure 1. Consequently, the natural choice is the evolution of damage to be defined in terms of damage part of velocity gradient, see for instance (Brünig, 2001; Brünig, 2003; Brünig et al., 2011a), which, from the dissipation inequalities (3.9) and (3.11), leads to the definition of the damage potential in terms of (Mandel stress like) conjugate force $\bar{\mathbf{C}}_d\bar{\mathbf{S}}$. However, available experimental data and material characterisation have been done for the classical approach widely used in continuum damage mechanics, where the damage state variable and its conjugate force are the second order damage tensor and damage energy release rate, respectively. Consequently, the relationship between the kinematic and kinetic quantities of these two formulations needed to be established.

Damage deformation gradient and corresponding kinematics, which physically represent a loss of load carrying capacity of the material i.e. reduction of the material effective load carrying area, are defined to some extent similar to (Murakami, 1988). The relationship between an effective differential area vector in the isoclinic configuration, $\mathrm{d}\bar{\mathbf{S}}_1$, and the corresponding area vector in damaged elastically unloaded intermediate configuration, $\mathrm{d}\mathbf{s}_{dp}$, is defined by Nanson's formula (Holzapfel, 2000) as:

$$\mathrm{d}\mathbf{s}_{dp} = \bar{J}_d \bar{\mathbf{F}}_d^{-T} \mathrm{d}\bar{\mathbf{S}}_1 \qquad \text{where} \quad \bar{J}_d = \det \bar{\mathbf{F}}_d \tag{4.1}$$

As a generalisation of the 1D problem, where the damage variable represents the reduction of the effective area, the linear mapping (4.1) can alternatively be defined via second order damage tensor $\bar{\boldsymbol{\omega}}$, the principle values of which are the effective area reductions in the principle directions. The formulation is capable of representing orthotropic distribution (state) of damage in a material.

Second order damage tensor $\bar{\boldsymbol{\omega}}$ in this work is defined via differential area, which is normalised by the inverse of the determinant of damage deformation gradient i.e. $\mathrm{d}\mathbf{s}_{dp}^n = \bar{J}_d^{-1}\mathrm{d}\mathbf{s}_{dp}$, as:

$$\mathrm{d}\mathbf{s}_{dp}^n = \left(\mathbf{I} - \bar{\boldsymbol{\omega}}\right)^{-1} \mathrm{d}\bar{\mathbf{S}}_1 \tag{4.2}$$

where $\left(\mathbf{I}-\bar{\boldsymbol{\omega}}\right)$ is usually refer to as integrity tensor. Note that vectors $\mathrm{d}\mathbf{s}_{dp}^{n}$ and $\mathrm{d}\mathbf{s}_{dp}$ have the same direction.

The normalised area vector (4.2) defines a traction vector in the elastically unloaded intermediate configuration in terms of Kirchhoff type stress tensor, $\boldsymbol{\tau}_{dp}=\bar{J}_d\tilde{\mathbf{S}}$ as:

$$\mathbf{t}_{dp}^{n}\mathrm{d}s_{dp}^{n}=\boldsymbol{\tau}_{dp}\mathrm{d}\mathbf{s}_{dp}^{n}=\bar{J}_d\tilde{\mathbf{S}}\bar{J}_d^{-1}\mathrm{d}\mathbf{s}_{dp}=\tilde{\mathbf{S}}\mathrm{d}\mathbf{s}_{dp}=\mathbf{t}_{dp}\mathrm{d}s_{dp} \tag{4.3}$$

By assuming that the traction vector, $\mathbf{t}_1$, acting on the effective area in the isoclinic configuration is equal to the vector (4.3) pulled back to this configuration by $\bar{\mathbf{F}}_d$ (Djordjevic, 2011):

$$\mathbf{t}_{dp}^{n}\mathrm{d}s_{dp}^{n}=\bar{\mathbf{F}}_d\bar{\mathbf{t}}_1\,\mathrm{d}S_1=\bar{\mathbf{F}}_d\bar{\mathbf{S}}\mathrm{d}\bar{\mathbf{S}}_1 \tag{4.4}$$

The relationship between the stress tensors in the two configurations can be defined as:

$$\boldsymbol{\tau}_{dp}\mathrm{d}\mathbf{s}_{dp}^{n}=\boldsymbol{\tau}_{dp}\bar{\mathbf{F}}_d^{-T}\mathrm{d}\bar{\mathbf{S}}_1=\bar{\mathbf{F}}_d\bar{\mathbf{S}}\mathrm{d}\bar{\mathbf{S}}_1 \tag{4.5}$$

$$\boldsymbol{\tau}_{dp}=\bar{\mathbf{F}}_d\bar{\mathbf{S}}\bar{\mathbf{F}}_d^{T} \tag{4.6}$$

Furthermore, using the definitions (2.7) (4.1) and (4.2), one can obtain the damage deformation and damage velocity gradient in terms of integrity tensor and the rate of change of damage tensor as:

$$\bar{\mathbf{C}}_d=\bar{\mathbf{F}}_d^{T}\bar{\mathbf{F}}_d=\left[\mathbf{I}-\bar{\boldsymbol{\omega}}\right]^2 \tag{4.7}$$

$$\bar{\mathbf{l}}_d=\bar{\mathbf{F}}_d^{-1}\dot{\bar{\mathbf{F}}}_d=\left[\mathbf{I}-\bar{\boldsymbol{\omega}}\right]^{-1}\left(-\dot{\bar{\boldsymbol{\omega}}}\right)=-\left[\mathbf{I}-\bar{\boldsymbol{\omega}}\right]^{-1}\dot{\bar{\boldsymbol{\omega}}} \tag{4.8}$$

In order to define the thermodynamic force $\bar{\mathbf{Y}}$ conjugate to the symmetric damage tensor $\bar{\boldsymbol{\omega}}$, equations (4.7) and (4.8) was substituted in the equation for damage part of dissipation (3.11), i.e.

$$\begin{aligned}\Delta_{dam}&=\bar{\mathbf{S}}:\bar{\mathbf{C}}_d\,\bar{\mathbf{l}}_d-\bar{\rho}\frac{\partial u_d}{\partial\omega^H}\dot{\omega}^H=\bar{\mathbf{S}}:\left(\bar{\mathbf{F}}_d^{T}\bar{\mathbf{F}}_d\bar{\mathbf{F}}_d^{-1}\dot{\bar{\mathbf{F}}}_d\right)-\bar{\rho}\frac{\partial u_d}{\partial\omega^H}\dot{\omega}^H=\bar{\mathbf{S}}:\left[\mathbf{I}-\bar{\boldsymbol{\omega}}\right]\left(-\dot{\bar{\boldsymbol{\omega}}}\right)-\bar{\rho}\frac{\partial u_d}{\partial\omega^H}\dot{\omega}^H=\\&=-\left[\mathbf{I}-\bar{\boldsymbol{\omega}}\right]\bar{\mathbf{S}}:\dot{\bar{\boldsymbol{\omega}}}-\bar{\rho}\frac{\partial u_d}{\partial\omega^H}\dot{\omega}^H\end{aligned} \tag{4.9}$$

$$\Delta_{dam}=\bar{\mathbf{Y}}:\dot{\bar{\boldsymbol{\omega}}}-\frac{\partial u_d}{\partial\omega^H}\dot{\omega}^H\geq 0 \tag{4.10}$$

where:

$$\bar{\mathbf{Y}}=-\left[\mathbf{I}-\bar{\boldsymbol{\omega}}\right]\bar{\mathbf{S}} \tag{4.11}$$

Damage energy release rate (4.11), was used in the definition of damage potential used in the remainder of this subsection.

Using the push forward and pull back operations and relationships between the damage kinetics and kinematics with the damage tensor, i.e. expressions (4.5) to (4.7), one can relate the tensor variables in the intermediate and isoclinic configuration as:

$$\tilde{\mathbf{E}}_e=\bar{\mathbf{F}}_d^{-T}\bar{\mathbf{E}}_e\bar{\mathbf{F}}_d^{-1}=\left[\mathbf{I}-\bar{\boldsymbol{\omega}}\right]^{-1}\bar{\mathbf{E}}_e\left[\mathbf{I}-\bar{\boldsymbol{\omega}}\right]^{-1} \tag{4.12}$$

$$\tilde{\mathbf{S}}=\bar{\mathbf{F}}_d\bar{\mathbf{S}}\bar{\mathbf{F}}_d^{T}=\left[\mathbf{I}-\bar{\boldsymbol{\omega}}\right]\bar{\mathbf{S}}\left[\mathbf{I}-\bar{\boldsymbol{\omega}}\right]^{-1} \tag{4.13}$$

$$\tilde{\mathbb{C}}=\bar{\mathbf{F}}_d\bar{\mathbf{F}}_d\bar{\mathbb{C}}\bar{\mathbf{F}}_d^{T}\bar{\mathbf{F}}_d^{T}=\left[\mathbf{I}-\bar{\boldsymbol{\omega}}\right]\left[\mathbf{I}-\bar{\boldsymbol{\omega}}\right]\bar{\mathbb{C}}\left[\mathbf{I}-\bar{\boldsymbol{\omega}}\right]^{T}\left[\mathbf{I}-\bar{\boldsymbol{\omega}}\right]^{T} \tag{4.14}$$

Note that the relationship between the material stiffness tensors in the two configurations are the same to the expressions obtained with the energy equivalence principle:

$$\bar{\psi}^{(damaged)} = \frac{1}{2}\bar{\mathbf{E}}_e : \bar{\mathbb{C}} : \bar{\mathbf{E}}_e = \frac{1}{2}\left[\mathbf{I}-\bar{\boldsymbol{\omega}}\right]^T \tilde{\mathbf{E}}_e \left[\mathbf{I}-\bar{\boldsymbol{\omega}}\right] : \bar{\mathbb{C}} : \left[\mathbf{I}-\bar{\boldsymbol{\omega}}\right]^T \tilde{\mathbf{E}}_e \left[\mathbf{I}-\bar{\boldsymbol{\omega}}\right] = \frac{1}{2}\bar{\mathbf{E}}_e : \bar{\mathbb{C}} : \bar{\mathbf{E}}_e = \frac{1}{2}\left[\mathbf{I}-\bar{\boldsymbol{\omega}}\right]^T \tilde{\mathbf{E}}_e \left[\mathbf{I}-\bar{\boldsymbol{\omega}}\right] : \bar{\mathbb{C}} : \left[\mathbf{I}-\bar{\boldsymbol{\omega}}\right]^T \tilde{\mathbf{E}}_e \left[\mathbf{I}-\bar{\boldsymbol{\omega}}\right] = \tag{4.15}$$

4.1.2 Damage potential

The damage potential is defined in terms of damage energy release rate $\bar{\mathbf{Y}}$ and the thermodynamic force conjugate to damage hardening variable Ω. Similarly to the Helmholtz free energy given in (3.6) and (3.13), damage potential for an orthotropic material is defined in terms of the irreducible set of invariants and pseudo invariants of damage energy release rate and structural tensors (2.2) as:

$$\begin{aligned} &\bar{I}_{Y1} = \mathbf{I} : \bar{\mathbf{Y}} && \bar{I}_{Y2} = \mathbf{I} : \left(\bar{\mathbf{Y}}\right)^2 \\ &\bar{I}_{Y3} = \mathbf{I} : \left(\bar{\mathbf{Y}}\right)^3 && \\ &\bar{I}_{Y4} = \mathbf{I} : \left(\bar{\mathbf{M}}^1 \bar{\mathbf{Y}}\right) && \bar{I}_{Y5} = \mathbf{I} : \left(\bar{\mathbf{M}}^1 \left(\bar{\mathbf{Y}}\right)^2\right) \\ &\bar{I}_{Y6} = \mathbf{I} : \left(\bar{\mathbf{M}}^2 \bar{\mathbf{Y}}\right) && \bar{I}_{Y7} = \mathbf{I} : \left(\bar{\mathbf{M}}^2 \left(\bar{\mathbf{Y}}\right)^2\right) \end{aligned} \tag{4.16}$$

The quadratic form of damage potential can now be defined as:

$$f_d\left(\bar{\mathbf{Y}}, \bar{\mathbf{M}}^1, \bar{\mathbf{M}}^2, \Omega\right) = \frac{1}{2}\bar{\gamma}_1 \bar{I}_{Y1}^2 + \bar{\gamma}_2 \bar{I}_{Y2} + \frac{1}{2}\bar{\gamma}_3 \bar{I}_{Y4}^2 + \bar{\gamma}_4 \bar{I}_5 + \frac{1}{2}\bar{\gamma}_5 \bar{I}_{Y6}^2 + \bar{\gamma}_6 \bar{I}_{Y7} + \bar{\gamma}_7 \bar{I}_{Y1}\bar{I}_{Y4} + \bar{\gamma}_8 \bar{I}_{Y1}\bar{I}_{Y6} + \bar{\gamma}_9 \bar{I}_{Y4}\bar{I}_{Y6} - \left(\Omega_0 + \Omega\left(\omega^H\right)\right)^2 \tag{4.17}$$

where $\bar{\gamma}_1$ to $\bar{\gamma}_9$ are material parameters and Ω_0 is an initial damage hardening conjugate force. Second derivative of damage potential with respect to the damage energy release rate is a damage characteristic tensor:

$$\bar{\mathbb{J}} = \frac{\partial^2 f_d}{\partial \bar{\mathbf{Y}}^2} = \bar{\gamma}_1 \mathbf{I}\otimes\mathbf{I} + 2\bar{\gamma}_2 \mathbb{I} + \bar{\gamma}_3 \bar{\mathbf{M}}^1 \otimes \bar{\mathbf{M}}^1 + \bar{\gamma}_5 \bar{\mathbf{M}}^2 \otimes \bar{\mathbf{M}}^2 + \bar{\gamma}_4 \mathbb{F}^1 + \bar{\gamma}_6 \mathbb{F}^2 + \bar{\gamma}_7\left(\mathbf{I}\otimes\bar{\mathbf{M}}^1 + \bar{\mathbf{M}}^1 \otimes \mathbf{I}\right) + \bar{\gamma}_8\left(\mathbf{I}\otimes\bar{\mathbf{M}}^2 + \bar{\mathbf{M}}^2 \otimes \mathbf{I}\right) + \bar{\gamma}_9\left(\bar{\mathbf{M}}^1 \otimes \bar{\mathbf{M}}^2 + \bar{\mathbf{M}}^2 \otimes \bar{\mathbf{M}}^1\right) \tag{4.18}$$

where $\mathbb{I}$ is an identity tensor of the fourth order, $\bar{\mathbb{F}}^1_{ijkl} = \left(\bar{\mathbf{M}}^1_{ik}\delta_{jl} + \delta_{ik}\bar{\mathbf{M}}^1_{lj}\right)$ and $\bar{\mathbb{F}}^2_{ijkl} = \left(\bar{\mathbf{M}}^2_{ik}\delta_{jl} + \delta_{ik}\bar{\mathbf{M}}^2_{lj}\right)$.

Note that the damage characteristic tensor in (4.18) is a symmetric tensor of the fourth order, and it was assumed constant in the current model development. This assumption has limited thermodynamics consistency but still gives satisfactory results demonstrated in Section 7 and (Djordjevic, 2011). A simplified form of the damage characteristic tensor used in this work is described in the subsection 6.1.

The damage characteristic tensor (4.18), written in Voigt notation as a second order tensor is:

$$\overline{\mathbf{J}} = 2\begin{bmatrix} J_{11} & J_{12} & J_{13} & 0 & 0 & 0 \\ J_{12} & J_{22} & J_{23} & 0 & 0 & 0 \\ J_{13} & J_{23} & J_{33} & 0 & 0 & 0 \\ 0 & 0 & 0 & J_{44} & 0 & 0 \\ 0 & 0 & 0 & 0 & J_{55} & 0 \\ 0 & 0 & 0 & 0 & 0 & J_{66} \end{bmatrix} \tag{4.19}$$

Consequently, the damage potential given in terms of damage characteristic tensor (Hansen and Schreyer, 1994) is:

$$f_d\left(\overline{\mathbf{Y}},\Omega\right) = \left(\frac{1}{2}\overline{\mathbf{Y}} : \overline{\mathbf{J}} : \overline{\mathbf{Y}}\right)^{\frac{1}{2}} - \Omega\left(\omega^H\right) = 0 \tag{4.20}$$

where the first term of the potential is referred to as equivalent damage energy release rate Y_{eq}. According to (De Borst and Feenstra, 1990), the form of damage potential (4.20) has shown some advantages in terms of the convergence of solution, relative to the form (4.17).

Evolution of the damage surface is controlled by the thermodynamic force Ω, which was assumed to be a linear function of the damage hardening parameter ω^H:

$$\Omega\left(\omega^H\right) = \Omega_0 + \omega_{t1}\omega^H \tag{4.21}$$

where the coefficient ω_{t1} is a slope of the hardening curve $Y_{eq}\left(\omega_{eq}\right)$, shown in Figure 3 in the Section 6.

A definition of the damage hardening parameter is based on a modified Klepaczko criterion (Klepaczko, 1990), which accounts for thermally activated physical (micromechanical) damage mechanisms. Klepaczko's criterion is based on the Tuler Bucher time to failure concept updated by (Dremin and Molodets, 1985) as:

$$\dot{\phi} = \dot{\phi}_0 \exp\left(-\frac{\Delta U}{k\theta}\right) \qquad 1 = \int_0^{t_c} \dot{\phi} dt \qquad \dot{\phi}_0 = \frac{1}{t_{c0}} \tag{4.22}$$

where ϕ is a convenient damage accumulation rate function of the stress, σ, ΔU is free energy of damage activation, t_c is time to failure, t_{c0} is a characteristic time to failure which corresponds to the minimum threshold stress σ_0 for which material failure can occur and k is a Boltzmann constant. By assuming that the free energy is a function of stress, Klepaczko defined it as:

$$\Delta U = \Delta U_0 \ln\left(\frac{\frac{\sigma_0}{\mu_0}}{\frac{\sigma}{\mu(\theta)}}\right) \tag{4.23}$$

where $\mu(\theta)$ and μ_0 are current and initial shear moduli and ΔU_0 is the reference damage activation energy for a body at the reference stress and temperature. Making use of the normalised activation energy, introduced by Follansbee and Kocks (Follansbee and Kocks, 1988):

$$u_0 = \frac{\Delta U_0}{\mu(\theta) b^3} \tag{4.24}$$

where b is Burgers vector, the model was made consistent with the MTS model, used for the evolution of plastic flow stress. Consequently, free activation energy becomes:

$$\Delta U = \mu(\theta) b^3 u_0 \ln\left(\frac{\frac{\sigma_0}{\mu_0}}{\frac{\sigma}{\mu(\theta)}}\right) \tag{4.25}$$

Finally, by substituting the free activation energy (4.25) in the expression for the damage accumulation function given in the integral form in (4.22), the damage hardening parameter assumes the following form:

$$\omega^H = \frac{\varepsilon}{\varepsilon_{c0}} \frac{1}{\left(\left(\frac{\mu(\theta) b^3 u_0}{k\theta}\right)+1\right)} \left(\frac{\frac{\sigma(\varepsilon)}{\mu(\theta)}}{\frac{\sigma_0}{\mu_0}}\right)^{\left(\frac{\mu(\theta) b^3 u_0}{k\theta}\right)} \tag{4.26}$$

where ε and ε_0 are respectively current and critical strain at the time of failure. Note that the solution (4.26) is obtained by the integration in the strain domain, assuming the constant strain rate which agrees with the experimental procedure for strain rate material characterisation. The material constants σ_0, t_{c0} and u_0 are obtained from the plate impact test data as outlined in Section 6.

The damage rate of change tensor $\dot{\bar{\boldsymbol{\omega}}}$ and rate of change of hardening parameter $\dot{\omega}^H$ are obtained from the principle of maximum dissipation (3.16) and (3.17), introduced in (Hill, 1950). The rates $\dot{\bar{\boldsymbol{\omega}}}$ and $\dot{\omega}^H$ are collinear and proportional to their conjugate forces. The proportionality is determined by the monotonically increasing Lagrange multiplier $\dot{\lambda}_d$:

$$\dot{\bar{\boldsymbol{\omega}}} = \dot{\lambda}_d \frac{\partial f_d}{\partial \bar{\mathbf{Y}}} = \dot{\lambda}_d \frac{\bar{\mathbf{J}} : \bar{\mathbf{Y}}}{\left(\frac{1}{2}\bar{\mathbf{Y}} : \bar{\mathbf{J}} : \bar{\mathbf{Y}}\right)^{\frac{1}{2}}} \tag{4.27}$$

$$\dot{\omega}^H = -\dot{\lambda}_d \frac{\partial f_d}{\partial \Omega} = \dot{\lambda}_d \tag{4.28}$$

The Lagrange multiplier for damage deformation is calculated from the consistency condition $\dot{f}_d = 0$, when damage is evolving:

$$\dot{f}_d\left(\bar{\mathbf{Y}},\Omega\right)=\frac{\partial f_d}{\partial\bar{\mathbf{Y}}}:\dot{\bar{\mathbf{Y}}}+\frac{\partial f_d}{\partial\Omega}\dot{\Omega}=0 \tag{4.29}$$

Rate of change of damage energy release rate is calculated from Equation (4.11), described in detail in Appendix B, as:

$$\dot{\bar{\mathbf{Y}}}=\dot{\lambda}_d\left(\frac{\partial f_d}{\partial\bar{\mathbf{Y}}}\bar{\mathbf{S}}-\left[\mathbf{I}-\bar{\boldsymbol{\omega}}\right]\bar{\mathbb{C}}:\left[\left[\mathbf{I}-\bar{\boldsymbol{\omega}}\right]\frac{\partial f_d}{\partial\bar{\mathbf{Y}}}\right]_{sym}\right)-\left[\mathbf{I}-\bar{\boldsymbol{\omega}}\right]\bar{\mathbb{C}}:\left[\bar{\mathbf{C}}_e\left(\bar{\mathbf{I}}-\bar{\mathbf{I}}_p\right)\right]_{sym} \tag{4.30}$$

whilst rate of change of the force conjugate to damage hardening parameter is obtained as:

$$\dot{\Omega}=\frac{\partial\Omega}{\partial\omega^H}\dot{\omega}^H=\dot{\lambda}_d\frac{\partial\Omega}{\partial\omega^H}=\dot{\lambda}_d\omega_{t1} \tag{4.31}$$

Making use of the expressions (4.30) and (4.31), the consistency condition (4.29), can now be solved for the damage Lagrange multiplier:

$$\begin{aligned}&\frac{\partial f_d}{\partial\bar{\mathbf{Y}}}:\left(\dot{\lambda}_d\left(\frac{\partial f_d}{\partial\bar{\mathbf{Y}}}\bar{\mathbf{S}}-\left[\mathbf{I}-\bar{\boldsymbol{\omega}}\right]\bar{\mathbb{C}}:\left[\left[\mathbf{I}-\bar{\boldsymbol{\omega}}\right]^T\frac{\partial f_d}{\partial\bar{\mathbf{Y}}}\right]_{sym}\right)-\left[\mathbf{I}-\bar{\boldsymbol{\omega}}\right]\bar{\mathbb{C}}:\left[\bar{\mathbf{C}}_e\left(\bar{\mathbf{I}}-\bar{\mathbf{I}}_p\right)\right]_{sym}\right)+\dot{\lambda}_d\frac{\partial f_d}{\partial\Omega}\frac{\partial\Omega}{\partial\omega^H}=0\\&\dot{\lambda}_d\left(\frac{\partial f_d}{\partial\bar{\mathbf{Y}}}:\left(\frac{\partial f_d}{\partial\bar{\mathbf{Y}}}\bar{\mathbf{S}}-\left[\mathbf{I}-\bar{\boldsymbol{\omega}}\right]\bar{\mathbb{C}}:\left[\left[\mathbf{I}-\bar{\boldsymbol{\omega}}\right]^T\frac{\partial f_d}{\partial\bar{\mathbf{Y}}}\right]_{sym}\right)+\frac{\partial f_d}{\partial\Omega}\frac{\partial\Omega}{\partial\omega^H}\right)-\frac{\partial f_d}{\partial\bar{\mathbf{Y}}}:\left[\mathbf{I}-\bar{\boldsymbol{\omega}}\right]\bar{\mathbb{C}}:\left[\bar{\mathbf{C}}_e\left(\bar{\mathbf{I}}-\bar{\mathbf{I}}_p\right)\right]_{sym}=0\end{aligned} \tag{4.32}$$

$$\dot{\lambda}_d=-\frac{\dfrac{\partial f_d}{\partial\bar{\mathbf{Y}}}:\left[\left[\mathbf{I}-\bar{\boldsymbol{\omega}}\right]\bar{\mathbb{C}}:\left[\bar{\mathbf{C}}_e\left(\bar{\mathbf{I}}-\bar{\mathbf{I}}_p\right)\right]_{sym}\right]}{\dfrac{\partial f_d}{\partial\bar{\mathbf{Y}}}:\left(\dfrac{\partial f_d}{\partial\bar{\mathbf{Y}}}\bar{\mathbf{S}}-\left[\mathbf{I}-\bar{\boldsymbol{\omega}}\right]\bar{\mathbb{C}}:\left[\left[\mathbf{I}-\bar{\boldsymbol{\omega}}\right]^T\dfrac{\partial f_d}{\partial\bar{\mathbf{Y}}}\right]_{sym}\right)+\dfrac{\partial f_d}{\partial\Omega}\dfrac{\partial\Omega}{\partial\omega^H}} \tag{4.33}$$

Lagrange multiplier in (4.33) is defined in the general form, for any functional form of damage potential. In the current form of the constitutive model, damage is described by damage deformation gradient (2.3), damage potential (4.20) and evolution equations for damage tensor and damage hardening rule, (4.27) and (4.28), respectively.

4.2 Plastic behaviour

Anisotropic properties of the material are pronounced during the inelastic deformation, so plastic potential and yield criterion are the functions of structural tensors in addition to their "isotropic" arguments. If the potential is defined as a function of deviatoric part of Mandel stress, temperature and internal variables, its invariance can be stated as:

$$f_{pl}\left(\bar{\boldsymbol{\Sigma}}^D,\bar{\mathbf{M}}^1,\bar{\mathbf{M}}^2,\sigma_{MTS}\left(\theta,\varepsilon_p,\dot{\varepsilon}_p\right)\right)=f_{pl}\left(\mathbf{Q}^T\bar{\boldsymbol{\Sigma}}^D\mathbf{Q},\mathbf{Q}^T\bar{\mathbf{M}}^1\mathbf{Q},\mathbf{Q}^T\bar{\mathbf{M}}^2\mathbf{Q},\sigma_{MTS}\right) \tag{4.34}$$

where $\mathbf{Q}$ is a rotation that belongs to the group of orthotropic transformations (Boehler, 1987), $\bar{\boldsymbol{\Sigma}}^D$ is a deviatoric Mandel stress and σ_{MTS} is referential flow stress calculated by the MTS model (Follansbee and Kocks, 1988). Assuming the symmetry of deviatoric Mandel stress, an irreducible set of invariants for the yield function given in (4.34) consists of seven invariants (Boehler, 1987; Spencer, 1971):

$$\bar{I}_1 = \mathbf{I} : \bar{\boldsymbol{\Sigma}}^D = 0 \qquad \bar{I}_2 = \mathbf{I} : \left(\bar{\boldsymbol{\Sigma}}^D\right)^2$$
$$\bar{I}_3 = \mathbf{I} : \left(\bar{\boldsymbol{\Sigma}}^D\right)^3 \tag{4.35}$$
$$\bar{I}_4 = \mathbf{I} : \left(\bar{\mathbf{M}}^1 \bar{\boldsymbol{\Sigma}}^D\right) \qquad \bar{I}_5 = \mathbf{I} : \left(\bar{\mathbf{M}}^1 \left(\bar{\boldsymbol{\Sigma}}^D\right)^2\right)$$
$$\bar{I}_6 = \mathbf{I} : \left(\bar{\mathbf{M}}^2 \bar{\boldsymbol{\Sigma}}^D\right) \qquad \bar{I}_7 = \mathbf{I} : \left(\bar{\mathbf{M}}^2 \left(\bar{\boldsymbol{\Sigma}}^D\right)^2\right)$$

The plastic potential is defined as a quadratic function in deviatoric stress:

$$f_{pl}\left(\bar{\boldsymbol{\Sigma}}^D, \bar{\mathbf{M}}^1, \bar{\mathbf{M}}^2, \sigma_{MTS}\right) = \bar{\beta}_1 \bar{I}_2 + \frac{1}{2}\bar{\beta}_2 \bar{I}_4^2 + \frac{1}{2}\bar{\beta}_3 \bar{I}_6^2 + \bar{\beta}_4 \bar{I}_5 + \bar{\beta}_5 \bar{I}_7 + \bar{\beta}_6 \bar{I}_4 \bar{I}_6 - \sigma_{MTS}^2 \tag{4.36}$$

where $\bar{\beta}_1$ to $\bar{\beta}_6$ are material parameters, which can be calculated from the coefficients in the Hill's yield function (Hill, 1950), given later in this section. Second derivative of the plastic potential with respect to the stress is a tensor of the fourth order denoted as $\bar{\mathbb{A}}$:

$$\bar{\mathbb{A}} = \frac{\partial^2 f_{pl}}{\partial \bar{\boldsymbol{\Sigma}}^D \partial \bar{\boldsymbol{\Sigma}}^D} = 2\bar{\beta}_1 \mathbb{I} + \bar{\beta}_2 \bar{\mathbf{M}}^1 \otimes \bar{\mathbf{M}}^1 + \bar{\beta}_3 \bar{\mathbf{M}}^2 \otimes \bar{\mathbf{M}}^2 + \\ + \bar{\beta}_4 \bar{\mathbb{F}}^1 + \bar{\beta}_5 \bar{\mathbb{F}}^2 + \bar{\beta}_6 \left(\bar{\mathbf{M}}^1 \otimes \bar{\mathbf{M}}^2 + \bar{\mathbf{M}}^2 \otimes \bar{\mathbf{M}}^1\right) \tag{4.37}$$

Convexity of the yield surface requires tensor $\bar{\mathbb{A}}$ to be positive semi definite (Itskov and Aksel, 2004). For the same arguments described for the damage potential and in (De Borst and Feenstra, 1990), the yield function expressed in terms of $\bar{\mathbb{A}}$ is used in the remaining of this section as:

$$f_{pl}\left(\bar{\boldsymbol{\Sigma}}^D, \bar{\mathbf{M}}^1, \bar{\mathbf{M}}^2, \sigma_{MTS}\right) = \left(\frac{1}{2}\bar{\boldsymbol{\Sigma}}^D : \bar{\mathbb{A}} : \bar{\boldsymbol{\Sigma}}^D\right)^{\frac{1}{2}} - \sigma_{MTS}\left(\varepsilon_p, \dot{\varepsilon}_p, \theta\right) \tag{4.38}$$

where the first term in the equation is effective stress equivalent to the Hill's criterion (Hill, 1950) whilst ε_p and θ are parameters which define specific referential MTS curve.

Rate of plastic deformation and effective plastic strain are defined from the normality condition as:

$$\bar{\mathbf{d}}_p = \dot{\lambda}_{pl} \frac{\partial f_{pl}}{\partial \bar{\boldsymbol{\Sigma}}^D} = \dot{\lambda}_{pl} \frac{\bar{\mathbb{A}} : \bar{\boldsymbol{\Sigma}}^D}{\sqrt{\frac{1}{2}\bar{\boldsymbol{\Sigma}}^D : \bar{\mathbb{A}} : \bar{\boldsymbol{\Sigma}}^D}} \tag{4.39}$$

$$\dot{\varepsilon}_p = -\dot{\lambda}_{pl} \frac{\partial f_{pl}}{\partial \sigma_{MTS}} = \dot{\lambda}_{pl} \tag{4.40}$$

Lagrange multiplier $\dot{\lambda}_{pl}$ in (4.39) and (4.40) is obtained from the consistency condition:

$$\dot{f}_{pl} = \frac{\partial f_{pl}}{\partial \bar{\boldsymbol{\Sigma}}^D} : \dot{\bar{\boldsymbol{\Sigma}}}^D + \frac{\partial f_{pl}}{\partial \sigma_{MTS}} \dot{\sigma}_{MTS} = \frac{\partial f_{pl}}{\partial \bar{\boldsymbol{\Sigma}}^D} : \left(\dot{\bar{\mathbf{C}}}_e \bar{\mathbf{S}} + \bar{\mathbf{C}}_e \dot{\bar{\mathbf{S}}} \right) - \frac{\partial \sigma_{MTS}}{\partial \hat{\sigma}} \frac{\partial \hat{\sigma}}{\partial \varepsilon_p} \dot{\varepsilon}_p = 0 \tag{4.41}$$

$$\begin{aligned}
\dot{f}_{pl} &= \frac{\partial f_{pl}}{\partial \bar{\boldsymbol{\Sigma}}^D} : \left(2\left[\bar{\mathbf{C}}_e \left(\bar{\mathbf{I}} - \bar{\mathbf{I}}_p \right) \right]_{sym} \bar{\mathbf{S}} + \bar{\mathbf{C}}_e \left(\bar{\mathbb{C}} : \left(\left[\bar{\mathbf{C}}_e \left(\bar{\mathbf{I}} - \bar{\mathbf{I}}_p \right) \right]_{sym} - \left[\bar{\mathbf{C}}_d \bar{\mathbf{I}}_d \right]_{sym} \right) \right) \right) - \frac{\partial \sigma_{MTS}}{\partial \hat{\sigma}} \frac{\partial \hat{\sigma}}{\partial \varepsilon_p} \dot{\varepsilon}_p = \\
&= \left(2\bar{\mathbf{C}}_e \frac{\partial f_{pl}}{\partial \bar{\boldsymbol{\Sigma}}^D} \bar{\mathbf{S}} + \frac{\partial f_{pl}}{\partial \bar{\boldsymbol{\Sigma}}^D} : \bar{\mathbf{C}}_e \left(\bar{\mathbf{C}}_e \bar{\mathbb{C}} \right) \right) : \left[\bar{\mathbf{I}} \right]_{sym} - \frac{\partial f_{pl}}{\partial \bar{\boldsymbol{\Sigma}}^D} : \bar{\mathbf{C}}_e \bar{\mathbb{C}} : \left[\bar{\mathbf{C}}_d \bar{\mathbf{I}}_d \right]_{sym} - \\
&\quad \dot{\lambda}_{pl} \left(\left(2\bar{\mathbf{C}}_e \frac{\partial f_{pl}}{\partial \bar{\boldsymbol{\Sigma}}^D} \bar{\mathbf{S}} + \frac{\partial f_{pl}}{\partial \bar{\boldsymbol{\Sigma}}^D} : \bar{\mathbf{C}}_e \left(\bar{\mathbf{C}}_e \bar{\mathbb{C}} \right) \right) : \left[\frac{\partial f_{pl}}{\partial \bar{\boldsymbol{\Sigma}}^D} \right]_{sym} + \frac{\partial \sigma_{MTS}}{\partial \hat{\sigma}} \frac{\partial \hat{\sigma}}{\partial \varepsilon_p} \right)
\end{aligned} \tag{4.42}$$

Substituting the rates of kinematic and kinetic measures in the latter expression, the solution for the multiplier is obtained in terms of total velocity gradient given in the isoclinic configuration:

$$\dot{\lambda}_{pl} = \dot{\varepsilon}_p = \frac{\left(2\bar{\mathbf{C}}_e \frac{\partial f_{pl}}{\partial \bar{\boldsymbol{\Sigma}}^D} \bar{\mathbf{S}} + \frac{\partial f_{pl}}{\partial \bar{\boldsymbol{\Sigma}}^D} : \bar{\mathbf{C}}_e \left(\bar{\mathbf{C}}_e \bar{\mathbb{C}} \right) \right) : \left[\bar{\mathbf{I}} \right]_{sym} - \frac{\partial f_{pl}}{\partial \bar{\boldsymbol{\Sigma}}^D} : \bar{\mathbf{C}}_e \bar{\mathbb{C}} : \left[\bar{\mathbf{C}}_d \bar{\mathbf{I}}_d \right]_{sym}}{\left(2\bar{\mathbf{C}}_e \frac{\partial f_{pl}}{\partial \bar{\boldsymbol{\Sigma}}^D} \bar{\mathbf{S}} + \frac{\partial f_{pl}}{\partial \bar{\boldsymbol{\Sigma}}^D} : \bar{\mathbf{C}}_e \left(\bar{\mathbf{C}}_e \bar{\mathbb{C}} \right) \right) : \left[\frac{\partial f_{pl}}{\partial \bar{\boldsymbol{\Sigma}}^D} \right]_{sym} + \frac{\partial \sigma_{MTS}}{\partial \hat{\sigma}} \frac{\partial \hat{\sigma}}{\partial \varepsilon_p}} \tag{4.43}$$

Making use of the last result, rate of plastic deformation (4.39) in terms of total strain rate is:

$$\bar{\mathbf{d}}_p = \dot{\lambda}_{pl} \frac{\partial f_{pl}}{\partial \bar{\boldsymbol{\Sigma}}^D} = \frac{\frac{\partial f_{pl}}{\partial \bar{\boldsymbol{\Sigma}}^D} \left(2\bar{\mathbf{C}}_e \frac{\partial f_{pl}}{\partial \bar{\boldsymbol{\Sigma}}^D} \bar{\mathbf{S}} + \frac{\partial f_{pl}}{\partial \bar{\boldsymbol{\Sigma}}^D} : \bar{\mathbf{C}}_e \left(\bar{\mathbf{C}}_e \bar{\mathbb{C}} \right) \right) : \left[\bar{\mathbf{I}} \right]_{sym} - \frac{\partial f_{pl}}{\partial \bar{\boldsymbol{\Sigma}}^D} \frac{\partial f_{pl}}{\partial \bar{\boldsymbol{\Sigma}}^D} : \bar{\mathbf{C}}_e \bar{\mathbb{C}} : \left[\bar{\mathbf{C}}_d \bar{\mathbf{I}}_d \right]_{sym}}{\left(2\bar{\mathbf{C}}_e \frac{\partial f_{pl}}{\partial \bar{\boldsymbol{\Sigma}}^D} \bar{\mathbf{S}} + \frac{\partial f_{pl}}{\partial \bar{\boldsymbol{\Sigma}}^D} : \bar{\mathbf{C}}_e \left(\bar{\mathbf{C}}_e \bar{\mathbb{C}} \right) \right) : \left[\frac{\partial f_{pl}}{\partial \bar{\boldsymbol{\Sigma}}^D} \right]_{sym} + \frac{\partial \sigma_{MTS}}{\partial \hat{\sigma}} \frac{\partial \hat{\sigma}}{\partial \varepsilon_p}} \tag{4.44}$$

A specific plastic potential of Hill's type (4.38) and the MTS hardening model (Follansbee and Kocks, 1988) can now be substituted in (4.43) and (4.44).

The tensor $\bar{\mathbb{A}}$ is a state variable, determined by the structural tensors given in the isoclinic configuration. It is assumed to be constant in the current development of material model; hence the constants from $\bar{\beta}_1$ to $\bar{\beta}_6$ in (4.36) and (4.37) can be expressed in terms of Hill's coefficients (4.45) (Hill, 1950) as follows:

$$f_{pl} = \left(F\left(\bar{\boldsymbol{\Sigma}}^D_{22} - \bar{\boldsymbol{\Sigma}}^D_{33} \right)^2 + G\left(\bar{\boldsymbol{\Sigma}}^D_{33} - \bar{\boldsymbol{\Sigma}}^D_{11} \right)^2 + H\left(\bar{\boldsymbol{\Sigma}}^D_{11} - \bar{\boldsymbol{\Sigma}}^D_{22} \right)^2 + 2L\bar{\boldsymbol{\Sigma}}^D_{23} + 2M\bar{\boldsymbol{\Sigma}}^D_{31} + 2N\bar{\boldsymbol{\Sigma}}^D_{12} \right)^{\frac{1}{2}} - \sigma_{MTS} \tag{4.45}$$

$$\begin{aligned}
\bar{\beta}_1 &= M + L - N & \bar{\beta}_2 &= 2\left(F + 4G + H - 2M \right) \\
\bar{\beta}_3 &= 2\left(4F + G + H - 2L \right) & \bar{\beta}_4 &= 2\left(N - L \right) \\
\bar{\beta}_5 &= 2\left(N - M \right) & \bar{\beta}_6 &= 2F - H + 2G - L - M + N
\end{aligned} \tag{4.46}$$

Material constants given in (4.46) are determined from the experimental data as described in Section 6.

The effective plastic strain rate in the plastic potential (4.38) can be obtained from the equivalence of the rate of work of Mandel stress and effective stress as:

$$\dot{\varepsilon}_p = \frac{1}{\sigma_{MTS}} \bar{\boldsymbol{\Sigma}} \; : \bar{\mathbf{d}}_p \tag{4.47}$$

Consequently, $\dot{\varepsilon}_p$ when expressed in terms of invariants of the plastic rate of deformation (Pereda et al., 1993) is:

$$\dot{\varepsilon}_p = \left[c_1 \bar{J}_2 + c_2 \bar{J}_4^2 + c_3 \bar{J}_6^2 + c_4 \bar{J}_5 + c_5 \bar{J}_7 + c_6 \bar{J}_4 \bar{J}_6 \right]^{\frac{1}{2}} \tag{4.48}$$

The set of invariants, equivalent to the sets (4.35), is defined as:

$$\begin{aligned} \bar{J}_1 &= \mathbf{I} : \bar{\mathbf{d}}_p & \bar{J}_2 &= \mathbf{I} : \bar{\mathbf{d}}_p^2 \\ \bar{J}_3 &= \mathbf{I} : \bar{\mathbf{d}}_p^3 & & \\ \bar{J}_4 &= \mathbf{I} : \left(\bar{\mathbf{M}}^1 \bar{\mathbf{d}}_p \right) & \bar{J}_5 &= \mathbf{I} : \left(\bar{\mathbf{M}}^1 \bar{\mathbf{d}}_p^2 \right) \\ \bar{J}_6 &= \mathbf{I} : \left(\bar{\mathbf{M}}^2 \bar{\mathbf{d}}_p \right) & \bar{J}_7 &= \mathbf{I} : \left(\bar{\mathbf{M}}^2 \bar{\mathbf{d}}_p^2 \right) \end{aligned} \tag{4.49}$$

where the coefficients from c_1 to c_6 are respectively given in terms of Hill's coefficients are:

$$\begin{aligned} c_1 &= \frac{1}{L} + \frac{1}{M} - \frac{1}{N} & c_2 &= \frac{F+G}{FG+GH+HF} - \frac{2}{M} \\ c_3 &= \frac{F+H}{FG+GH+HF} - \frac{2}{L} & c_4 &= 2\left(-\frac{1}{L} + \frac{1}{N} \right) \\ c_5 &= -\frac{1}{M} + \frac{1}{N} & c_6 &= 2\left(\frac{H}{FG+GH+HF} - \frac{1}{L} + \frac{1}{M} - \frac{1}{N} \right) \end{aligned} \tag{4.50}$$

MTS is a physically based model, derived from the analysis of dislocation motions in a metal undergoing plastic deformation (Follansbee and Kocks, 1988). The model provides scalar-valued flow stress as a function of plastic strain rate and temperature, given in the following form:

$$\sigma_{MTS} = \sigma_a + \frac{\mu}{\mu_0} \left(\hat{\sigma} - \sigma_a \right) s\left(\theta, \dot{\varepsilon}_p \right) = \sigma_a + \frac{\mu}{\mu_0} \left(\hat{\sigma} - \sigma_a \right) \left[1 - \left(\frac{k\theta \ln\left(\frac{\dot{\varepsilon}_0}{\dot{\varepsilon}_p} \right)}{\mu b^3 g_0} \right)^{\frac{1}{q}} \right]^{\frac{1}{p}} \tag{4.51}$$

where σ_a is an athermal rate independent component of flow stress, $\hat{\sigma}$ is internal parameter of the material structure, $\dot{\varepsilon}_p$ is plastic strain rate, whilst $s\left(\theta, \dot{\varepsilon} \right)$ is thermal interaction factor, obtained from the Arrhenius expression for strain rate and free activation energy. The other parameters in the Equation (4.51) are: g_0 is normalized activation energy, p and q are the material micromechanical constants.

The evolution of parameter of the structure $\hat{\sigma}$, according to original work of Follansbee and Kocks (Follansbee and Kocks, 1988), can be expressed via strain hardening rate Θ, as a balance of the two competing processes: dislocation accumulation, determined by Θ_0, and dynamic recovery,

determined by $\Theta\left(\dot{\varepsilon},\theta,\hat{\sigma}\right)$. For a number of metals (aluminium alloys) of interest, strain hardening rate changes linearly within the range of stresses and strains but exhibits the saturation behaviour, especially for the higher strain and stress levels. In order to describe this saturation the hyperbolic functions are used in the definition of the strain hardening rate:

$$\Theta = \frac{\partial \hat{\sigma}}{\partial \varepsilon_p} = \Theta_0 \left(1 - \frac{\tanh\left(\alpha \frac{\hat{\sigma}}{\hat{\sigma}_s} \right)}{\tanh\left(\alpha\right)} \right) \tag{4.52}$$

where the initial strain hardening rate Θ_0 and saturation threshold stress $\hat{\sigma}_s$ are defined as:

$$\Theta_0 = a_0 + a_1 \ln\left(\dot{\varepsilon}_p\right) + a_2 \dot{\varepsilon}_p^n \tag{4.53}$$

$$\hat{\sigma}_s = \hat{\sigma}_{s0} \left(\frac{\dot{\varepsilon}_p}{\dot{\varepsilon}_{s0}} \right)^{\frac{k\theta}{\mu A b^3}} \tag{4.54}$$

In the Equation (4.53) a_0, a_1, a_2 and n are material parameters (fitting constants), whilst $\hat{\sigma}_{s0}$ and $\dot{\varepsilon}_{s0}$ in (4.54) are, respectively, a reference saturation stress threshold at $0K$ and reference strain rate; A is a material parameter.

Note that Equations (4.52) and consequently (4.51) are nonlinear differential equations which cannot be explicitly solved for structural parameter $\hat{\sigma}$, except in a special case for the constant strain rate and temperature. Hence, for the sake of simplicity and computational convenience, it is assumed that strain rate and temperature do not change within the time step. This assumption means that the material state changes along one stress strain curve during the time step, which can be physically justified to some extent, but was primarily driven by convenience of numerical implementation. Hence the reference hardening rate is calculated as:

$$\frac{\partial \sigma_{MTS}}{\partial \hat{\sigma}} \frac{\partial \hat{\sigma}}{\partial \varepsilon_p} = \frac{\mu}{\mu_0} s\left(\theta, \dot{\bar{\varepsilon}}_p\right) \Theta_0 \left(1 - \left[\frac{\tanh\left(\alpha \frac{\hat{\sigma}}{\hat{\sigma}_s} \right)}{\tanh\left(\alpha\right)} \right] \right) \tag{4.55}$$

The last equation completes the description of the plastic behaviour in the material model.

5 System of equations of constitutive model and numerical implementation

The system of equations, which define the constitutive model in the rate form, is given below:

- Piola Kirchhoff stress rate, Mandel stress rate and Cauchy stress rate:

$$\dot{\bar{\mathbf{S}}} = \bar{\mathbb{C}} : \dot{\bar{\mathbf{E}}}_e - \boldsymbol{\beta}\dot{\theta} = \bar{\mathbb{C}} : \left(\left[\bar{\mathbf{C}}_e \left(\bar{\mathbf{I}} - \bar{\mathbf{I}}_p \right) \right]_{sym} - \left[\bar{\mathbf{C}}_d \bar{\mathbf{I}}_d \right]_{sym} \right) - \boldsymbol{\beta}\dot{\theta}$$
$$= \bar{\mathbf{C}}_e \bar{\mathbb{C}} : \bar{\mathbf{I}} - \dot{\lambda}_p \bar{\mathbf{C}}_e \bar{\mathbb{C}} : \left[\frac{\partial f_{pl}}{\partial \bar{\boldsymbol{\Sigma}}^D} \right]_{sym} + \dot{\lambda}_d \bar{\mathbb{C}} : \left[\left[\mathbf{I} - \bar{\boldsymbol{\omega}} \right] \frac{\partial f_d}{\partial \bar{\mathbf{Y}}} \right]_{sym} - \boldsymbol{\beta}\dot{\theta} \tag{5.1}$$

$$\dot{\bar{\boldsymbol{\Sigma}}} = \dot{\bar{\mathbf{C}}}_e \bar{\mathbf{S}} + \bar{\mathbf{C}}_e \dot{\bar{\mathbf{S}}} =$$
$$= 2\bar{\mathbf{C}}_e \bar{\mathbf{I}} \bar{\mathbf{S}} + \bar{\mathbf{C}}_e^2 \bar{\mathbb{C}} : \bar{\mathbf{I}} - \dot{\lambda}_p \left(2\bar{\mathbf{C}}_e \left[\frac{\partial f_{pl}}{\partial \boldsymbol{\Sigma}^D} \right]_{sym} \bar{\mathbf{S}} + \bar{\mathbf{C}}_e^2 \bar{\mathbb{C}} : \left[\frac{\partial f_{pl}}{\partial \bar{\boldsymbol{\Sigma}}^D} \right]_{sym} \right) + \dot{\lambda}_d \bar{\mathbf{C}}_e \bar{\mathbb{C}} : \left(\left[\mathbf{I} - \boldsymbol{\omega} \right] \left[\frac{\partial f_d}{\partial \bar{\mathbf{Y}}} \right]_{sym} \right) \tag{5.2}$$

$$\dot{\boldsymbol{\sigma}} = J_e^{-1} \bar{J}_d^{-1} \left[\mathbf{F}_e \bar{\mathbf{F}}_d \dot{\bar{\mathbf{S}}} \bar{\mathbf{F}}_d^T \mathbf{F}_e + \left(\mathbf{l}_e + \mathbf{l}_d \right) \boldsymbol{\sigma} + \boldsymbol{\sigma} \left(\mathbf{l}_e^T + \mathbf{l}_d^T \right) \right] - \left(J_e^{-2} \bar{J}_d^{-1} \dot{J}_e + J_e^{-1} \bar{J}_d^{-2} \dot{\bar{J}}_d \right) \boldsymbol{\sigma} \tag{5.3}$$

- Damage energy release rate:

$$\dot{\bar{\mathbf{Y}}} = \dot{\lambda}_d \left(\frac{\partial f_d}{\partial \bar{\mathbf{Y}}} \bar{\mathbf{S}} - \left[\mathbf{I} - \bar{\boldsymbol{\omega}} \right] \bar{\mathbb{C}} : \left[\left[\mathbf{I} - \bar{\boldsymbol{\omega}} \right]^T \frac{\partial f_d}{\partial \bar{\mathbf{Y}}} \right]_{sym} \right) - \left[\mathbf{I} - \bar{\boldsymbol{\omega}} \right] \bar{\mathbb{C}} : \left[\bar{\mathbf{C}}_e \left(\bar{\mathbf{I}} - \bar{\mathbf{I}}_p \right) \right]_{sym} \tag{5.4}$$

- Damage surface/potential:

$$f_d = \left(\frac{1}{2} \bar{\mathbf{Y}} : \bar{\mathbf{J}} : \bar{\mathbf{Y}} \right)^{\frac{1}{2}} - \left(\Omega_0 + \Omega\left(\omega^H \right) \right) \le 0 \tag{5.5}$$

- Yield surface/potential:

$$f_{pl} = \left(\frac{1}{2} \bar{\boldsymbol{\Sigma}}^D : \bar{\mathbb{A}} : \bar{\boldsymbol{\Sigma}}^D \right)^{\frac{1}{2}} - \sigma_{MTS}\left(\varepsilon_p, \dot{\varepsilon}_p, \theta \right) \le 0 \tag{5.6}$$

- Loading/unloading and consistency conditions:

$$f_d \le 0 \qquad \dot{\lambda}_d \ge 0 \qquad \dot{\lambda}_d f_d = 0 \tag{5.7}$$
$$f_{pl} \le 0 \qquad \dot{\lambda}_{pl} \ge 0 \qquad \dot{\lambda}_{pl} f_{pl} = 0 \tag{5.8}$$

- Flow rules:

$$\dot{\bar{\boldsymbol{\omega}}} = \dot{\lambda}_d \frac{\bar{\mathbf{J}} : \bar{\mathbf{Y}}}{\left(\frac{1}{2} \bar{\mathbf{Y}} : \bar{\mathbf{J}} : \bar{\mathbf{Y}} \right)^{\frac{1}{2}}} \qquad \bar{\mathbf{d}}_p = \dot{\lambda}_p \frac{\bar{\mathbb{A}} : \bar{\boldsymbol{\Sigma}}^D}{\left(\frac{1}{2} \bar{\boldsymbol{\Sigma}}^D : \bar{\mathbb{A}} : \bar{\boldsymbol{\Sigma}}^D \right)^{\frac{1}{2}}} \tag{5.9}$$

$$\omega^H = \dot{\lambda}_d \qquad \dot{\varepsilon}_p = \dot{\lambda}_p \tag{5.10}$$

- Damage isotropic hardening:

$$\dot{\Omega}\left(\omega^H \right) = \omega_{t1} \dot{\omega}^H = \omega_{t1} \dot{\lambda}_d \tag{5.11}$$

- Plastic isotropic hardening:

$$\dot{\sigma}_{MTS} = \frac{\mu}{\mu_0} \left(\hat{\sigma} - \sigma_a \right) \left[1 - \left(\frac{k\theta \ln\left(\frac{\dot{\varepsilon}_0}{\dot{\varepsilon}_p} \right)}{\mu b^3 g_0} \right)^{\frac{1}{q}} \right]^{\frac{1}{p}} \Theta_0 \left(1 - \frac{\tanh\left(\alpha \frac{\hat{\sigma} - \hat{\sigma}_a}{\hat{\sigma}_s - \hat{\sigma}_a} \right)}{\tanh\left(\alpha \right)} \right) \dot{\lambda}_p \tag{5.12}$$

- Evolution of temperature is determined as:

$$\dot{\theta}=\frac{1}{c}\left(Q_e+Q_p+Q_d\right)=\frac{1}{c}\theta\bar{\boldsymbol{\beta}}:\bar{\mathbf{C}}_e\bar{\mathbf{I}}-\dot{\lambda}_p\left(\frac{1}{c}\theta\bar{\mathbf{C}}_e\bar{\boldsymbol{\beta}}:\frac{\partial f_{pl}}{\partial\bar{\boldsymbol{\Sigma}}^D}+\bar{\boldsymbol{\Sigma}}:\frac{\partial f_{pl}}{\partial\bar{\boldsymbol{\Sigma}}^D}-\Upsilon\right)+\dot{\lambda}_d\left(\left[\mathbf{I}-\bar{\boldsymbol{\omega}}\right]\frac{\partial f_d}{\partial\bar{\mathbf{Y}}}+\bar{\mathbf{Y}}:\frac{\partial f_d}{\partial\bar{\mathbf{Y}}}-\Omega\right) \quad (5.13)$$

- Gruneisen Equation of state (Steinberg, 1991):

$$p\left(\mu,E\right)=\frac{\rho_0C^2\mu\left[1+\left(1-\frac{\gamma_0}{2}\right)\mu-\frac{a}{2}\mu^2\right]}{\left[1-\left(S_1-1\right)\mu-S_2\frac{\mu^2}{\mu+1}-S_3\frac{\mu^3}{\left(\mu+1\right)^2}\right]}+\left(\gamma_0+a\mu\right)E \quad (5.14)$$

5.1 Stress update

One of the key components of numerical implementation of a nonlinear constitutive model is stress update which requires calculation of the tangent stiffness tensor which relates increment of stress to increment of total strain. Tangent stiffness tensors for the two nonlinear inelastic processes, plastic deformation and damage, were derived and presented the following subsections.

Coupling between the plasticity related part and damage part of the model is based on the approach introduced in (Lemaitre and Chaboche, 1990), which assumes that as the material starts deforming inelastically, plastic deformation is dominant dissipative process until the plastic hardening rate reaches the critical value of zero (for numerical implementation set to a small positive number, e.g. 1.0 e-06). Once this critical hardening rate is reached, damage is initiated and damage evolution becomes the dominant dissipation process. This rate based criterion for damage initiation avoids some of the difficulties related to the localised nature of the inelastic deformation described in (Brünig et al., 2011a; Driemeier et al., 2010). Note that plasticity does not directly contribute to the damage development and that damage does not directly contribute to the plasticity in the current material model development (Djordjevic, 2011).

In terms of kinematics of deformation, the three modes of material deformation; elastic, elastic-damage and elastic-plastic can be, respectively, defined as:

$$\bar{\mathbf{I}}\neq 0 \qquad \bar{\mathbf{I}}_e\neq 0 \qquad \bar{\mathbf{I}}_p=0 \qquad \bar{\mathbf{I}}_d=0 \quad (5.15)$$

$$\bar{\mathbf{I}}\neq 0 \qquad \bar{\mathbf{I}}_e\neq 0 \qquad \bar{\mathbf{I}}_p=0 \qquad \bar{\mathbf{I}}_d\neq 0 \quad (5.16)$$

$$\bar{\mathbf{I}}\neq 0 \qquad \bar{\mathbf{I}}_e\neq 0 \qquad \bar{\mathbf{I}}_p\neq 0 \qquad \bar{\mathbf{I}}_d=0 \quad (5.17)$$

5.1.1 Thermo-elastic damage deformation

Tangent stiffness tensor for the damage thermo-elastic deformation was obtained, starting from the rate of second Piola Kirchhoff stress expressed in the isoclinic configuration:

$$\dot{\bar{\mathbf{S}}} = \bar{\mathbf{C}}_e \bar{\mathbb{C}} : \bar{\mathbf{d}} - \dot{\lambda}_p \bar{\mathbf{C}}_e \bar{\mathbb{C}} : \left[\frac{\partial f_{pl}}{\partial \bar{\bar{\boldsymbol{\Sigma}}}^D} \right]_{sym} - \dot{\lambda}_d \bar{\mathbb{C}} : \left[\bar{\mathbf{C}}_d \left(\left[\mathbf{I} - \bar{\boldsymbol{\omega}} \right]^{-1} \frac{\partial f_d}{\partial \bar{\bar{\mathbf{Y}}}} \right) \right]_{sym} - \boldsymbol{\beta} \dot{\theta} =$$

$$= \bar{\mathbf{C}}_e \bar{\mathbb{C}} : \bar{\mathbf{d}} + \bar{\mathbb{C}} : \left[\left[\mathbf{I} - \bar{\boldsymbol{\omega}} \right] \frac{\frac{\partial f_d}{\partial \bar{\bar{\mathbf{Y}}}} \frac{\partial f_d}{\partial \bar{\bar{\mathbf{Y}}}} : \left[\left[\mathbf{I} - \bar{\boldsymbol{\omega}} \right] \bar{\mathbb{C}} : \left[\bar{\mathbf{C}}_e \left(\bar{\mathbf{I}} - \bar{\mathbf{I}}_p \right) \right]_{sym} \right]}{\frac{\partial f_d}{\partial \bar{\bar{\mathbf{Y}}}} : \left(\frac{\partial f_d}{\partial \bar{\bar{\mathbf{Y}}}} \bar{\mathbf{S}} - \left[\mathbf{I} - \bar{\boldsymbol{\omega}} \right] \bar{\mathbb{C}} : \left[\left[\mathbf{I} - \bar{\boldsymbol{\omega}} \right]^T \frac{\partial f_d}{\partial \bar{\bar{\mathbf{Y}}}} \right]_{sym} \right) + \frac{\partial f_d}{\partial \Omega} \frac{\partial \Omega}{\partial \omega^H}} \right] - \boldsymbol{\beta} \dot{\theta} = \quad (5.18)$$

$$= \bar{\mathbb{C}}_T^{ed} : \bar{\mathbf{d}} - \boldsymbol{\beta} \dot{\theta}$$

where $\bar{\mathbb{C}}$ denotes elastic stiffness tensor of the virgin material and the tangent stiffness tensor $\bar{\mathbb{C}}_T^{ed}$ for elastic damage deformation is:

$$\bar{\mathbb{C}}_T^{ed} = \bar{\mathbf{C}}_e \bar{\mathbb{C}} + \bar{\mathbb{C}} : \left[\left[\mathbf{I} - \bar{\boldsymbol{\omega}} \right] \frac{\frac{\partial f_d}{\partial \bar{\bar{\mathbf{Y}}}} \frac{\partial f_d}{\partial \bar{\bar{\mathbf{Y}}}} : \bar{\mathbf{C}}_e \left[\mathbf{I} - \bar{\boldsymbol{\omega}} \right] \bar{\mathbb{C}}}{\frac{\partial f_d}{\partial \bar{\bar{\mathbf{Y}}}} : \left(\frac{\partial f_d}{\partial \bar{\bar{\mathbf{Y}}}} \bar{\mathbf{S}} - \left[\mathbf{I} - \bar{\boldsymbol{\omega}} \right] \bar{\mathbb{C}} : \left[\left[\mathbf{I} - \bar{\boldsymbol{\omega}} \right]^T \frac{\partial f_d}{\partial \bar{\bar{\mathbf{Y}}}} \right]_{sym} \right) + \frac{\partial f_d}{\partial \Omega} \frac{\partial \Omega}{\partial \omega^H}} \right] \quad (5.19)$$

Note that plastic term in the expression (5.18) (the second term in the first equation) is set to zero, since the plastic deformation and damage evolution do not occur simultaneously in the current implementation of the constitutive model. Damage thermo-elastic mode of deformation is characterised by $\dot{\lambda}_p = 0$, $\dot{\lambda}_d \neq 0$.

5.1.2 Thermo-elastic plastic deformation

Similarly to the previous derivation, the tangent stiffness tensor for thermo-elastic plastic behaviour was obtained starting from the rate of Piola Kirchhoff stress tensor given in the isoclinic configuration, $\dot{\bar{\mathbf{S}}}$, as:

$$\dot{\bar{\mathbf{S}}} = \bar{\mathbf{C}}_e \bar{\mathbb{C}} : \bar{\mathbf{d}} - \dot{\lambda}_p \bar{\mathbf{C}}_e \bar{\mathbb{C}} : \left[\frac{\partial f_{pl}}{\partial \bar{\bar{\boldsymbol{\Sigma}}}^D} \right]_{sym} - \dot{\lambda}_d \bar{\mathbb{C}} : \left[\bar{\mathbf{C}}_d \left(\left[\mathbf{I} - \bar{\boldsymbol{\omega}} \right]^{-1} \frac{\partial f_d}{\partial \bar{\bar{\mathbf{Y}}}} \right) \right]_{sym} - \boldsymbol{\beta} \dot{\theta} =$$

$$= \bar{\mathbf{C}}_e \bar{\mathbb{C}} : \bar{\mathbf{d}} - \bar{\mathbf{C}}_e \bar{\mathbb{C}} : \left[\frac{\frac{\partial f_{pl}}{\partial \bar{\bar{\boldsymbol{\Sigma}}}^D} \left(2 \bar{\mathbf{C}}_e \frac{\partial f_{pl}}{\partial \bar{\bar{\boldsymbol{\Sigma}}}^D} \bar{\mathbf{S}} + \frac{\partial f_{pl}}{\partial \bar{\bar{\boldsymbol{\Sigma}}}^D} : \bar{\mathbf{C}}_e \left(\bar{\mathbf{C}}_e \bar{\mathbb{C}} \right) \right) : \bar{\mathbf{d}}}{\left(2 \bar{\mathbf{C}}_e \frac{\partial f_{pl}}{\partial \bar{\bar{\boldsymbol{\Sigma}}}^D} \bar{\mathbf{S}} + \frac{\partial f_{pl}}{\partial \bar{\bar{\boldsymbol{\Sigma}}}^D} : \bar{\mathbf{C}}_e \left(\bar{\mathbf{C}}_e \bar{\mathbb{C}} \right) \right) : \left[\frac{\partial f_{pl}}{\partial \bar{\bar{\boldsymbol{\Sigma}}}^D} \right]_{sym} + \frac{\partial \sigma_{MTS}}{\partial \hat{\sigma}} \frac{\partial \hat{\sigma}}{\partial \varepsilon_p}} \right]_{sym} - \boldsymbol{\beta} \dot{\theta} = \quad (5.20)$$

$$= \bar{\mathbb{C}}_T^{ep} : \bar{\mathbf{d}} - \boldsymbol{\beta} \dot{\theta}$$

where a general form of the tangent stiffness tensor in the isoclinic configuration $\bar{\mathbb{C}}_T^{ep}$ during the thermo-elastic plastic deformation is given as:

$$\bar{\mathbb{C}}_T^{ep} = \bar{\mathbf{C}}_e\bar{\mathbb{C}} - \bar{\mathbf{C}}_e\bar{\mathbb{C}} : \left[\frac{\dfrac{\partial f_{pl}}{\partial \bar{\boldsymbol{\Sigma}}^D}\left(2\bar{\mathbf{C}}_e \dfrac{\partial f_{pl}}{\partial \bar{\boldsymbol{\Sigma}}^D}\bar{\mathbf{S}} + \dfrac{\partial f_{pl}}{\partial \bar{\boldsymbol{\Sigma}}^D} : \bar{\mathbf{C}}_e\left(\bar{\mathbf{C}}_e\bar{\mathbb{C}}\right)\right)}{\left(2\bar{\mathbf{C}}_e \dfrac{\partial f_{pl}}{\partial \bar{\boldsymbol{\Sigma}}^D}\bar{\mathbf{S}} + \dfrac{\partial f_{pl}}{\partial \bar{\boldsymbol{\Sigma}}^D} : \bar{\mathbf{C}}_e\left(\bar{\mathbf{C}}_e\bar{\mathbb{C}}\right)\right) : \left[\dfrac{\partial f_{pl}}{\partial \bar{\boldsymbol{\Sigma}}^D}\right]_{sym} + \dfrac{\partial \sigma_{MTS}}{\partial \hat{\sigma}}\dfrac{\partial \hat{\sigma}}{\partial \varepsilon_p}} \right]_{sym} \tag{5.21}$$

Having in mind that thermo-elastic/plastic mode of deformation is characterised by $\dot{\lambda}_p \neq 0, \dot{\lambda}_d = 0$ the damage term in the Equation (5.20) (last term in the first equation) is set to zero.

5.1.3 Numerical implementation

The new material model was implemented in Lawrence Livermore National Laboratory (LLNL) DYNA3D (Liu, 2004) using radial return algorithms for plasticity and damage (Djordjevic, 2011). Once the system of equations from (5.1) to (5.13) is integrated, the updated nominal stress is used in integration of the momentum equation.

The model was validated by numerical simulations of Taylor anvil tests for AA7010, given in the Section 7.

6 Determination of the material parameters

This section provides an outline description of the material characterisation required in order to determine parameters for the new material model. A detailed description of the material characterisation process including all experimental data can be found in (Panov, 2006).

6.1 Material parameters for damage potential

Anisotropy of damage is represented in the damage potential through the damage characteristic tensor (4.19), which is in general determined by nine material parameters from $\bar{\gamma}_1$ to $\bar{\gamma}_9$. The relationships between the members of the tensor and material parameters are:

$$\begin{aligned}
\bar{\gamma}_1 &= J_{33} + J_{44} - J_{55} - J_{66} & \bar{\gamma}_2 &= \frac{1}{2}\left(J_{55} + J_{66} - J_{44}\right) \\
\bar{\gamma}_3 &= J_{11} + J_{33} - 2J_{66} - 2J_{13} & \bar{\gamma}_4 &= J_{44} - J_{55} \\
\bar{\gamma}_5 &= J_{22} + J_{33} - 2J_{55} - 2J_{23} & \bar{\gamma}_6 &= J_{44} - J_{66} \\
\bar{\gamma}_7 &= J_{13} - J_{33} - J_{44} + J_{55} + J_{66} & \bar{\gamma}_8 &= J_{23} - J_{33} - J_{44} + J_{55} + J_{66} \\
\bar{\gamma}_9 &= J_{12} - J_{13} - J_{23} + J_{33} + J_{44} - J_{55} - J_{66}
\end{aligned} \tag{6.1}$$

Due to the lack of experimental data, a simplified form of the damage characteristic tensor is used in this work, motivated by the definition of the tensor proposed in (Zhu and Cescotto, 1995; Habraken et al., 1998). The damage model, in its current form, was intended primarily for modelling of tensile damage. Therefore, the diagonal components in (4.19) which correspond to shear damage (J_{44} , J_{55}

and J_{66}) were set to zero. The remaining members were expressed in terms of the constants J_1, J_2 and J_3, experimentally determined for the principal direction of damage orthotropy for a material as:

$$J_{11}=J_1 \qquad J_{12}=\sqrt{J_2} \qquad J_{13}=\sqrt{J_3} \qquad (6.2)$$
$$J_{22}=J_2 \qquad J_{23}=\sqrt{J_2 J_3} \qquad J_{33}=J_3$$

The constants J_1, J_2 and J_3 in (6.2) are calculated by making use of the energy equivalence principle, which is schematically illustrated in Figure 3. The equivalent damage energy release rate in the definition of damage potential (the first term in (4.20)), determined by damage characteristic tensor, is equal to the damage energy release rate in reference direction. For the linear hardening model illustrated in the Figure 3, the equivalent damage work is:

$$W_{eq}=\frac{1}{2}\omega_t\left(Y_{eq}+Y_0\right)=\frac{1}{2}\frac{\left(Y_{eq}-Y_0\right)}{\omega_{eq}}\left(Y_{eq}+Y_0\right)=\frac{1}{2\omega_{eq}}\left(Y_{eq}^2-Y_0^2\right) \qquad (6.3)$$

Where the equivalent damage variable ω_{eq} work conjugate to Y_{eq} can be obtained from power equivalence $Y_{eq}\omega_{eq}=\bar{\mathbf{Y}}:\bar{\boldsymbol{\omega}}$. Consequently, the rate of change of damage tensor can be expressed as:

$$\bar{\boldsymbol{\omega}}=\omega_{eq}\frac{\partial f_d}{\partial \bar{\mathbf{Y}}}=\omega_{eq}\frac{\mathbb{J}:\bar{\mathbf{Y}}}{2Y_{eq}} \qquad (6.4)$$

Double contraction of this expression with itself leads to the expression for $\omega_{eq}=\sqrt{2\bar{\boldsymbol{\omega}}:\mathbb{J}^{-1}:\bar{\boldsymbol{\omega}}}$.

Similarly, damage work done in direction *i* is the area below the curve $Y_i\left(\omega_i\right)$ defined as:

$$W_{di}=\frac{1}{2\omega_i}\left(Y_i^2-Y_{i0}^2\right) \qquad (6.5)$$

where: ω_{ti} is a slope of the $Y_i\left(\omega_i\right)$ curve and Y_{10} is an initial damage energy release rate in i-direction; $i=1,2,3$.

Near Figure 3

Equivalence between the damage work (6.5) done in each principle direction *i* of damage orthotropy and the equivalent damage work (6.3), yields a solution for the coefficients J_1 to J_3. If the reference direction coincides with direction 1, the coefficients have the following form:

$$J_1=\left(\frac{Y_1}{Y_1}\right)^2=1$$
$$J_2=\left(\frac{Y_1}{Y_2}\right)^2=\frac{Y_1^2}{\left(\frac{\omega_{t2}}{\omega_{t1}}\right)\left(Y_1^2-Y_{10}^2\right)+Y_{20}^2} \qquad J_3=\left(\frac{Y_1}{Y_3}\right)^2=\frac{Y_1^2}{\left(\frac{\omega_{t3}}{\omega_{t1}}\right)\left(Y_1^2-Y_{10}^2\right)+Y_{30}^2} \qquad (6.6)$$

In order to determine of members of damage characteristic tensor $\mathbf{J}$, it is necessary to determine the damage energy released rate as a function of damage. Damage energy release rate as a function of damage can be determined from the cyclic tensile tests (Zhu and Cescotto, 1995). Instead of the quasi static cyclic tests, a novel approach was used in this work. Given a stress strain curve from the uniaxial tensile test for aluminium alloy AA7010, damage as a function of strain for the loading direction i was calculated using modified Klepaczko failure criterion (Klepaczko, 1990):

$$\omega_i(\varepsilon_i) = \frac{\varepsilon_i}{\varepsilon_{c0}} \frac{1}{\left(\left(\frac{\mu(\theta) b^3 u_0}{k\theta}\right)+1\right)} \left(\frac{\frac{\sigma_i(\varepsilon_i)}{\mu(\theta)}}{\frac{\sigma_0}{\mu_0}} \right)^{\left(\frac{\mu(\theta) b^3 u_0}{k\theta}\right)} \tag{6.7}$$

The terms in the equation (6.7) and material constants were introduced in the subsection 4.1. Note that the stress in the equation (6.7) is expressed as a function of strain. The material constants σ_0, t_{c0} and u_0 are obtained from the experimental data following the procedure outlined at the end of this subsection and described in detail in (Panov, 2006).

It is easy to demonstrate that the energy release rate as a function of strain in the case of uniaxial stress state aligned with a principal damage direction is given by (6.8).

$$-Y_i = \frac{\sigma^2{}_i(\varepsilon_i)}{E_i(1-\omega_i(\varepsilon_i))^3} \tag{6.8}$$

Again, making use of the experimentally determined stress strain curves and the relationship (6.7) for $\omega_i(\varepsilon_i)$ one can calculate $Y_i\ (\omega_i)$ curves for the two principle directions of damage orthotropy; and the results are given in Figure 4. In absence of data for the third principle direction, it was assumed that the behaviour was equivalent to the behaviour in the direction 1 (Zhu and Cescotto, 1995; Panov, 2006).

Near Figure 4

A number of the experimental tensile test stress strain curves are accurately approximated by the corresponding curves obtained with the proposed material model (with and without damage effects) for a range of temperatures and strain rates as shown in Figure 5, using martial parameters determined by the procedure described in this section.

Near Figure 5

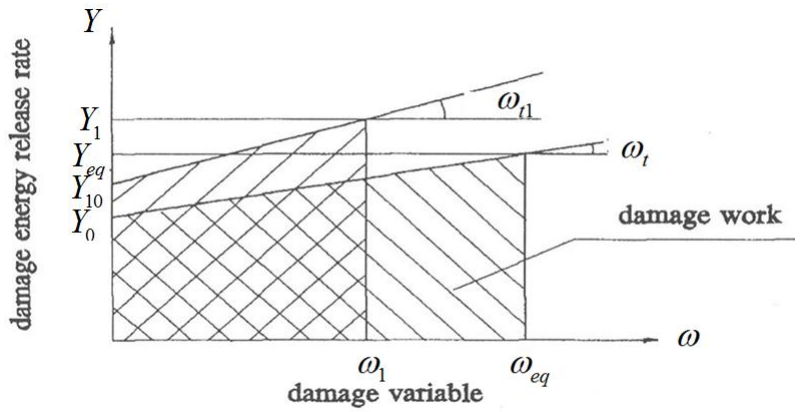

Figure 3 Method of equivalence of damage work for calculation of damage characteristic tensor (Zhu and Cescotto, 1995)

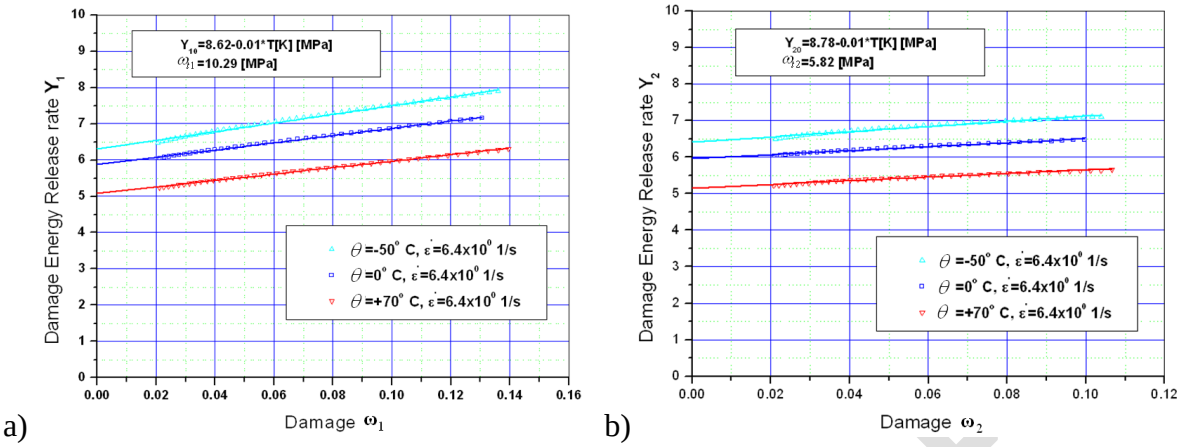

a) b)

Figure 4 Energy released rate vs. damage in the principle direction 1 (a) and 2 (b) for AA7010 at $\dot{\varepsilon} = 6.4\,s^{-1}$

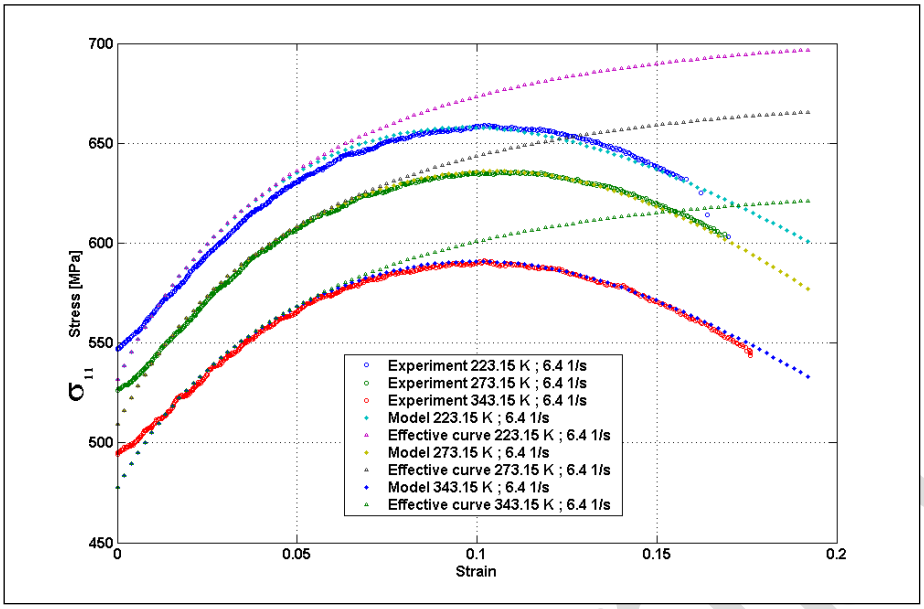

Figure 5 Experimental, Effective (MTS) and Model (MTS + damage) stress-strain curves of AA7010 at $\dot{\varepsilon} = 6.4 s^{-1}$

Material constants $\sigma_0 = 1.05GPa$, $t_{c0} = 2\mu s$ and $u_0 = 0.0087$ in the expression for the damage hardening variable (6.7) were obtained from the published data for spall strength for aluminium alloy AA 7020 (Chevrier, 1996). This was done by plotting the spall strength normalised with the shear modulus as a function of critical loading time t_c, given in Figure 6, and fitting the curve with the expression for normalised stress. As already stated this expression was derived on the basis of Klepaczko's criterion (Klepaczko, 1990).

$$\frac{\sigma}{\mu(\theta)} = \frac{\sigma_0}{\mu_0}\left[\left(\frac{u_0 b^3 \mu(\theta)}{k\theta} + 1\right)\frac{t_{c0}}{t_c}\right]^{\left(\frac{k\theta}{u_0 b^3 \mu(\theta)}\right)} \tag{6.9}$$

The values for the damage parameters, discussed in this section, for AA 7010 are given in the Table 9 in the Section 7 where they were used in validation of the new constitutive model.

Near Figure 6

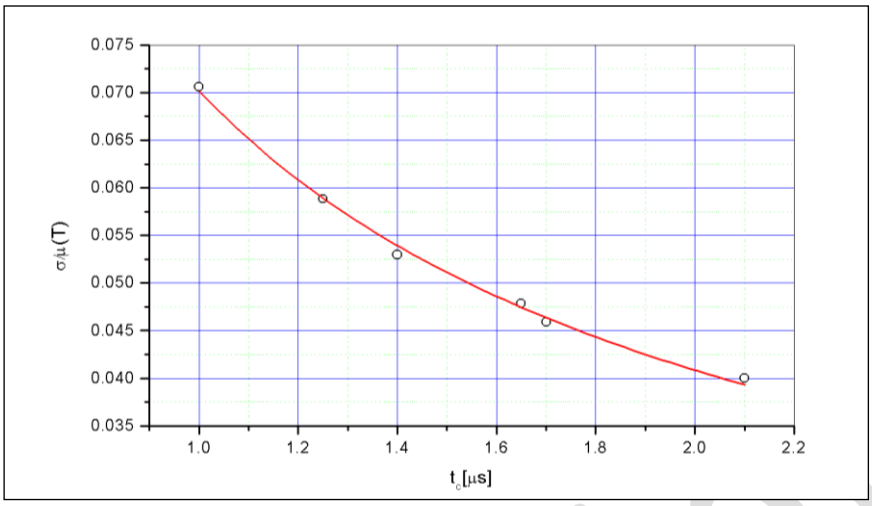

Figure 6 Normalized critical spall stress versus critical time of loading for AA7020

6.2 Material parameters for plastic potential

Material constants in the equations (4.46) were calculated from the Hill's coefficients, which were obtained using a novel procedure which combines standard tensile tests (Hill, 1950) with data from Taylor anvil test. The required experimental data consists of: yield stress under the uniaxial loading for three directions, and Lankford coefficient $R_0 = \dot{\varepsilon}^p_{y'} \big/ \dot{\varepsilon}^p_{z'}$, obtained from the Taylor anvil test. In the characterisation of the AA7010 yield stresses were measured for the angles 0°, 45°, 90° relative to the rolling direction for the range of strain rates between $6.4\times10^{-4}\ s^{-1}$ and $6.4\times10^{1}\ s^{-1}$ and at temperatures –50°, 0°, +70°, +140° and +200° C. For instance, the yield stresses obtained for the strain rate $6.4\ s^{-1}$ (for which the damage energy release rates are shown in Figure 4) and temperature +70°C are: $\boldsymbol{\sigma}_{Y0} = 496.7MPa$, $\boldsymbol{\sigma}_{Y45} = 493.5MPa$ and $\boldsymbol{\sigma}_{Y90} = 467.4MPa$ (the other values and a detailed description of the experimental procedure can be found in (Panov, 2006)).

A number of Taylor tests of AA7010 were performed with the cylindrical specimens shown in Figure 7 a). The impact direction (z direction in the Figure 7) was aligned with material rolling direction. The Lankford coefficient $R_0 = 0.894$ determined from the data for the test performed at impact velocity 200 m/s given in the Figure 7 b). The values for yield stresses given above and Lankford coefficient were sufficient for calculation of the values for the Hill's coefficients, given in the Table 9. The following expressions were used to obtain the values for F, G, H and N:

$$F = \frac{1}{\sigma_{90}{}^2} - \frac{R_0}{\sigma_{90}{}^2(1+R_0)} \qquad G = \frac{1}{\sigma_0{}^2(1+R_0)} \qquad H = \frac{R_0}{\sigma_0{}^2(1+R_0)} \qquad (6.10)$$

$$N = \frac{1}{2}\left(\frac{4}{\sigma^2{}_{45}} - \frac{1}{\sigma^2{}_{90}} + \frac{R_0 - 1}{\sigma_0{}^2(1+R_0)}\right)$$

Near Figure 7

a) 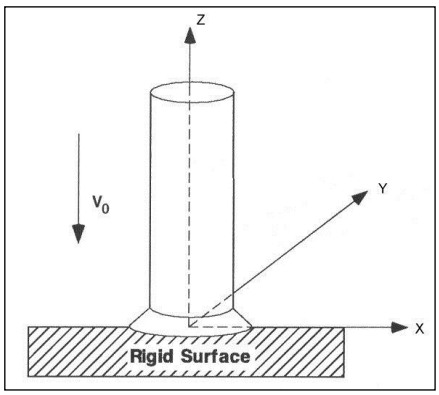

b) 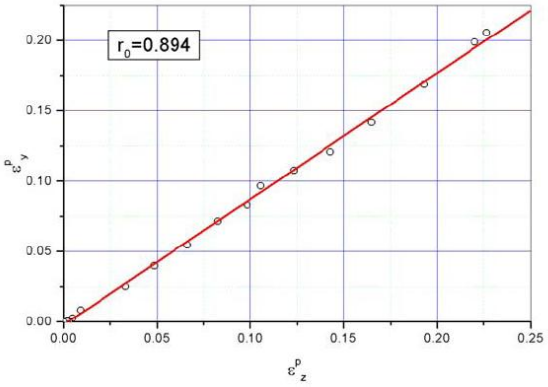

Figure 7 a) Taylor impact specimen and the reference coordinate system b) Lankford coefficient observed from Taylor test of AA7010 at (a) $v = 200m/s$

A geometrical representation of the initial Hill's yield surface for plane stress state represented in the stress space $(\sigma_x, \sigma_y, \sigma_{xy})$ (Szczepiński and Miastkowski, 1968) based on the material parameters for AA7010 at $\theta = +70^{\circ} C$, and in the strain rate $\dot{\varepsilon} = 6.4 s^{-1}$ is given in Figure 8.

Near Figure 8

Note, Hill's coefficients in the proposed method were calculated using the measured yield stresses and the plastic strains, assuming that the results obtained by measuring either the yield stresses or the final plastic strains are equivalent. In other words, assuming that the yield surfaces determined from stress ratios or plastic strain ratios are the same. Although Hill (Hill, 1950) suggested independent measurements of the plastic strain ratios and yield stress ratios in order to validate the theory, it has been shown in some experiments that the combination of the measured parameters didn't significantly affect the shape of the yield function (Cazacu and Barlat, 2003; Malo et al., 1998).

The material constants for the MTS model were obtained following the procedure given in (Meyers, 1994) and are given in the Table 9 along with the other material parameters required by the constitutive model. The experimentally obtained stress strain curves and their MTS model equivalents (based on the data from Table 9) for a range of strain rates from $\dot{\varepsilon} = 6.4 \times 10^{0} s^{-1}$ to $\dot{\varepsilon} = 6.4 \times 10^{-4} s^{-1}$ are shown in Figure 9.

Near Figure 9

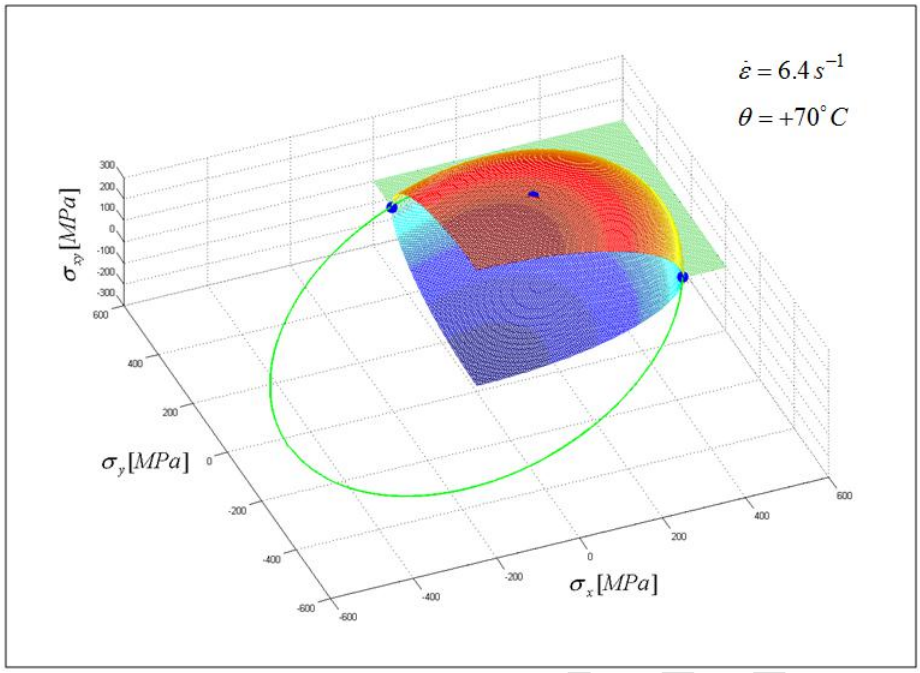

Figure 8 Yield surface for AA7010 alloy plate as predicted by Hill's criterion at $\dot{\varepsilon} = 6.4\,s^{-1}$ and $\theta = +70^{\circ}C$

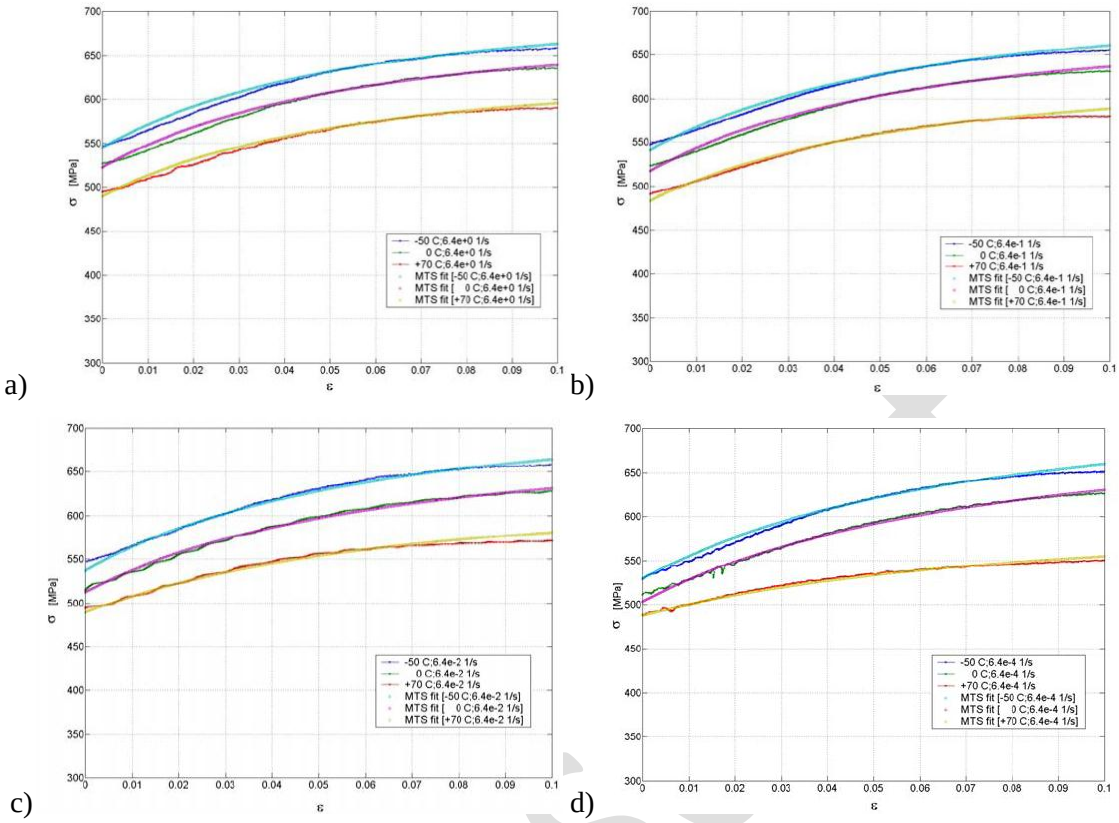

Figure 9 Experimental stress strain curves fitted with Mechanical Threshold Stress (MTS model) for the following strain rates: a) $\dot{\varepsilon} = 6.4\times10^{0}\, s^{-1}$**; b)** $\dot{\varepsilon} = 6.4\times10^{-1} s^{-1}$**; c)** $\dot{\varepsilon} = 6.4\times10^{-2} s^{-1}$**; d)** $\dot{\varepsilon} = 6.4\times10^{-4}\, s^{-1}$

7 Validation of the new model

The developed constitutive model was validated in two main stages. The first stage comprised systematic validation of each part of the new material model, i.e. the validation of elastic isotropic behaviour, the validation of orthotropic elastic behaviour, the validation of orthotropic elastic-plastic behaviour and the validation of orthotropic elastic-plastic-damage behaviour. This stage of the validation process allowed for each important part of the proposed formulation and its implementation into DYNA3D to be examined. The second stage of the validation process comprised comparison of the results generated by the proposed material model against the available experimental data for Plate Impact test and Taylor anvil test. A schematic representation of the whole validation process is given in Figure 10. The first stage validation is described in Section 7.1 and the second stage in Section 7.2.

Near Figure 10

7.1 The first stage validation

In this stage the validation was performed by conducting a serous of a single element analysis a uniaxial strain test and uniaxial stress test. In order to speed up the validation, both types of analyses (uniaxial strain and uniaxial stress) were performed with the single element models. The formulations of elastic isotropy, elastic orthotropy and elastic plastic orthotropy (with and without hardening) of the new material were examined and validated against an appropriate reference material model. The following existing DYNA3D material models were employed: Isotropic elastic-plastic, orthotropic elastic and orthotropic elastic-plastic. The final step, in this validation stage was comparison of the whole model (including elastic, plastic and damage orthotropy) against the tensile test experimental data.

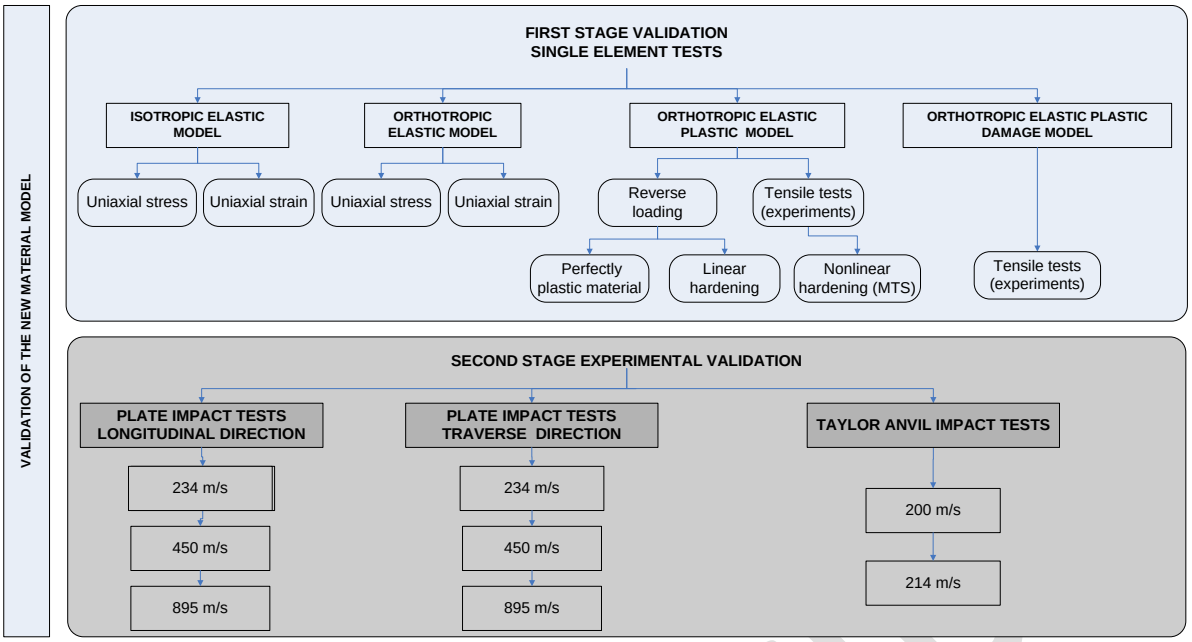

Figure 10 A schematic representation of the validation process for the new material model

7.1.1 Single element model

In order to speed up the comparison process in the single element analyses, two solid elements with identical geometry, boundary conditions and loading, as shown in Figure 11 and Table 1, were used in each simulation. In this model one element was assigned the new material model (node numbering from 1 to 8) and the other a reference material model available in DYNA3D (node numbering from 9 to 16). The principle directions of material orthotropy were aligned with the x, y, z axis of the global coordinate system. This allowed for effective comparison of the new material model against the reference material models. The node numbering used to define boundary conditions is shown in Figure 11. The displacement boundary conditions, based on the node numbering in Figure 11, used in these tests are summarized in Table 1. Loading in compression and tension was applied to the elements by prescribing displacement load curves to nodes 5, 6, 7 and 8 (consequently). The equivalent tests were performed for the x, y and z directions. For brevity, only the results for the test performed in the x direction are presented and discussed.

Near Figure 11

Table 1 Displacements boundary conditions defined for a uniaxial stress and a uniaxial strain tests in the x direction

Node	Uniaxial Stress	Uniaxial Strain
1 & 9	Constrained x, y and z displacements	Constrained x, y and z displacements
2 & 10	Constrained x displacement	Constrained x, y and z displacements
3 & 11	Constrained x displacement	Constrained x, y and z displacements
4 & 12	Constrained x displacement	Constrained x, y and z displacements
5 & 13	No constraints	Constrained y and z displacements
6 & 14	No constraints	Constrained y and z displacements
7 & 15	No constraints	Constrained y and z displacements
8 & 16	No constraints	Constrained y and z displacements

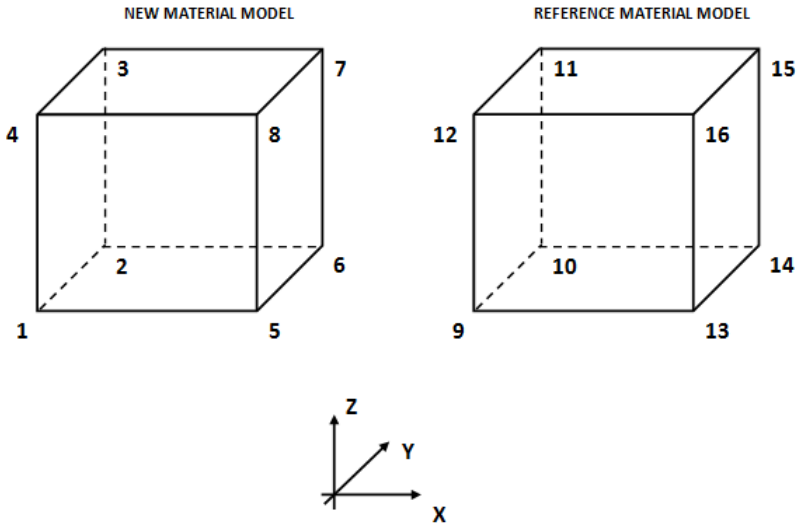

Figure 11 The finite element model used in the single element analysis

7.1.2 Validation of the Elastic Isotropy Formulation

These tests were intended to ensure that the new material model is capable of reproducing isotropic behaviour. For this purpose the Isotropic-Elastic-Plastic-Hydrodynamic material (Liu, 2004) was used as the reference material for comparison with the elastic part of the new material when the same material properties were given for the three principal directions of orthotropy. The reference material was given the same elastic properties and a high value for yield stress in order to prevent the material from yielding for the range of deformations applied. The elastic material properties used in these analyses are given in Table 2.

Table 2 Aluminium material properties for elastic isotropy analysis

Parameter	Description	Nominal value
E	Initial elastic modulus	$71GPa$
ν	Poisson's ratio	0.30
G	Shear modulus	$26.75GPa$
K	Bulk modulus	$69.75GPa$
ρ	Density	$2.81g/cm^3$

The data from the uniaxial stress test, the true stress vs. true strain curves for the x, y and z directions were plotted for both material models (the curves for the x direction are shown in Figure 12). The stress strain curves, in the x direction, for the new and the reference material were identical. The values of Young's modulus calculated from the slopes of the stress strain curves was the same as the value in the input file. Therefore, it can be concluded that the new material model is capable of correctly reproducing uniaxial stress states of elastically isotropic materials.

Near Figure 12

Similarly, the true stress vs. true strain curves, from the uniaxial strain tests, for the reference and the new material for the x, y and z directions were compared. The values for the material stiffness in each direction, calculated from the slopes of these curves, was equal to $K+4G/3$ (where K is bulk modulus and G shear elastic modulus). As illustrated in Figure 13 for the loading in the x direction, the stress strain curves for the new and the reference material were identical. Therefore, it can be concluded that the new material model is capable of correctly reproducing uniaxial strain states for elastically isotropic materials.

Near Figure 13

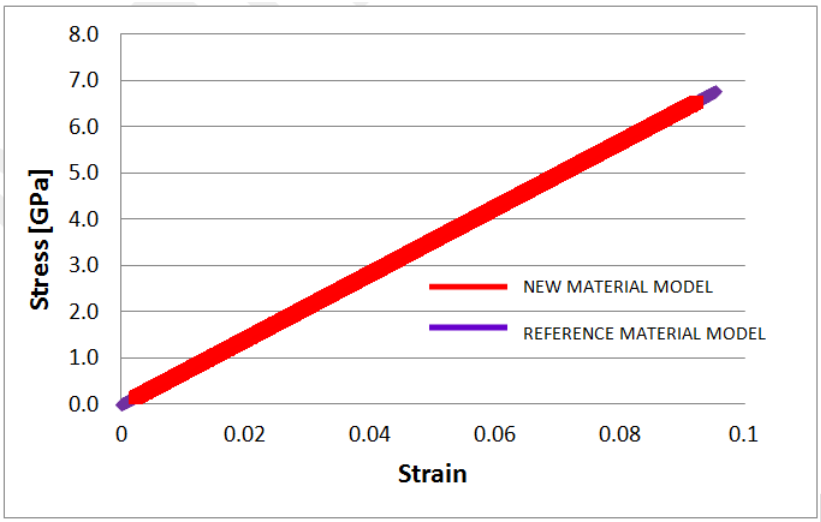

Figure 12 Stress strain curves for reference material (isotropic elastic plastic) and the new material in the x direction; uniaxial stress

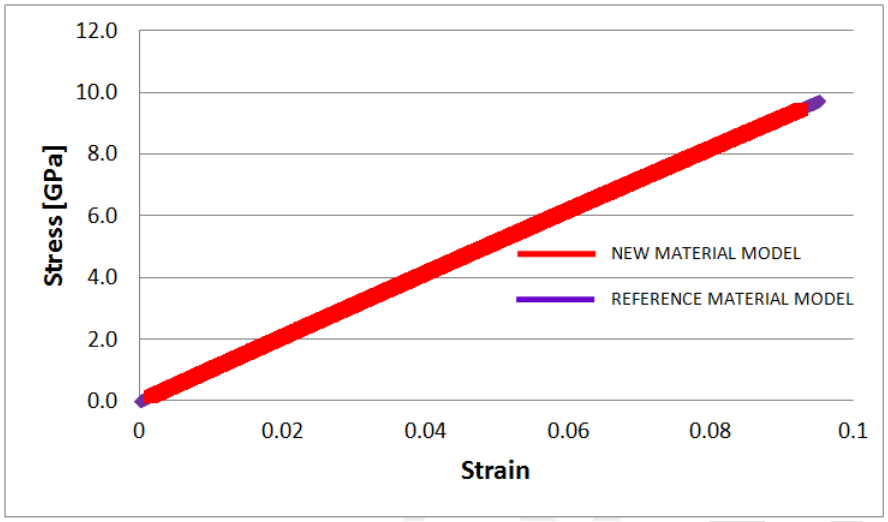

Figure 13 Stress strain curves for reference material (isotropic elastic plastic) and the new material in the x direction; uniaxial strain

7.1.3 Validation of Elastic Orthotropy Formulation

The reference material was elastic orthotropic (DYNA3D material 22) (Liu, 2004). The same two element model, described above, was used but this time with the orthotropic elastic material properties as given in Table 3.

Table 3 Orthotropic material properties of Aluminium alloy

Parameter	Description	Nominal value
E_x	Young's modulus in x direction	$70.6 GPa$
E_y	Young's modulus in y direction	$71.1 GPa$
E_z	Young's modulus in z direction	$60.6 GPa$
ν_{xy}	Poisson's ration	0.342
ν_{zx}	Poisson's ration	0.342
ν_{yz}	Poisson's ration	0.342
G_{xy}	Shear modulus for xy	026.3
G_{yz}	Shear modulus for yz	$26.5 GPa$
G_{zx}	Shear modulus for zx	0.342

The stress strain curves obtained in the uniaxial stress analyses for the new and the reference materials were identical, as illustrated in Figure 14 (for the analysis in the x direction only). The orthotropic elastic material properties determined from the numerically obtained stress strain curves are given in Table 4. The values for Young's module obtained for the new material agree well with the values obtained for the reference material.

Table 4 Comparison of Young's module of elastic orthotropy, uniaxial stress analyses

Material direction	Reference material model	New material model
x	$71.1 GPa$	$71.1 GPa$
y	$71.1 GPa$	$71.1 GPa$
z	$70.58 GPa$	$70.60 GPa$

Near Figure 14

Similarly, the uniaxial strain single element analyses were performed as the next step in the validation of the elastic orthotropic part of the new model. The results of the analyses for the x, y and z directions are given in Table 5. The x direction test stress - strain curves are given in Figure 15.

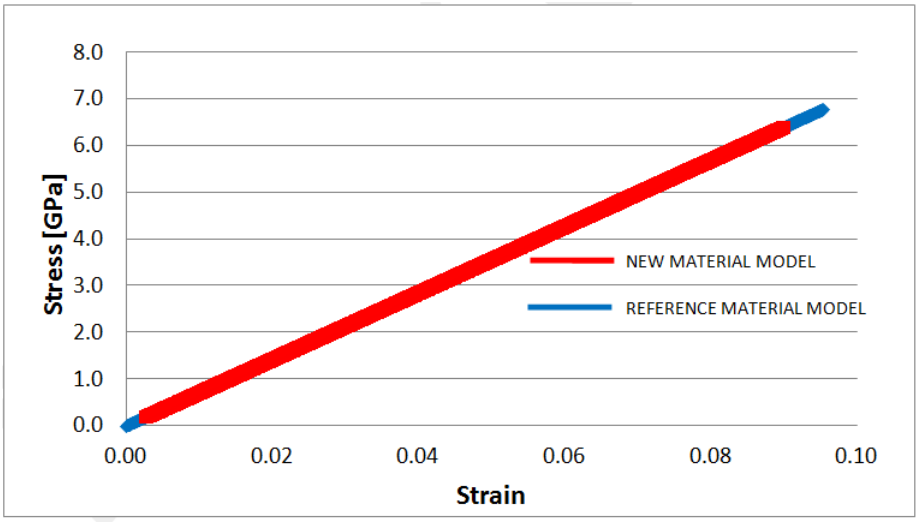

Figure 14 Stress strain curves for elastic orthotropic reference material and the new material, loading in the x direction; uniaxial stress

Table 5 Comparison of Young's modulus of elastic orthotropy, uniaxial strain analyses

Material direction	Reference material model	New material model
x	$110.32 GPa$	$110.30 GPa$
y	$109.44 GPa$	$109.41 GPa$
z	$109.65 GPa$	$109.62 GPa$

Near Figure 15

7.1.4 Validation of Elastic-Plastic part of the model

In this part of the validation process the plasticity part of the new material model was assessed. The first set of tests included validation of the Hill's yield criterion for the isotropic elastic-perfectly plastic material and the second set of tests covered the orthotropic elastic-plastic material with hardening. The first set of tests was performed with isotropic aluminium material properties, while the second set of tests was performed with orthotropic tantalum material properties (a material with pronounced anisotropy). The specific values of the material properties used are given in Table 6 and Table 7, respectively.

In the isotropic material tests Hill's coefficients were given values as follows, $F = G = H = 0.5$ and $L = M = N = 3/2$ in order to reduce the Hill's yield criterion to the von Misses yield criterion. More specifically, Hill's coefficients had to be converted into Lankford parameters $R, P, Q_{ab}, Q_{ba}, Q_{ca}$ given in Table 6 and Table 7, as required by DYNA3D.

Table 6 Aluminium material properties used in the isotropic elastic-plastic analysis

Parameter	Description	Nominal value
$E_x = E_y = E_z$	Young's modulus	$70.6 GPa$
$\nu_{xy} = \nu_{yz} = \nu_{zx}$	Poisson's ration	0.342
$G_{xy} = G_{yz} = G_{zx}$	Shear modulus	$26.48 GPa$
σ_Y	Yield stress in x direction	$564 MPa$
R	Hill's parameter	0.5
P	Hill's parameter	1.0
Q_{bc}	Hill's parameter	1.0
Q_{ba}	Hill's parameter	1.0
Q_{ca}	Hill's parameter	0.5

Table 7 Tantalum material properties used in the orthotropic elastic-plastic analysis

Parameter	Description	Nominal value
E_x	Young's modulus in x direction	$191.35 GPa$

E_y	Young's modulus in y direction	$195.75 GPa$
E_z	Young's modulus in z direction	$208.38 GPa$
ν_{xy}	Poisson's ration	0.371
ν_{yz}	Poisson's ration	0.331
ν_{zx}	Poisson's ration	0.306
G_{xy}	Shear modulus	$70.86 GPa$
G_{yz}	Shear modulus	$62.31 GPa$
G_{zx}	Shear modulus	$64.63 GPa$
σ_Y	Yield stress in reference direction	$172 MPa$
H	Tangent plastic modulus for reference direction	$2.2 GPa$
R	Hill's parameter	1.5760
P	Hill's parameter	1.5760
Q_{bc}	Hill's parameter	0.4125
Q_{ba}	Hill's parameter	0.3553
Q_{ca}	Hill's parameter	0.4049

The prescribed displacement load curves were defined so that the material is first brought to yield in tension and then the loading was reversed to force the material to yield in compression (the reversed loading tests).

In these tests a single element was loaded in tension and compression in the x, y and z directions. The material orthotropic properties were set to isotropic case, i.e. given the same values. The performance of the model was assessed by evaluating the yield stress and the Young's modulus from the output stress strain curves for each direction and in tension and compression. The results of this analysis are shown in Figure 16 for the x direction only. The slope of the initial elastic loading part of the curve was the same as the slope of elastic unloading – loading in compression part of the curve and equal to the inputted Young's modulus E=70.8 GPa.

Near Figure 16

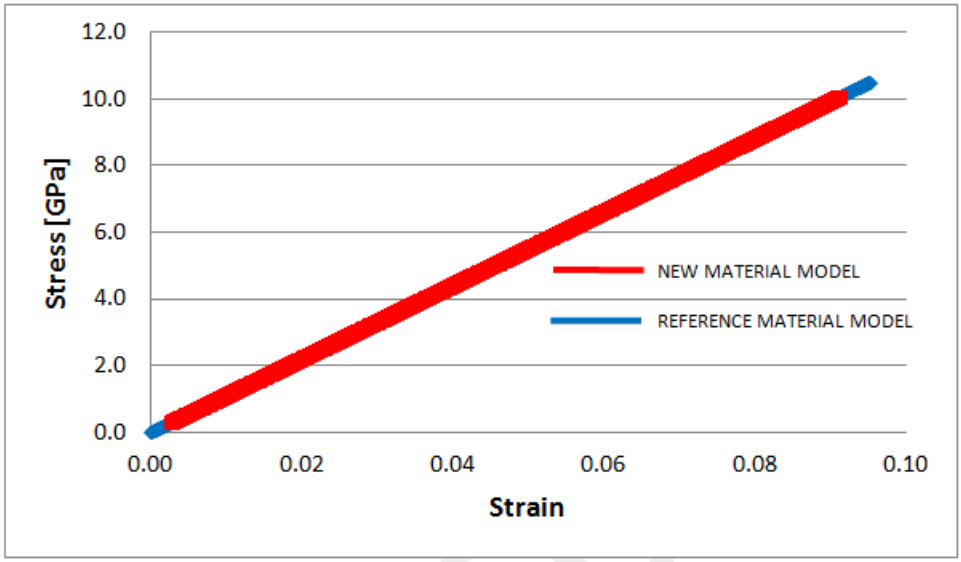

Figure 15 Stress strain curves for elastic orthotropic reference material and the new material, loading in the x direction; uniaxial strain

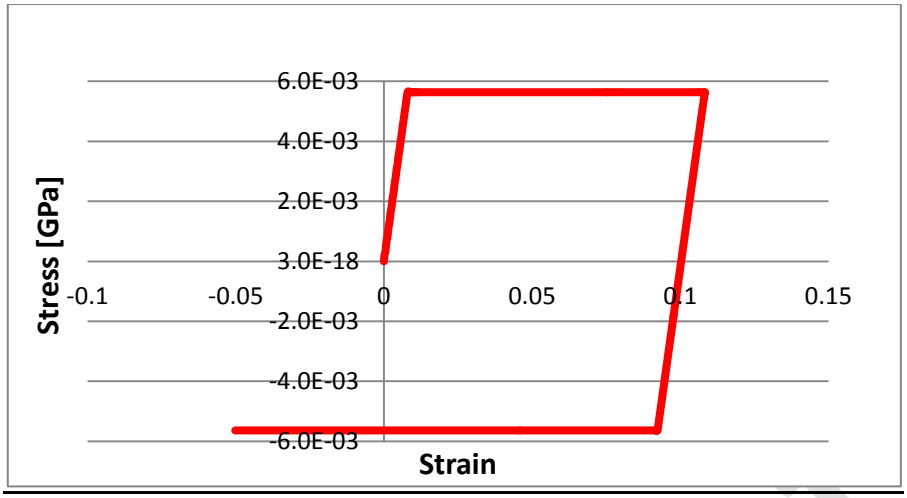

Figure 16 Stress strain curves for elastic –perfectly plastic response of the new material, reversed loading uniaxial stress test in X direction

The results of the above analyses are, summarized in Table 8, represent the evidence that the new material model can accurately reproduce the behaviour of isotropic elastic-perfectly plastic materials (von Misses yield surface) since the yield stress for the x, y and z directions had the same (within the bounds of numerical round off error) values for the three directions.

Table 8 Summary of uniaxial reversed loading test for elastic-perfectly plastic analysis

Parameter	Description	Tension	Compression
E_x	Young's modulus in x direction	$70.6 GPa$	$70.6 GPa$
σ_{Yx}	Yield stress in x direction	$563.9 MPa$	$564 MPa$
E_y	Young's modulus in y direction	$70.6 GPa$	$70.6 GPa$
σ_{Yy}	Yield stress in y direction	$564.1 MPa$	$564 MPa$
E_z	Young's modulus in z direction	$70.58 GPa$	$70.6 GPa$
σ_{Yz}	Yield stress in z direction	$563.8 MPa$	$564 MPa$

The next step was to demonstrate that this material model was capable of describing the elastic-plastic behaviour of hardening metals. The results obtained with the new material model were compared directly with the results produced by the reference orthotropic elastic – plastic material with hardening, which is available in DYNA3D (material 33) (Liu, 2004). To simplify the comparison, the isotropic hardening controlled by the MTS model was switched off and instead the constant tangent plastic modulus given in Table 6 was used to define plastic hardening.

The reversed loading single element tests used in the previous analysis (see Figure 17) were repeated but this time with a linearly hardening material.

Near Figure 17

It can be seen in Figure 17, the stress strain curves obtained by the reference material (elastic-plastic with linear hardening) and the new material were identical for the x direction. The same agreement was obtained for the y and z directions. The yield stress was accurately determined in each of the tests. Furthermore, the slopes of the elastic and plastic parts of the curves for both isotropic and orthotropic cases were correctly calculated by the new model.

The following single element tests were performed in order to validate the MTS hardening law used to control the evolution of the yield surface. For this purpose the new material model, with the MTS hardening law switched on, was used over a range of strain rates and temperatures. The specific elastic and yield surface parameters for Aluminium 7010 used in these analyses are given in , whereas the data for the MTS model is provided in Table 9.

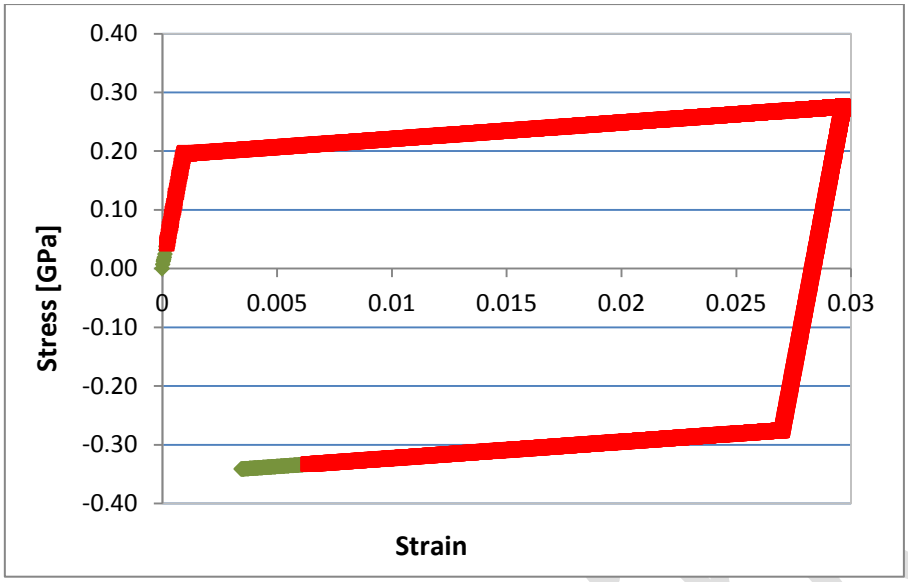

Figure 17 Stress strain curves for elastic – plastic with linear hardening for the reference material and the new material in the *x* direction, reversed loading uniaxial stress test in *x* direction

Table 9 Material model parameters

Parameter	Description	Nominal value
E_1	Initial elastic modulus	71.100 GPa
E_2	Initial elastic modulus	70.326 GPa
E_3	Initial elastic modulus	71.100 GPa
	Damage part of constitutive model	
Y_{10}	Initial damage energy release rate in 1 direction	$(8.62-0.01)MPa$
ω_{t1}	Damage hardening in direction 1	10.29
Y_{20}	Initial damage energy release rate in 2 direction	$(8.78-0.01T)MPa$
ω_{t2}	Damage hardening in direction 2	$5.82Mpa$
Y_{30}	Initial damage energy release rate in 3 direction	$(8.62-0.01T)MPa$
ω_{t3}	Damage hardening in direction 3	$10.29MPa$
σ_0	Threshold stress	$1.05GPa$
u_0	Normalised activation energy	0.0087
t_{c0}	Characteristic time for the threshold stress	$2\mu s$
	Coefficients for Hill's potential	
F	Hill's material constant	0.5524
G	Hill's material constant	0.5447
H	Hill's material constant	0.4553
N	Hill's material constant	1.6870
	Material constants for the MTS material model	
σ_a	Athermal rate independent threshold stress	$10.0\,MPa$
σ_0	Initial plastic stress at zero plastic strain	$600.0\,MPa$
$g_{0\varepsilon}$	Normalised activation energy	1.606
$\dot{\varepsilon}_{0\varepsilon}$	Reference strain rate	$1\times10^{7}\ s^{-1}$
p	Free energy equation exponent	1.0
q	Free energy equation exponent	1.0
A	Saturation stress equation material constant	5.542
$\hat{\sigma}_{s0}$	Saturation stress at 0K	$801.01\ MPa$
$\dot{\varepsilon}_{\varepsilon 0}$	Saturation stress reference strain rate	$1\times10^{7}\ s^{-1}$
a_0	Hardening function constant	$67604.6\ MPa$
a_1	Hardening function constant	$1816.9\ MPa$
a_2	Hardening function constant	$202.3\ MPa$
k	Boltzmann's constant	$1.38\times10^{-23}\,JK^{-1}$
b	Burgers vector	$0.286\times10^{-9}\,m$
b_0	Shear modulus at 0K	$28.83GPa$
b_1	Material constant for shear modulus	$4.45GPa$
b_2	Material constant for shear modulus	$248.5K$
θ_r	Reference temperature	$293.15\ K$
ρ	Density	$2810\ kgm^{-3}$
C_p	Heat capacity	$869\ Jkg^{-1}K^{-1}$

Mie Gruneisen Equation of State		
C_0	Bulk sound speed	0.5386 $cm/\mu s$
S_1	First Hugoniot slope coefficient	1.339
S_3	Third Hugoniot slope coefficient	0
γ_0	Gruneisen coefficient	1.97
B	First order volume correction coefficient	0.48
E_0	Initial internal energy	0.0
V_0	Initial relative volume	1.0

Since DYNA3D does not offer a material model that could be used as a reference material in these validation tests the numerical results were compared with the experimental data from the tensile tests (Panov, 2006).

The validation was performed for the x, y and z directions for strain rates between $6.4\times10^{-4}s^{-1}$ and $6.4\times10^{1}s^{-1}$ and temperature range between $-50^{\circ}C$ and $70^{\circ}C$. In order to illustrate the performance of the model in this validation stage the stress strain curves from the simulated tensile tests in the x direction for the strain rate $6.4s^{-1}$ and temperatures $-50^{\circ}C$ and $+70^{\circ}C$ and for the range of strain rates at $+70^{\circ}C$ are given in Figure 18 and Figure 19, respectively. It can be seen the MTS model is capable of reproducing the stress, strain rate and temperature effects experimentally observed for the orthotropic AA 7010.

Near Figure 18

Near Figure 19

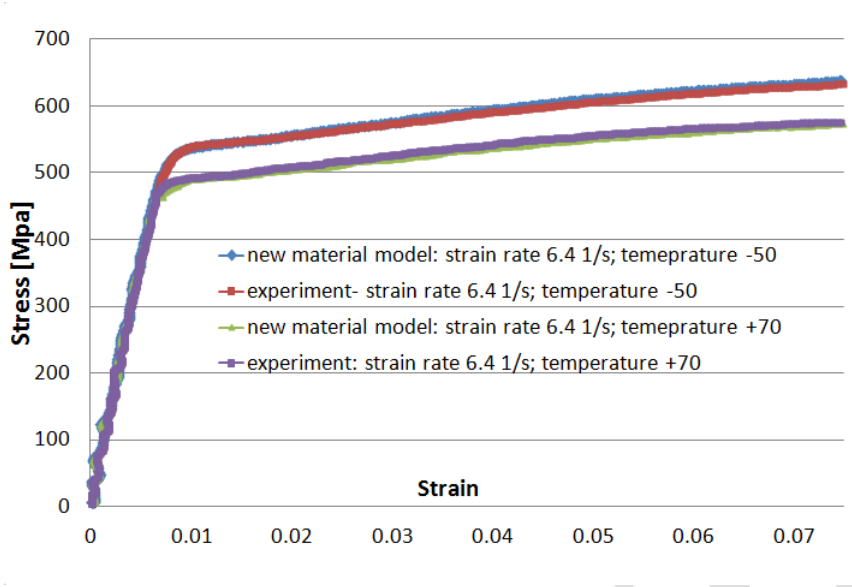

Figure 18 Validation of the new material model against the experimental data obtained in the tensile tests for the strain rate $6.4 s^{-1}$ performed at two temperatures $-50^{\circ}C$ and $+70^{\circ}C$

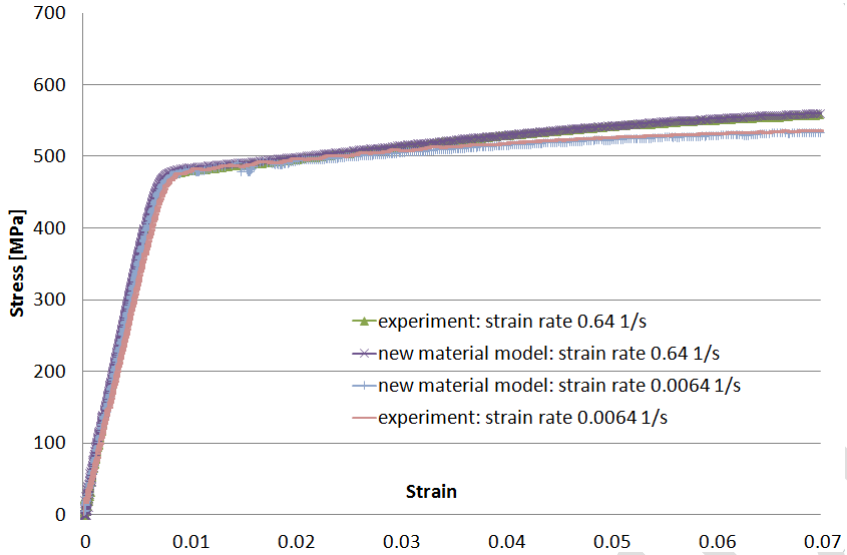

Figure 19 Validation of the new material model against the experimental data obtained in the tensile tests for the range of strain rates performed at temperature $+70^{\circ}C$

7.1.5 Validation of Elastic-Plastic – Damage part of the model

The first stage of the material validation is completed with the validation of the damage model coupled with the orthotropic elastic plastic part of the model with the hardening controlled by MTS. The material parameters for elastic, plastic and damage part of the model, used in these simulations, are given in Table 9. As before, the simulation results were compared directly to the tensile test experimental results, which were performed for the range of strain rates and temperatures. The performance of the model is illustrated in Figure 20 for the strain rate of $6.4s^{-1}$ and two temperatures ($-50^{\circ}C$ and $70^{\circ}C$), from which one can conclude that the new material model accurately reproduced experimentally observed elastic plastic behaviour including damage for orthotropic AA7010.

Near Figure 20

7.1.6 The First Stage Validation Summary

Based on the results generated by the new material model in the first validation stage it can be concluded that the implementation of the new material model into DYNA3D was done correctly. The elastic responses for both isotropic and orthotropic cases were correctly calculated. The implementation of the Hill's yield criterion was also validated as the results were accurate for both isotropic validation cases. The yield points in all analysis involving plastic deformation were accurately determined.

Similarly, the plastic hardening algorithm correctly implemented. The MTS model captured the evolution of the yield surface observed in the experiments for the range of strain rates and temperatures. The damage part of the new model accurately reproduced the experimentally observed stress softening in the tensile tests.

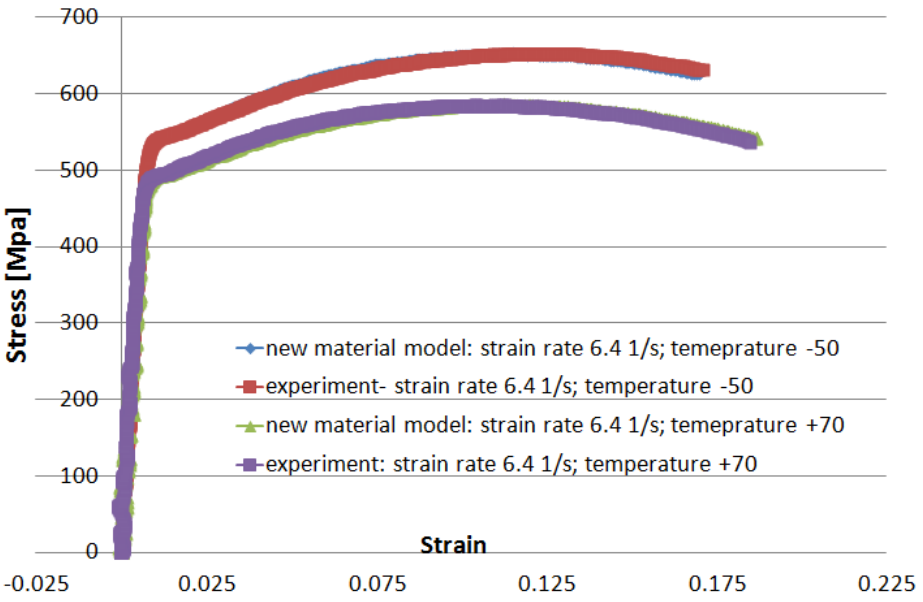

Figure 20 Validation of the new material model against the experimental data obtained in the tensile tests for the strain rate $6.4 s^{-1}$ performed at two temperatures $-50^{\circ}C$ and $+70^{\circ}C$

7.2 The second stage validation

This stage of the new model validation process was done by modelling specific Taylor anvil and plate impact tests and comparing the numerical results with the corresponding experimental data. The experimental results from Taylor anvil tests are described in the Sub Section 7.2.1, whilst their comparison to the numerical results is given in Sub Section 7.2.2. The numerical simulations of the plate impact test are validated in Section 7.2.3.

7.2.1 Taylor anvil experiments

The experimental procedure used in these tests is described in detail in (Panov, 2006). Taylor cylinder specimens used had a diameter D=9.30mm and length L=46.50mm (length-to-diameter ratio, L/D=5) and were manufactured from AA7010 rolled plate. The experimental coordinate system (X, Y, Z) adopted for the tests had the Z-axis aligned with the longitudinal cylinder direction (material rolling direction), as shown in Figure 7.

The tests were performed at velocities of 200 m/s and 214 m/s, using a smooth-bore, single-stage gas gun. Photographs of the side profiles and footprints of the recovered samples are given in Figure 21. Final specimen heights were 42.2 mm for specimen impacted at 200 m/s, and 42.1 mm for the specimen impacted at 214 m/s. The observed elliptical shape of the footprints was a direct consequence of material orthotropy.

Near Figure 21

The recovered deformed specimens were scanned using a 3D scanning machine. This allowed for determination of side profiles and deformed cross-sections along the cylinder length (see Figure 22).

Near Figure 22

Figure 22 provides comparisons between the digitised footprints of initial and post-test geometries for the Taylor specimens. Eccentricity (ratio of major to minor diameters) for the specimen impacted at 200 m/s was 1.04, and for the specimen impacted at 214m/s, was 1.06. Figure 23 shows a comparison of minor and major side profiles of post-test geometry plotted as radial strain vs. distance.

Near Figure 23

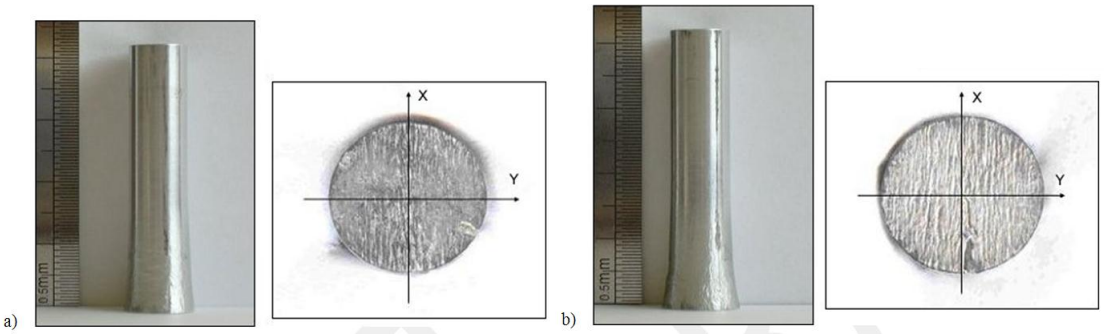

Figure 21 Photographs of the post-test geometry for the AA 7010 Taylor specimen for the impact velocities: a) v=200m/s and b) v=214m/s

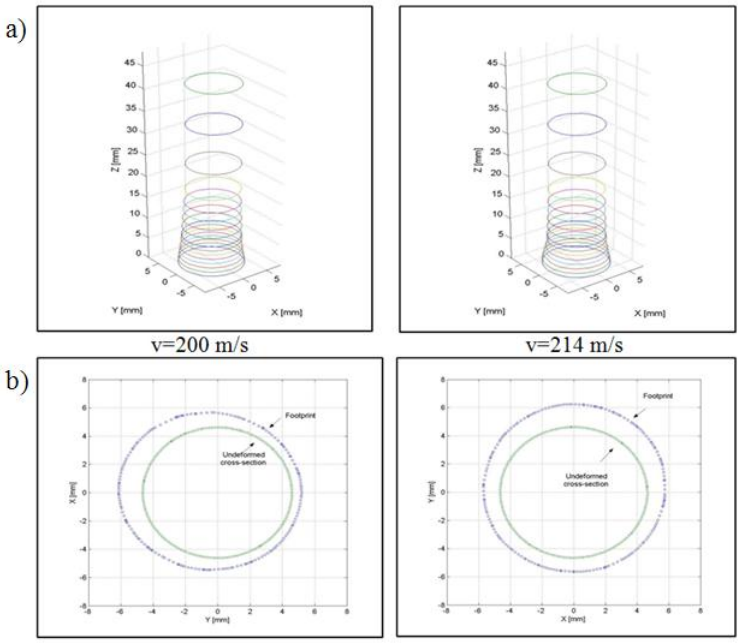

Figure 22 Digitised post-test geometry for the AA 7010 Taylor specimens: a) side profile and b) footprint

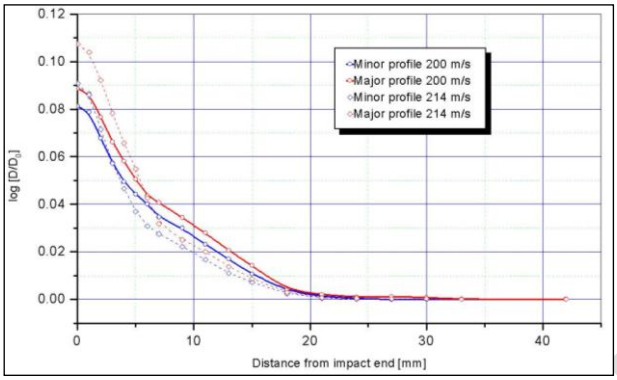

Figure 23 Comparisons of the major and minor side profiles of post-test geometry for the AA 7010 Taylor specimens impacted at 200 m/s and 214 m/s plotted as radial strain vs. distance

7.2.2 Numerical simulations of Taylor anvil tests

Taylor anvil tests are frequently used in validation of constitutive models for metals because in order to accurately reproduce experimental data the model has to accurately capture strain, strain rate and thermal effects and initiation and evolution of damage.

In the validation described below, the Taylor tests model comprised only a quarter of the cylinder due to presence of two plains of symmetry. The cylinder was modelled with 18900 solid elements. Impact velocities of 200 m/s and 214 m/s were simulated. The system of units used in the simulations was cm – g – μs. The material elastic parameters (Young's moduli for principle directions of material orthotropy), parameters for the plasticity and damage model, for AA7010, are given in Table 9. The proposed material model was coupled with the Gruneisen Equation of State, for which material parameters are also given at the end of Table 9.

The post test distribution of damage in Taylor specimen at two response times t= 9 μs and t=25μs, for the impact velocities of 200 m/s are shown in Figure 24. Due to impact, the longitudinal compressive and lateral release waves were generated in the material. Interaction of the release waves results in the high levels of tensile stresses in the centre of the plastically deformed part of the cylinder. The same behaviour was observed by Brünig (Brünig and Driemeier, 2007), in a number of Taylor tests of stainless steel specimens with different initial geometry (length-to-diameter ratio). Following plastic deformation, damage was locally initiated and evolved according to the proposed model. The red elements in Figure 24 indicate failed material. The location and the extent of damage correlate well with damage distribution observed in Taylor tests (Maudlin et al., 1999a; Maudlin et al., 1999b; Bronkhorst et al., 2006).

Near Figure 24

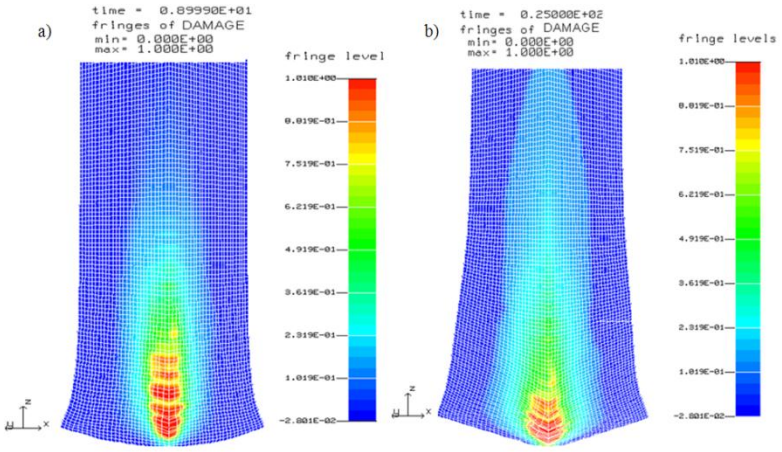

Figure 24 Damage distribution (ω_{eq}) in AA7010 Taylor specimen (a) 9μs and (b) 25μs after the impact at 200m/s

The simulation results and the test data for the specimen post test profiles are compared in Figure 25. In the numerical simulations the plastically deformed zone has propagated slightly further down the cylinder than in the experiments. The two main modelling aspects that lead to this difference are overestimated speed of plastic waves and the initial damage evolution rate slower than the experimentally observed.

The total error $\left|\ln\left(D/D_0\right)_{symulation} - \ln\left(D/D_0\right)_{experimental}\right| \Big/ \ln\left(D/D_0\right)_{experimental}$ integrated over the length of cylinder from 0 to 20mm of the un-deformed cylinder length was 7.98%. The numerically obtained footprint size and shape agree well with the experimental data. Consequently, it can be concluded that the proposed model is capable of accurately modelling elastic and large plastic deformation of orthotropic metals including initiation and evolution of damage.

Near Figure 25

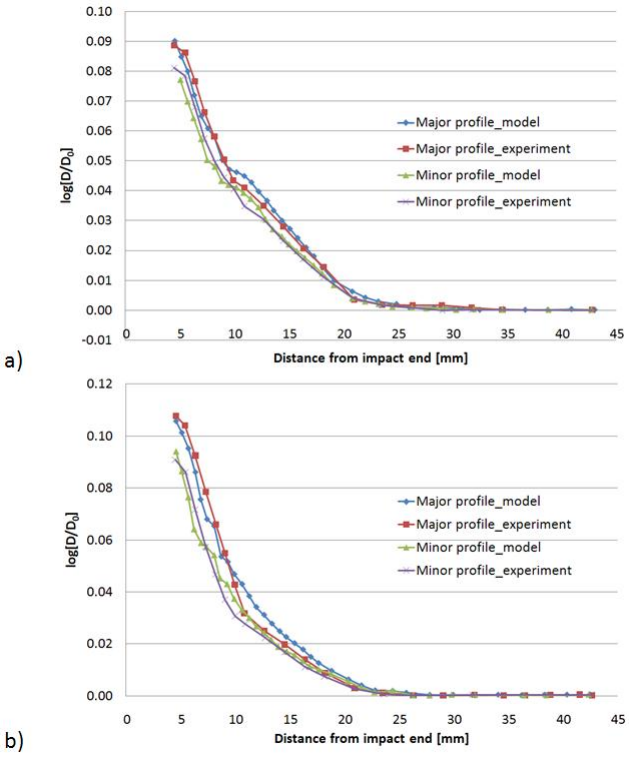

Figure 25 Comparison of experimental and simulation results for major and minor distributions of plastic strains of Taylor cylinder test impacted at a) 200 m/s and b) 214 m/s

7.2.3 Plate impact test

Plate impact test is a standard method conducted at Cranfield University for studying the material behaviour undergoing shock loading (Vignjevic et al., 2002; Gray et al., 2003; Paris et al., 2011). Assuming an ideally parallel contact between the flyer and target plates, a uniaxial strain state is developed in the target material. For a sufficiently high impact velocity this state results in generation and propagation of shock waves in both target and flyer plate. The experimental work consisted of impact tests in the rolling and transverse directions for a range of velocity between 234 m/s and 897 m/s and was published in (Vignjevic et al., 2002). All test trials were conducted with the 2.5 mm thick flyer plates made of aluminium alloy 6082-T6, which impacted a 5 mm thick target plate made of AA7010 alloy. The target plates were supported by a 12 mm thick block of polymethil methacrylate (PMMA).

The symmetry of the geometry and uniaxial loading of these tests allowed for certain simplifications of the FE model, which is illustrated in Figure 26. Each plate was modelled as a rectangular bar with 4x4 elements in cross section and four symmetry boundary conditions defined on the side of the bars. The bars were modelled with the hexagonal solid elements with one integration point: flyer plate was modelled with 24 elements along the impact axes; the target was modelled with 75 elements along the axes and 12 mm thick PMMA was modelled with 99 elements in the impact direction. Surface to surface contact definition was used for the contact between the flyer and target plates.

The flyer plate was modelled with kinematic/isotropic elastic plastic material, available in DYNA3D as material 3 (Liu, 2004), whilst the PMMA was modelled as an isotropic elastic plastic hydrodynamic model (material 10).

Near Figure 26

Two configurations of the target plates were considered: impact in the longitudinal (rolling) direction (rolling direction aligned with the through thickness direction) and impact in the short traverse (the through thickness direction aligned with the traverse direction).

A stress pulse obtained in the numerical simulation is compared to the corresponding stress trace recorded by manganin stress gauge at the back of the target plate. The comparison of the results for the plate impact in longitudinal direction at 455 m/s and impact in the traverse direction at 443m/s are illustrated in Figure 27.

Near Figure 27

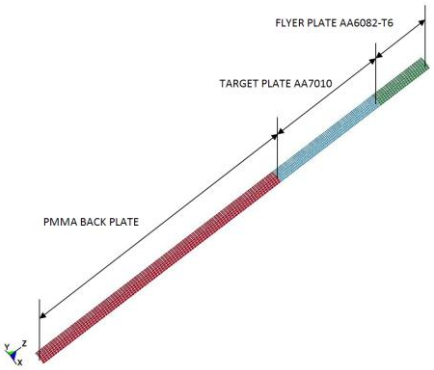

Figure 26 Finite element model of a symmetric plate impact test of AA7010

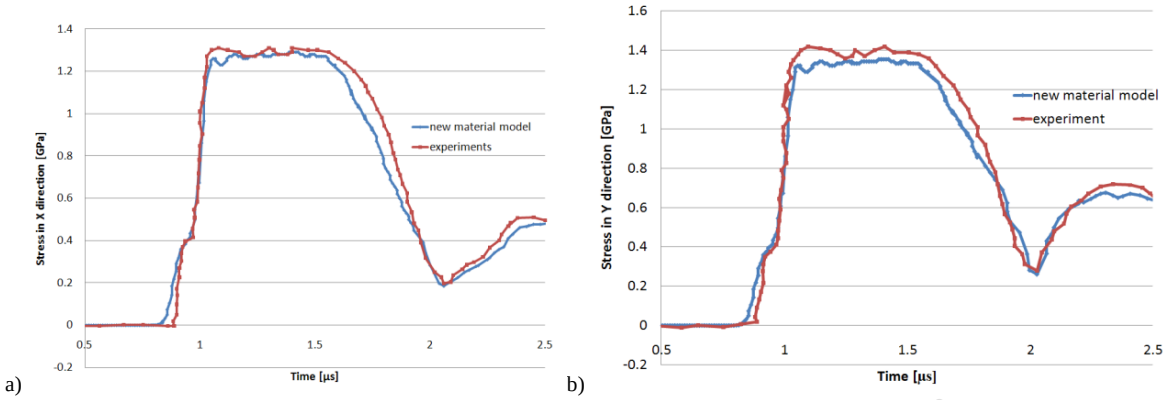

Figure 27 Comparison of experimental data and simulation of the plate impact test: a) in the rolling (longitudinal) direction at 455 m/s and b) in the short traverse direction at 443 m/s

In both test cases considered, the numerical simulations replicated a typical shape of the stress pulse observed in the experiments. More specifically, in the compression phase Hugoniot Elastic Limit was captured accurately for both the longitudinal and the transverse direction. The difference between the numerical and the experimental average longitudinal stress behind the shockwave was 1% for the longitudinal direction and 4% for the transverse direction indicating that the coupling between the strength model and the shock equation of state was done correctly. The release phase (the shape of the unloading part of the curves) is influenced by damage evolution in the material. It can be observed that the new model reproduced accurately the experimentally observed behaviour especially in the vicinity of the spall failure point. The errors in the prediction of spall strengths were 5% for the longitudinal direction and 6% for the transverse direction. Note that the numerically obtained time of the spall agrees well with the experiment. Furthermore, it is important to note that the slops of the post failure reloading part of the curves replicate the experimental data very accurately. These slopes are a direct indicator of the amount of damage present in the material.

8 Conclusions

.

A constitutive model for orthotropic metals is developed in the framework of continuum irreversible thermodynamics with internal variables. The model is integrated in the isoclinic configuration, defined using the multiplicative decomposition of deformation gradient, which allows for modelling finite deformation hyperelastic, plastic and damage problems. Thermodynamic (state and dissipation) potentials, which describe each part of the model behaviour, are given in terms of an irreducible set of orthotropic invariants, using the structural tensors and assuming that the principle direction of elastic plastic and damage orthotropy of the material do not evolve.

The model was implemented into the public domain version of the non-linear finite element code DYNA3D (Liu, 2004) originating from Lawrence Livermore National Laboratory (LLNL).

Validation of the model was done through comparison with relevant existing DYNA3D material models (reference models) and experimental data from tensile, Taylor anvil and plate impact tests. The validation demonstrated that the new model can accurately reproduce results obtained with the reference models for elastic plastic behaviour of isotopic and orthotropic materials. Furthermore, good agreement between the experimental data and the corresponding numerical results demonstrates that the proposed model can accurately capture dynamic elastic plastic behaviour of orthotropic metals including evolution of damage for the cases considered.

The proposed model has a number of novel aspects:

- the definition of damaged configuration and mapping $\bar{\mathbf{F}}_d^{-T} = \left[\mathbf{I} - \bar{\boldsymbol{\omega}}\right]^{-1}$ between the damaged and undamaged configuration, and consequently a definition of damage part of velocity gradient in the form of $\bar{\mathbf{l}}_d = \left(\mathbf{I} - \bar{\boldsymbol{\omega}}\right)^{-1} \dot{\bar{\boldsymbol{\omega}}}$;
- isoclinic configuration which includes kinematics of damage, i.e. damaged intermediate configurations (see Figure 1);
- damage initiation based on critical plastic hardening rate
- damage potential which is defined in terms of set of invariants of tensor Y (see (4.17));
- thermally activated damage evolution, which is "coupled" with (thermally activated) MTS model;
- the use of Taylor impact tests for identification of the coefficients of the Hill's potential.

Acknowledgements: the authors are grateful and would like to acknowledge that this work was sponsored by AWE.

References

Bammann, D. J. and Solanki, K. N. (2010), "On kinematic, thermodynamic, and kinetic coupling of a damage theory for polycrystalline material", *International Journal of Plasticity,* vol. 26, no. 6, pp. 775-793.

Bielski, J., Skrzypek, J. J. and Kuna-Ciskał, H. (2006), "Implementation of a model of coupled elastic-plastic unilateral damage material to finite element code", *International Journal of Damage Mechanics,* vol. 15, no. 1, pp. 5-40.

Binning, M. S. and Partridge, P. G. (1984), "Subzero tensile properties of 7010 aluminium alloy and Ti-6A1-4V and IMI550 titanium alloys in sheet form", *Cryogenics,* vol. 24, no. 2, pp. 97-105.

Boehler, J. P. (1987), "Applications of tensor functions in solid mechanics", *Applications of Tensor Functions in Solid Mechanics,* .

Bronkhorst, C. A., Cerreta, E. K., Xue, Q., Maudlin, P. J., Mason, T. A. and Gray III, G. T. (2006), "An experimental and numerical study of the localization behavior of tantalum and stainless steel", *International Journal of Plasticity,* vol. 22, no. 7, pp. 1304-1335.

Brünig, M. (2001), "A framework for large strain elastic-plastic damage mechanics based on metric transformations", *International Journal of Engineering Science,* vol. 39, no. 9, pp. 1033-1056.

Brünig, M. (2003), "An anisotropic ductile damage model based on irreversible thermodynamics", International Journal of Plasticity, vol. 19, no. 10, pp. 1679-1713.

Brünig, M., Albrecht, D. and Gerke, S. (2011a), "Modeling of ductile damage and fracture behavior based on different micromechanisms", *International Journal of Damage Mechanics,* vol. 20, no. 4, pp. 558-577.

Brünig, M., Albrecht, D. and Gerke, S. (2011b), "Numerical Analyses of Stress-triaxiality-dependent Inelastic Deformation Behavior of Aluminum Alloys", *International Journal of Damage Mechanics*, vol. 20, no. 2, pp. 299-317.

Brünig, M. and Driemeier, L. (2007), "Numerical simulation of Taylor impact tests", *International Journal of Plasticity*, vol. 23, no. 12, pp. 1979-2003.

Brünig, M. and Gerke, S. (2011), "Simulation of damage evolution in ductile metals undergoing dynamic loading conditions", *International Journal of Plasticity*, .

Butcher, B. M. (1968), "Spallation of 6061-T6 Aluminum: Behavior of Dense Media under High Dynamic Pressure", in *Behaviour of Dense Media under High Dynamic Pressure*, Gordon and Breach, New York, pp. 245.

Cazacu, O. and Barlat, F. (2003), "Application of the theory of representation to describe yielding of anisotropic aluminum alloys", *International Journal of Engineering Science*, vol. 41, no. 12, pp. 1367-1385.

Chen, S. and Gray, G. (1996), "Constitutive behavior of tantalum and tantalum-tungsten alloys", *Metallurgical and Materials Transactions A*, vol. 27, no. 10, pp. 2994-3006.

Chen, S.R., Maudlin, P. J. and Gray, G. T. (1998), "Mechanical properties and constitutive relations for molybdenum under high rate deformation, Molybdenum and Molybdenum Alloys", in Crowson, A., Chen, E. S., Shields, J. A., et al (eds.) The Minerals, Metals and Materials Society, Warrenddale, PA, pp. 155-172.

Chen, Y. and Ghosh, S. (2011), "Micromechanical analysis of strain rate-dependent deformation and failure in composite microstructures under dynamic loading conditions", *International Journal of Plasticity*, xx, no. xx, in press

Chevrier, P. (1996), "Spalling of aluminium alloy 7020-T6, experimental and theoretical analysis", *Mechanisms and mechanics of damage and failure*, vol. 1.

Colvin, J. D., Minich, R. W. and Kalantar, D. H. (2009), "A model for plasticity kinetics and its role in simulating the dynamic behavior of Fe at high strain rates", *International Journal of Plasticity*, vol. 25, no. 4, pp. 603-611.

De Borst, R. and Feenstra, P. H. (1990), "Studies in anisotropic plasticity with reference to the hill criterion", *International Journal for Numerical Methods in Engineering*, vol. 29, no. 2, pp. 315-336.

Dillon, O. W. (1967), "Plastic deformation waves and heat generated near the yield point of annealed aluminium", in *Mechanical Behaviour of Materials under Dynamic Loading*, .

Djordjevic, N. (2011), *Modelling of inelastic behaviour of orthotropic materials under dynamic loading including high velocity impact* (PhD thesis), Cranfield University, Cranfield.

Dremin, A. N. and Molodets, A. M. (1985), "On the spall strength of metals", Beijing, Pergamon Press, pp. 13.

Driemeier, L., Brünig, M., Micheli, G. and Alves, M. (2010), "Experiments on stress-triaxiality dependence of material behavior of aluminum alloys", *Mechanics of Materials*, vol. 42, no. 2, pp. 207-217.

Egner, H. and Skoczeń, B. (2010), "Ductile damage development in two-phase metallic materials applied at cryogenic temperatures", *International Journal of Plasticity*, vol. 26, no. 4, pp. 488-506.

Ekh, M., Lillbacka, R. and Runesson, K. (2004), "A model framework for anisotropic damage coupled to crystal (visco)plasticity", *International Journal of Plasticity*, vol. 20, no. 12, pp. 2143-2159.

Farren, W. S. and Taylor, G. I. (1925), "The Heat Developed during Plastic Extension of Metals", *Proceedings of the Royal Society of London.Series A, Containing Papers of a Mathematical and Physical Character*, vol. 107, no. 743, pp. pp. 422-451.

Follansbee, P. S. and Kocks, U. F. (1988), "A constitutive description of the deformation of copper based on the use of the mechanical threshold stress as an internal state variable", *Acta Metallurgica*, vol. 36, no. 1, pp. 81-93.

Furnish, M. D. and Chhabildas, L. C. (1998), "Alumina strength degradation in the elastic regime", *AIP Conference Proceedings*, vol. 429, no. 1, pp. 501-504.

Gerke, S. and Brünig, M. (2010), "Modeling and numerical simulations of rate and temperature-dependent damage and fracture in aluminum alloys", *PAMM*, vol. 10, no. 1, pp. 113-114.

Germain, P. and Lee, E. H. (1973), "On shock waves in elastic-plastic solids", *Journal of the Mechanics and Physics of Solids*, vol. 21, no. 6, pp. 359-382.

Goto, D. M., Bingert, J. F., Chen, S. R., Gray III, G. T. and Garrett Jr., R. K. (2000), "The mechanical threshold stress constitutive-strength model description of HY-100 steel", *Metallurgical and Materials Transactions A: Physical Metallurgy and Materials Science*, vol. 31, no. 8, pp. 1985-1996.

Gray, G. T., Bourne, N. K. and Millett, J. C. F. (2003), "Shock response of tantalum: Lateral stress and shear strength through the front", *Journal of Applied Physics*, vol. 94, no. 10, pp. 6430-6436.

Gray, G., Chen, S. and Vecchio, K. (1999), "Influence of grain size on the constitutive response and substructure evolution of MONEL 400", *Metallurgical and Materials Transactions A*, vol. 30, no. 5, pp. 1235-1247.

Habraken, A. M., Charles, J. F. and Cescotto, S. (1998), "Calibration and validation of an anisotropic elasto-plastic damage model for sheet metal forming", *Damage Mechanics in Engineering Materials*, vol. 46, no. C, pp. 401-420.

Hansen, N. R. and Schreyer, H. L. (1994), "A thermodynamically consistent framework for theories of elastoplasticity coupled with damage", *International Journal of Solids and Structures*, vol. 31, no. 3, pp. 359-389.

Hiermaier, S. J. (2008), *Structures Under Crash and Impact electronic resource : Continuum Mechanics, Discretization and Experimental Characterization*, Springer Science+Business Media, LLC, Boston, MA.

Hill, R., (1950), *The mathematical theory of plasticity*, Clarendon Press, Oxford.

Holzapfel, G. A. (2000), "Nonlinear solid mechanics: A continuum approach for engineering", *Wiley, Chichester, New York, pp xiv*, vol. 455.

Itskov, M. and Aksel, N. (2004), "A constitutive model for orthotropic elasto-plasticity at large strains", *Archive of Applied Mechanics*, vol. 74, no. 1-2, pp. 75-91.

Jaric, J. (1988), *Continuum Mechanics*, IRO Gradjevinska knjiga, Belgrade, YU.

Neil, J. C. and Agnew, S. R. (2009), "Crystal plasticity-based forming limit prediction for non-cubic metals: Application to Mg alloy AZ31B", *International Journal of Plasticity*, vol. 25, no. 3, pp. 379-398.

Kanel, G. I., Zaretsky, E. B., Rajendran, A. M., Razorenov, S. V., Savinykh, A. S. and Paris, V. (2009), "Search for conditions of compressive fracture of hard brittle ceramics at impact loading", *International Journal of Plasticity*, vol. 25, no. 4, pp. 649-670.

Khan, A. S., Kazmi, R. and Farrokh, B. (2007a), "Multiaxial and non-proportional loading responses, anisotropy and modeling of Ti–6Al–4V titanium alloy over wide ranges of strain rates and temperatures", *International Journal of Plasticity*, vol. 23, no. 6, pp. 931-950.

Khan, A. S., Kazmi, R., Farrokh, B. and Zupan, M. (2007b), "Effect of oxygen content and microstructure on the thermo-mechanical response of three Ti–6Al–4V alloys: Experiments and modeling over a wide range of strain-rates and temperatures", *International Journal of Plasticity*, vol. 23, no. 7, pp. 1105-1125.

Khan, A. S., Kazmi, R., Pandey, A. and Stoughton, T. (2009), "Evolution of subsequent yield surfaces and elastic constants with finite plastic deformation. Part-I: A very low work hardening aluminum alloy (Al6061-T6511)", *International Journal of Plasticity*, vol. 25, no. 9, pp. 1611-1625.

Khan, A. S. and Meredith, C. S. (2010), "Thermo-mechanical response of Al 6061 with and without equal channel angular pressing (ECAP)", *International Journal of Plasticity*, vol. 26, no. 2, pp. 189-203.

Klepaczko, J. R. (1990), "Dynamic crack initiation, some experimental methods and modelling", in Klepaczko, J. R. (ed.) *Crack dynamics in metallic materials*, Springer-Verlag, Vienna, pp. 428-445.

Krajcinovic, D. (1996), *Damage mechanics*, Elsevier, Amsterdam ; New York.

Krajcinovic, D. (1989), "Damage mechanics", *Mechanics of Materials*, vol. 8, no. 2-3, pp. 117-197.

Lemaitre, J. and Chaboche, J. (1990), *Mechanics of solid materials*, Cambridge University Press, Cambridge.

Li, Y. and Karr, D. G. (2009), "Prediction of ductile fracture in tension by bifurcation, localization, and imperfection analyses", *International Journal of Plasticity*, vol. 25, no. 6, pp. 1128-1153.

Li, Y. and Wierzbicki, T. (2010), "Prediction of plane strain fracture of AHSS sheets with post-initiation softening", *International Journal of Solids and Structures*, vol. 47, no. 17, pp. 2316-2327.

Liu, J., (2004), *Dyna3D: A Nonlinear, Explicit, Three-Dimensional Finite Element Code for Solid and Structural Mechanics*, University of California, Lawrence Livermore National Laboratory, Livermore, (CA) USA.

Lubliner, J. (1972), "On the thermodynamic foundations of non-linear solid mechanics", *International Journal of Non-Linear Mechanics*, vol. 7, no. 3, pp. 237-254.

Malo, K. A., Hopperstad, O. S. and Lademo, O. G. (1998), "Calibration of anisotropic yield criteria using uniaxial tension tests and bending tests", *Journal of Materials Processing Technology*, vol. 80-81, pp. 538-544.

Malvern, L. E. (1969), *Introduction to the mechanics of a continuous medium*, Prentice-Hall, Englewood Cliffs ; London.

Man, C. (1995), "On the correlation of elastic and plastic anisotropy in sheet metals", *Journal of Elasticity*, vol. 39, no. 2, pp. 165-173.

Mandel, J. (1974), "Thermodynamics and plasticity", *Foundations of Continuum Thermodynamics*, , pp. 283-304.

Mandel, J. (1972), *Plasticite classique et viscoplasticite*. CISM course no. 97 ed, Springer, Vienna.

Maudlin, P. J., Bingert, J. F., House, J. W. and Chen, S. R. (1999a), "On the modeling of the Taylor cylinder impact test for orthotropic textured materials: Experiments and simulations", *International Journal of Plasticity*, vol. 15, no. 2, pp. 139-166.

Maudlin, P. J., Gray III, G. T., Cady, C. M. and Kaschner, G. C. (1999b), "High-rate material modelling and validation using the Taylor cylinder impact test", *Philosophical Transactions of the Royal Society A: Mathematical, Physical and Engineering Sciences*, vol. 357, no. 1756, pp. 1707-1729.

Menzel, A. and Steinmann, P. (2007), "On configurational forces in multiplicative elastoplasticity", *International Journal of Solids and Structures*, vol. 44, no. 13, pp. 4442-4471.

Meredith, C. S. and Khan, A. S. (2011), "Texture evolution and anisotropy in the thermo-mechanical response of UFG Ti processed via equal channel angular pressing", *International Journal of Plasticity*, xx, no xx. in press.

Meyers, M. A. (1994), *Dynamic Behaviour of Materials*, John Waley & Sons, Inc., New York.

Minich, R., Cazamias, J., Kumar, M. and Schwartz, A. (2004), "Effect of microstructural length scales on spall behavior of copper", *Metallurgical and Materials Transactions A*, vol. 35, no. 9, pp. 2663-2673.

Murakami, S. (1988), "Mechanical modeling of material damage", *Journal of Applied Mechanics, Transactions ASME*, vol. 55, no. 2, pp. 280-286.

Nakamachi, E., Tam, N. N. and Morimoto, H. (2007), "Multi-scale finite element analyses of sheet metals by using SEM-EBSD measured crystallographic RVE models", *International Journal of Plasticity*, vol. 23, no. 3, pp. 450-489.

Neil, C. J., Wollmershauser, J. A., Clausen, B., Tomé, C. N. and Agnew, S. R. (2010), "Modeling lattice strain evolution at finite strains and experimental verification for copper and stainless steel using in situ neutron diffraction", *International Journal of Plasticity*, vol. 26, no. 12, pp. 1772-1791.

Nicot, F., Sibille, L. and Darve, F. (2012), "Failure in rate-independent granular materials as a bifurcation toward a dynamic regime", *International Journal of Plasticity,* vol. 29, no. 1, pp. 136-154.

Panov, V. (2006), *Modelling of Behaviour of Metals at High Strain Rates* (PhD thesis), Cranfield University, Cranfield, UK.

Paris, V., Kalabukhov, S., Dariel, M. P., Frage, N. and Zaretsky, E. (2011), "High strain rate behavior of spark plasma sintered magnesium aluminate spinel", *International Journal of Impact Engineering,* vol. 38, no. 11, pp. 910-917.

Pereda, J. J., Aravas, N. and Bassani, J. L. (1993), "Finite deformations of anisotropic polymers", *Mechanics of Materials,* vol. 15, no. 1, pp. 3-20.

Reese, S. and Vladimirov, I. N. (2008), "Anisotropic Modelling of Metals in Forming Processes", *IUTAM Symposium on Theoretical, Computational and Modelling Aspects of Inelastic Media,* vol. 11, pp. 175-184.

Rosakis, P., Rosakis, A. J., Ravichandran, G. and Hodowany, J. (2000), "Thermodynamic internal variable model for the partition of plastic work into heat and stored energy in metals", *Journal of the Mechanics and Physics of Solids,* vol. 48, no. 3, pp. 581-607.

Rosenberg, Z., Luttwak, G., Yeshurun, Y. and Partom, Y. (1983), "Spall studies of differently treated 2024A1 specimens", *Journal of Applied Physics,* vol. 54, no. 5, pp. 2147-2152.

Rubin, M. B. (1990), "Analysis of weak shocks in 6061-T6 aluminium", in Schmidt, S. C., Johnson, J. N. and Davison, L. W. (eds.) *Shock Waves in Condensed Matter-1989,* American Institute of Physics, New York, pp. 321-328.

Sansour, C. and Bocko, J. (2003), "On the numerical implications of multiplicative inelasticity with an anisotropic elastic constitutive law", *International Journal for Numerical Methods in Engineering,* vol. 58, no. 14, pp. 2131-2160.

Schmidt, R. M., Davies, F. W., Lempriere, B. M. and Holsapple, K. A. (1978), "Temperature dependent spall threshold of four metal alloys", *Journal of Physics and Chemistry of Solids,* vol. 39, no. 4, pp. 375-385.

Sinha, S. and Ghosh, S. (2006), "Modeling cyclic ratcheting based fatigue life of HSLA steels using crystal plasticity FEM simulations and experiments", *International Journal of Fatigue,* vol. 28, no. 12, pp. 1690-1704.

Sitko, M., Skoczeń, B. and Wróblewski, A. (2010), "FCC-BCC phase transformation in rectangular beams subjected to plastic straining at cryogenic temperatures", *International Journal of Mechanical Sciences,* vol. 52, no. 7, pp. 993-1007.

Skoczeń, B., Bielski, J., Sgobba, S. and Marcinek, D. (2010), "Constitutive model of discontinuous plastic flow at cryogenic temperatures", *International Journal of Plasticity,* vol. 26, no. 12, pp. 1659-1679.

Smallman, R. E. (1985), *Modern physical metallurgy,* 4th ed, Butterworths, London.

Spencer, A. J. M. (1971), "Theory of invariants", *In Continuum Physics (Ed.A.C.Bringen), Vol.I.* Academic Press: New York., .

Steinberg, D. J. (1991), *Equation of state and strength properties of selected materials*, UCRL-MA-106439, Lawrence Livermore National Laboratory.

Stevens, A. L. and Tuler, F. R. (1971), "Effect of shock precompression on the dynamic fracture strength of 1020 steel and 6061-T6 aluminum", *Journal of Applied Physics*, vol. 42, no. 13, pp. 5665-5670.

Stojanovic, R., Djuric, S. and Vujosevic, L. (1964), "On finite thermal deformations", *Archiwum Mechaniki Stosowanej / Archives of Mechanics*, vol. 16, pp. 103-108.

Szczepiński, W. and Miastkowski, J. (1968), "An experimental study of the effect of the prestraining history on the yield surfaces of an aluminium alloy", *Journal of the Mechanics and Physics of Solids*, vol. 16, no. 3, pp. 153-162.

Vignjevic, R., Bourne, N. K., Millett, J. C. F. and De Vuyst, T. (2002), "Effects of orientation on the strength of the aluminum alloy 7010-T6 during shock loading: Experiment and simulation", *Journal of Applied Physics*, vol. 92, no. 8, pp. 4342-4348.

Vignjevic, R., Campbell, J. C., Bourne, N. K. and Djordjevic, N. (2008), "Modeling shock waves in orthotropic elastic materials", *Journal of Applied Physics*, vol. 104, no. 4.

Vladimirov, I. N., Pietryga, M. P. and Reese, S. (2008), "On the modelling of non-linear kinematic hardening at finite strains with application to springback - Comparison of time integration algorithms", *International Journal for Numerical Methods in Engineering*, vol. 75, no. 1, pp. 1-28.

Vujosevic, L. and Lubarda, V. A. (2002), "Finite-strain thermoelasticity based on multiplicative decomposition of deformation gradient", *Theoretical and Applied Mechanics*, vol. 28-29, pp. 379-399.

Zaretsky, E. B. and Kanel, G. I. (2011), "Plastic flow in shock-loaded silver at strain rates from 10[sup 4]s[sup - 1] to 10[sup 7]s[sup - 1] and temperatures from 296 K to 1233 K", *Journal of Applied Physics*, vol. 110, no. 7, pp. 073502.

Zhu, Y. Y. and Cescotto, S. (1995), "A fully coupled elasto-visco-plastic damage theory for anisotropic materials", *International Journal of Solids and Structures*, vol. 32, no. 11, pp. 1607-1641.

Appendix A

Constitutive equations for hyperelastic response of orthotropic material

The Helmholtz free energy function, assuming that the function exists, must be invariant to the rigid body rotation (Malvern, 1969). For an orthotropic material, the free energy is a function of

structural tensors in addition to deformation and temperature. A convenient isotropic form of free energy function is given in terms of irreducible set of invariants (Boehler, 1987; Spencer, 1971), for which the material symmetry restrictions are automatically satisfied. The irreducible set for orthotropic materials consists of the following seven invariants:

$$J_1 = \mathbf{I}:\bar{\mathbf{E}}_e \qquad J_2 = \mathbf{I}:\bar{\mathbf{E}}_e^2 \qquad (1.1)$$
$$J_3 = \mathbf{I}:\bar{\mathbf{E}}_e^3$$
$$J_4 = \mathbf{I}:\left(\bar{\mathbf{M}}^1\bar{\mathbf{E}}_e\right) \qquad J_5 = \mathbf{I}:\left(\bar{\mathbf{M}}^1\bar{\mathbf{E}}_e^2\right)$$
$$J_6 = \mathbf{I}:\left(\bar{\mathbf{M}}^2\bar{\mathbf{E}}_e\right) \qquad J_7 = \mathbf{I}:\left(\bar{\mathbf{M}}^2\bar{\mathbf{E}}_e^2\right)$$

The structural tensors and elastic Green-Lagrange strain tensors are given in the isoclinic configuration. Note that $\bar{\mathbf{E}}_e = \mathbf{0}$ and $\bar{\mathbf{S}} = \mathbf{0}$ for elastically undeformed material. Consequently the free energy function should satisfy this initial condition and is given in a quadratic form as:

$$\bar{\psi}\left(\bar{\mathbf{E}}_e, \bar{\mathbf{M}}^1, \bar{\mathbf{M}}^2, \theta\right) = \frac{1}{2}\alpha_1 J_1^2 + \alpha_2 J_2 + \frac{1}{2}\alpha_3 J_4^2 + \alpha_4 J_5 + \frac{1}{2}\alpha_5 J_6^2 + \alpha_6 J_7 + \alpha_7 J_1 J_4 + \alpha_8 J_1 J_6 + \alpha_9 J_4 J_6 \qquad (A.2)$$

where α_1 to α_9 are linearly independent material constants required for orthotropic materials. Stress tensor is defined as:

$$\bar{\mathbf{S}} = \frac{\partial \bar{\psi}}{\partial \bar{\mathbf{E}}_e} = \alpha_1 J_1 \frac{\partial J_1}{\partial \bar{\mathbf{E}}_e} + \alpha_2 \frac{\partial J_2}{\partial \bar{\mathbf{E}}_e} + \alpha_3 J_4 \frac{\partial J_4}{\partial \bar{\mathbf{E}}_e} + \alpha_4 \frac{\partial J_5}{\partial \bar{\mathbf{E}}_e} + \alpha_5 J_6 \frac{\partial J_6}{\partial \bar{\mathbf{E}}_e} + \alpha_6 \frac{\partial J_7}{\partial \bar{\mathbf{E}}_e} + \alpha_7 J_4 \frac{\partial J_1}{\partial \bar{\mathbf{E}}_e} + \alpha_7 J_1 \frac{\partial J_4}{\partial \bar{\mathbf{E}}_e} + \alpha_8 J_6 \frac{\partial J_1}{\partial \bar{\mathbf{E}}_e} + \alpha_8 J_1 \frac{\partial J_6}{\partial \bar{\mathbf{E}}_e} + \alpha_9 J_6 \frac{\partial J_4}{\partial \bar{\mathbf{E}}_e} + \alpha_9 J_4 \frac{\partial J_6}{\partial \bar{\mathbf{E}}_e} \qquad (A.3)$$

where the expressions for the derivatives of invariants are given in (A.11) at the end of this Appendix, so the result is obtained in the following form:

$$\bar{\mathbf{S}} = \alpha_1\left(\mathbf{I}:\bar{\mathbf{E}}_e\right)\mathbf{I} + 2\alpha_2\bar{\mathbf{E}}_e + \alpha_3\left(\mathbf{I}:\left(\bar{\mathbf{M}}^1\bar{\mathbf{E}}_e\right)\right)\bar{\mathbf{M}}^1 + \alpha_4\left(\bar{\mathbf{M}}^1\bar{\mathbf{E}}_e + \bar{\mathbf{E}}_e\bar{\mathbf{M}}^1\right) + \alpha_5\left(\mathbf{I}:\left(\bar{\mathbf{M}}^2\bar{\mathbf{E}}_e\right)\right)\bar{\mathbf{M}}^2 + \alpha_6\left(\bar{\mathbf{M}}^2\bar{\mathbf{E}}_e + \bar{\mathbf{E}}_e\bar{\mathbf{M}}^2\right) + \alpha_7\left(\mathbf{I}:\bar{\mathbf{M}}^1\bar{\mathbf{E}}_e\right)\mathbf{I} + \alpha_7\left(\mathbf{I}:\bar{\mathbf{E}}_e\right)\bar{\mathbf{M}}^1 + \alpha_8\left(\mathbf{I}:\bar{\mathbf{M}}^2\bar{\mathbf{E}}_e\right)\mathbf{I} + \alpha_8\left(\mathbf{I}:\bar{\mathbf{E}}_e\right)\bar{\mathbf{M}}^2 + \alpha_9\left(\mathbf{I}:\bar{\mathbf{M}}^2\bar{\mathbf{E}}_e\right)\bar{\mathbf{M}}^1 + \alpha_9\left(\mathbf{I}:\bar{\mathbf{M}}^1\bar{\mathbf{E}}_e\right)\bar{\mathbf{M}}^2 \qquad (A.4)$$

Similarly, stiffness tensor is defined as a derivative of stress with respect to the elastic strain:

$$\bar{\mathbb{C}} = \frac{\partial \bar{\mathbf{S}}}{\partial \bar{\mathbf{E}}_e} = \alpha_1 \frac{\partial J_1}{\partial \bar{\mathbf{E}}_e}\frac{\partial J_1}{\partial \bar{\mathbf{E}}_e} + \alpha_2 \frac{\partial^2 J_2}{\partial \bar{\mathbf{E}}_e \partial \bar{\mathbf{E}}_e} + \alpha_3 \frac{\partial J_4}{\partial \bar{\mathbf{E}}_e}\frac{\partial J_4}{\partial \bar{\mathbf{E}}_e} + \alpha_4 \frac{\partial^2 J_5}{\partial \bar{\mathbf{E}}_e \partial \bar{\mathbf{E}}_e} + \alpha_5 \frac{\partial J_6}{\partial \bar{\mathbf{E}}_e}\frac{\partial J_6}{\partial \bar{\mathbf{E}}_e} + \alpha_6 \frac{\partial^2 J_7}{\partial \bar{\mathbf{E}}_e \partial \bar{\mathbf{E}}_e} + \alpha_7\left(\frac{\partial J_1}{\partial \bar{\mathbf{E}}_e}\frac{\partial J_4}{\partial \bar{\mathbf{E}}_e} + \frac{\partial J_4}{\partial \bar{\mathbf{E}}_e}\frac{\partial J_1}{\partial \bar{\mathbf{E}}_e}\right) + \alpha_8\left(\frac{\partial J_1}{\partial \bar{\mathbf{E}}_e}\frac{\partial J_6}{\partial \bar{\mathbf{E}}_e} + \frac{\partial J_6}{\partial \bar{\mathbf{E}}_e}\frac{\partial J_1}{\partial \bar{\mathbf{E}}_e}\right) + \alpha_9\left(\frac{\partial J_4}{\partial \bar{\mathbf{E}}_e}\frac{\partial J_6}{\partial \bar{\mathbf{E}}_e} + \frac{\partial J_6}{\partial \bar{\mathbf{E}}_e}\frac{\partial J_4}{\partial \bar{\mathbf{E}}_e}\right) \qquad (A.5)$$

When the derivatives (A.11) and (A.12) are substituted in (A.5), the stiffness tensor in classic tensorial and index notation is written as:

$$\bar{\mathbb{C}} = \alpha_1\mathbf{I}\otimes\mathbf{I} + 2\alpha_2\mathbb{I} + \alpha_3\bar{\mathbf{M}}^1\otimes\bar{\mathbf{M}}^1 + \alpha_5\bar{\mathbf{M}}^2\otimes\bar{\mathbf{M}}^2 + \alpha_4\mathbb{F}^1 + \alpha_6\mathbb{F}^2 + \alpha_7\left(\mathbf{I}\otimes\bar{\mathbf{M}}^1 + \bar{\mathbf{M}}^1\otimes\mathbf{I}\right) + \alpha_8\left(\mathbf{I}\otimes\bar{\mathbf{M}}^2 + \bar{\mathbf{M}}^2\otimes\mathbf{I}\right) + \alpha_9\left(\bar{\mathbf{M}}^1\otimes\bar{\mathbf{M}}^2 + \bar{\mathbf{M}}^2\otimes\bar{\mathbf{M}}^1\right) \qquad (A.6)$$

$$\begin{aligned}\bar{\mathbb{C}}_{IJKL} &= \alpha_1\left(\delta_{IJ}\delta_{KL}\right)+2\alpha_2\left(\delta_{IK}\delta_{JL}\right)+\alpha_3\left(\bar{\mathbf{M}}^1_{IJ}\bar{\mathbf{M}}^1_{KL}\right)+\alpha_5\left(\bar{\mathbf{M}}^2_{IJ}\bar{\mathbf{M}}^2_{KL}\right)+\\ &\alpha_4\left(\delta_{IK}\bar{\mathbf{M}}^1_{JL}+\bar{\mathbf{M}}^1_{IK}\delta_{JL}\right)+\alpha_6\left(\delta_{IK}\bar{\mathbf{M}}^2_{JL}+\bar{\mathbf{M}}^2_{IK}\delta_{JL}\right)+\alpha_7\left(\delta_{IJ}\bar{\mathbf{M}}^1_{KL}+\bar{\mathbf{M}}^1_{IJ}\delta_{KL}\right)+\\ &\alpha_8\left(\delta_{IJ}\bar{\mathbf{M}}^2_{KL}+\bar{\mathbf{M}}^2_{IJ}\delta_{KL}\right)+\alpha_9\left(\bar{\mathbf{M}}^1_{IJ}\otimes\bar{\mathbf{M}}^2_{KL}+\bar{\mathbf{M}}^2_{IJ}\otimes\bar{\mathbf{M}}^1_{KL}\right)\end{aligned} \tag{A.7}$$

Expressions (A.2), (A.4) and (A.6) determine the constitutive model for hyperelastic response, whose principle axes of anisotropy do not evolve during the inelastic deformation.

Owing to the symmetry of the stress and strain tensor, stiffness tensor (A.6) and (A.7) can be written in the Voigt notation:

$$\bar{\mathbb{C}}=\begin{bmatrix} c_{1111} & c_{1122} & c_{1133} & 0 & 0 & 0\\ c_{1122} & c_{2222} & c_{2233} & 0 & 0 & 0\\ c_{1133} & c_{2233} & c_{3333} & 0 & 0 & 0\\ 0 & 0 & 0 & c_{1212} & 0 & 0\\ 0 & 0 & 0 & 0 & c_{2323} & 0\\ 0 & 0 & 0 & 0 & 0 & c_{3131} \end{bmatrix}=\begin{bmatrix} c_{11} & c_{12} & c_{13} & 0 & 0 & 0\\ c_{12} & c_{22} & c_{23} & 0 & 0 & 0\\ c_{13} & c_{23} & c_{33} & 0 & 0 & 0\\ 0 & 0 & 0 & c_{44} & 0 & 0\\ 0 & 0 & 0 & 0 & c_{55} & 0\\ 0 & 0 & 0 & 0 & 0 & c_{66} \end{bmatrix} \tag{A.8}$$

The relationships between the coefficients in the matrix form (A.8) and the coefficients in the invariance representation (A.6) and (A.7) are calculated as:

$$\begin{aligned} c_{11} &= \alpha_1+2\alpha_2+\alpha_3+2\alpha_4+2\alpha_7 & c_{12} &= \alpha_1+\alpha_7+\alpha_8+\alpha_9\\ c_{22} &= \alpha_1+2\alpha_2+\alpha_5+2\alpha_6+2\alpha_8 & c_{33} &= \alpha_1+2\alpha_2\\ c_{13} &= \alpha_1+\alpha_7 & c_{23} &= \alpha_1+\alpha_8 \end{aligned} \tag{A.9}$$

Or, expressed in terms of coefficients from α_1 to α_9 as:

$$\begin{aligned} \alpha_1 &= c_{33}-2\alpha_2 = c_{33}+c_{44}-c_{55}-c_{66} & \alpha_2 &= \frac{1}{2}\left(c_{55}+c_{66}-c_{44}\right)\\ \alpha_3 &= c_{11}-\alpha_1-2\alpha_2-2\alpha_4-2\alpha_7 = c_{11}+c_{33}-2c_{66}-2c_{13} & \alpha_4 &= c_{66}-2\alpha_2 = c_{44}-c_{55}\\ \alpha_5 &= c_{22}-\alpha_1-2\alpha_2-2\alpha_6-2\alpha_8 = c_{22}+c_{33}-2c_{55}-2c_{23} & \alpha_6 &= c_{55}-2\alpha_2 = c_{44}-c_{66}\\ \alpha_7 &= c_{13}-\alpha_1 = c_{13}-c_{33}-c_{44}+c_{55}+c_{66} & \alpha_8 &= c_{23}-\alpha_1 = c_{23}-c_{33}-c_{44}+c_{55}+c_{66}\\ \alpha_9 &= c_{12}-\alpha_1-\alpha_7-\alpha_8 = c_{12}-c_{13}-c_{23}+c_{33}+c_{44}-c_{55}-c_{66} \end{aligned} \tag{A.10}$$

Derivatives of the strain invariants for the hyperelastic part of constitutive model

Derivative of a tensor of the second order with respect to itself is an identity tensor of the forth order (Malvern, 1969), so the derivatives of invariants (1.1) with respect to the elastic strain are obtained as:

$$\begin{aligned} \frac{\partial J_1}{\partial\bar{\mathbf{E}}_e} &= \frac{\partial}{\partial\bar{\mathbf{E}}_e}\left(\mathbf{I}:\bar{\mathbf{E}}_e\right)=\left(\mathbf{I}:\mathbb{I}\right)=\mathbf{I} & \frac{\partial J_2}{\partial\bar{\mathbf{E}}_e} &= \frac{\partial}{\partial\bar{\mathbf{E}}_e}\left(\mathbf{I}:\bar{\mathbf{E}}_e^2\right)=\frac{\partial}{\partial\bar{\mathbf{E}}_e}\left(\bar{\mathbf{E}}_e^T:\bar{\mathbf{E}}_e\right)=2\left(\bar{\mathbf{E}}_e\right)\\ \frac{\partial J_3}{\partial\bar{\mathbf{E}}_e} &= \frac{\partial}{\partial\bar{\mathbf{E}}_e}\left(\mathbf{I}:\bar{\mathbf{E}}_e^3\right)=3\bar{\mathbf{E}}_e\bar{\mathbf{E}}_e & \frac{\partial J_4}{\partial\bar{\mathbf{E}}_e} &= \frac{\partial}{\partial\bar{\mathbf{E}}_e}\left(\mathbf{I}:\left(\bar{\mathbf{M}}^1\bar{\mathbf{E}}_e\right)\right)=\bar{\mathbf{M}}^1\\ \frac{\partial J_5}{\partial\bar{\mathbf{E}}_e} &= \frac{\partial}{\partial\bar{\mathbf{E}}_e}\left(\mathbf{I}:\left(\bar{\mathbf{M}}^1\bar{\mathbf{E}}_e^2\right)\right)=\bar{\mathbf{M}}^1\bar{\mathbf{E}}_e+\bar{\mathbf{E}}_e\bar{\mathbf{M}}^1 & \frac{\partial J_6}{\partial\bar{\mathbf{E}}_e} &= \frac{\partial}{\partial\bar{\mathbf{E}}_e}\left(\mathbf{I}:\left(\bar{\mathbf{M}}^2\bar{\mathbf{E}}_e\right)\right)=\bar{\mathbf{M}}^2 \end{aligned} \tag{A.11}$$

$$\frac{\partial J_7}{\partial \bar{\mathbf{E}}_e} = \frac{\partial}{\partial \bar{\mathbf{E}}_e}\left(\mathbf{I} : \left(\bar{\mathbf{M}}^2 \bar{\mathbf{E}}_e^2\right)\right) = \bar{\mathbf{M}}^2 \bar{\mathbf{E}}_e + \bar{\mathbf{E}}_e \bar{\mathbf{M}}^2$$

From the expressions (A.11), one can calculate the second derivatives of the strain invariants:

$$\frac{\partial^2 J_1}{\partial \bar{\mathbf{E}}_e \partial \bar{\mathbf{E}}_e} = 0 \qquad \frac{\partial^2 J_2}{\partial \bar{\mathbf{E}}_e \partial \bar{\mathbf{E}}_e} = \frac{\partial}{\partial \bar{\mathbf{E}}_e}\left(2\bar{\mathbf{E}}_e\right) = 2\bar{\mathbb{I}}$$

$$\frac{\partial^2 J_3}{\partial \bar{\mathbf{E}}_e \partial \bar{\mathbf{E}}_e} = \frac{\partial}{\partial \bar{\mathbf{E}}_e}\left(3\bar{\mathbf{E}}_e \bar{\mathbf{E}}_e\right) = 3\bar{\mathbb{k}} \qquad \bar{\mathbb{k}} = \delta_{ik}\bar{\mathbf{E}}_{lj} + \bar{\mathbf{E}}_{ik}\delta_{jl}$$

$$\frac{\partial^2 J_5}{\partial \bar{\mathbf{E}}_e \partial \bar{\mathbf{E}}_e} = \frac{\partial}{\partial \bar{\mathbf{E}}_e}\left(\bar{\mathbf{M}}^1 \bar{\mathbf{E}}_e + \bar{\mathbf{E}}_e \bar{\mathbf{M}}^1\right) = \bar{\mathbb{F}}^1 \qquad \bar{\mathbb{F}}^1_{ijkl} = \bar{\mathbf{M}}^1_{ik}\delta_{jl} + \delta_{ik}\bar{\mathbf{M}}^1_{lj} \tag{A.12}$$

$$\frac{\partial^2 J_7}{\partial \bar{\mathbf{E}}_e \partial \bar{\mathbf{E}}_e} = \frac{\partial}{\partial \bar{\mathbf{E}}_e}\left(\bar{\mathbf{M}}^2 \bar{\mathbf{E}}_e + \bar{\mathbf{E}}_e \bar{\mathbf{M}}^2\right) = \bar{\mathbb{F}}^2 \qquad \bar{\mathbb{F}}^2_{ijkl} = \bar{\mathbf{M}}^2_{ik}\delta_{jl} + \delta_{ik}\bar{\mathbf{M}}^2_{lj}$$

$$\frac{\partial^2 J_4}{\partial \bar{\mathbf{E}}_e \partial \bar{\mathbf{E}}_e} = \frac{\partial}{\partial \bar{\mathbf{E}}_e}\left(\bar{\mathbf{M}}^1\right) = 0 \qquad \frac{\partial^2 J_6}{\partial \bar{\mathbf{E}}_e \partial \bar{\mathbf{E}}_e} = \frac{\partial}{\partial \bar{\mathbf{E}}_e}\left(\bar{\mathbf{M}}^2\right) = 0$$

The invariants and derivatives are used in the formulation of free energy function and expressions for stress and stiffness tensors, given earlier in this Appendix.

Appendix B

Rate of change of damage conjugate force

Thermodynamics force conjugate to the second order damage tensor $\bar{\boldsymbol{\omega}}$, called damage energy release rate, is given in the following form (see equation (4.11)):

$$\bar{\mathbf{Y}} = -\left[\mathbf{I} - \bar{\boldsymbol{\omega}}\right]_{sym} \bar{\mathbf{S}} \tag{B.1}$$

The rate of change of the damage conjugate force (B.1) is calculated as:

$$\begin{aligned}
\dot{\bar{\mathbf{Y}}} &= \dot{\bar{\boldsymbol{\omega}}}\bar{\mathbf{S}} - \left[\mathbf{I} - \bar{\boldsymbol{\omega}}\right]\dot{\bar{\mathbf{S}}} = \dot{\lambda}_d \frac{\partial f_d}{\partial \bar{\mathbf{Y}}}\bar{\mathbf{S}} - \left[\mathbf{I} - \bar{\boldsymbol{\omega}}\right]\bar{\mathbb{C}} : \dot{\bar{\mathbf{E}}}_e = \\
&= \dot{\lambda}_d \frac{\partial f_d}{\partial \bar{\mathbf{Y}}}\bar{\mathbf{S}} - \left[\mathbf{I} - \bar{\boldsymbol{\omega}}\right]\bar{\mathbb{C}} : \left(\left[\bar{\mathbf{C}}_e\left(\bar{\mathbf{I}} - \bar{\mathbf{I}}_p\right)\right]_{sym} - \left[\bar{\mathbf{C}}_d \bar{\mathbf{I}}_d\right]_{sym}\right) = \\
&= \dot{\lambda}_d \left(\frac{\partial f_d}{\partial \bar{\mathbf{Y}}}\bar{\mathbf{S}} - \left[\mathbf{I} - \bar{\boldsymbol{\omega}}\right]\bar{\mathbb{C}} : \left[\left[\mathbf{I} - \bar{\boldsymbol{\omega}}\right]\frac{\partial f_d}{\partial \bar{\mathbf{Y}}}\right]_{sym}\right) - \left[\mathbf{I} - \bar{\boldsymbol{\omega}}\right]\bar{\mathbb{C}} : \left[\bar{\mathbf{C}}_e\left(\bar{\mathbf{I}} - \bar{\mathbf{I}}_p\right)\right]_{sym}
\end{aligned} \tag{B.2}$$

where the rate of stress tensor $\dot{\bar{\mathbf{S}}}$ and the rate of deformation $\dot{\bar{\mathbf{C}}}_e$ are expressed as:

$$\dot{\bar{\mathbf{S}}} = \bar{\mathbb{C}} : \dot{\bar{\mathbf{E}}}_e = \bar{\mathbb{C}} : \left(\left[\bar{\mathbf{C}}_e\left(\bar{\mathbf{I}} - \bar{\mathbf{I}}_p\right)\right]_{sym} - \left[\bar{\mathbf{C}}_d \bar{\mathbf{I}}_d\right]_{sym}\right) \tag{B.3}$$

$$\begin{aligned}
\dot{\bar{\mathbf{C}}}_e &= \dot{\bar{\mathbf{F}}}_d^T \mathbf{F}_e^T \mathbf{F}_e \bar{\mathbf{F}}_d + \bar{\mathbf{F}}_d^T \dot{\mathbf{F}}_e^T \mathbf{F}_e \bar{\mathbf{F}}_d + \bar{\mathbf{F}}_d^T \mathbf{F}_e^T \dot{\mathbf{F}}_e \bar{\mathbf{F}}_d + \bar{\mathbf{F}}_d^T \mathbf{F}_e^T \mathbf{F}_e \dot{\bar{\mathbf{F}}}_d = \\
&= \left(\bar{\mathbf{F}}_d \bar{\mathbf{I}}_d\right)^T \mathbf{F}_e^T \mathbf{F}_e \bar{\mathbf{F}}_d + \bar{\mathbf{F}}_d^T \left(\mathbf{F}_e \bar{\mathbf{F}}_d \bar{\mathbf{I}}_e \bar{\mathbf{F}}_d^{-1}\right)^T \mathbf{F}_e \bar{\mathbf{F}}_d + \bar{\mathbf{F}}_d^T \mathbf{F}_e^T \left(\mathbf{F}_e \bar{\mathbf{F}}_d \bar{\mathbf{I}}_e \bar{\mathbf{F}}_d^{-1}\right)\bar{\mathbf{F}}_d + \bar{\mathbf{F}}_d^T \mathbf{F}_e^T \mathbf{F}_e \left(\bar{\mathbf{F}}_d \bar{\mathbf{I}}_d\right) = \\
&= \bar{\mathbf{I}}_d^T \bar{\mathbf{C}}_e + \bar{\mathbf{I}}_e^T \bar{\mathbf{C}}_e + \bar{\mathbf{C}}_e \bar{\mathbf{I}}_e + \bar{\mathbf{C}}_e \bar{\mathbf{I}}_d = 2\left(\bar{\mathbf{C}}_e \bar{\mathbf{I}}_e + \bar{\mathbf{C}}_e \bar{\mathbf{I}}_d\right) = 2\bar{\mathbf{C}}_e\left(\bar{\mathbf{I}} - \bar{\mathbf{I}}_p\right)
\end{aligned} \tag{B.4}$$

Expressions from (B.2) to (B.4) are used in the consistency condition for associative damage evolution.